A SECTORAL CYLINDRICAL CAVITY-BACKED SLOT ARRAY ANTENNA

RANGSAN WONGSAN

A THESIS SUBMITTED IN PARTIAL FULFILLMENT OF
THE REQUIREMENT FOR THE DEGREE
DOCTOR OF ENGINEERING IN ELECTRICAL ENGINEERING
SCHOOL OF GRADUATE STUDIES
KING MONGKUT'S INSTITUTE OF TECHNOLOGY LADKRABANG
2003

ISBN 974-324-771-8

หัวข้อวิทยานิพนธ์	สายอากาศชนิดแถวลำดับแบบร่องบนเซกเตอร์ของโพรงทรงกระบอก
นักศึกษา	นายรังสรรค์ วงศ์สรรค์
รหัสประจำตัว	41060019
ปริญญา	วิศวกรรมศาสตรดุษฎีบัณฑิต
สาขาวิชา	วิศวกรรมไฟฟ้า
พ.ศ.	2546
อาจารย์ผู้ควบคุมวิทยานิพนธ์	รศ.ดร. โมไนย ไกรฤกษ์

บทคัดย่อ

วิทยานิพนธ์ฉบับนี้นำเสนอ สายอากาศชนิดแถวลำดับแบบร่องบนเซกเตอร์ของโพรงทรงกระบอก ซึ่งโครงสร้างของสายอากาศมีลักษณะเป็นแถวลำดับแบบร่องเจาะบนผิวตัวนำของเซกเตอร์ทรงกระบอกที่ป้อนสัญญาณด้วยโพรงตัวนำทรงกระบอกสองชั้นซ้อนกัน ถูกปิดด้วยผิวตัวนำที่มุมของเซกเตอร์ที่กำหนดและที่ปลายทั้งสองด้านของเซกเตอร์ โดยโครงสร้างดังกล่าวจะถูกกระตุ้นด้วยโพรบไฟฟ้าเส้นตรง ซึ่งติดตั้งอยู่ที่กึ่งกลางของผิวด้านในของโพรง ข้อดีของสายอากาศชนิดนี้ก็คือ จะมีโครงสร้างที่ง่ายและไม่ซับซ้อนเนื่องจากได้รวมเอาตัวแบ่งกำลังงานและระบบป้อนสัญญาณให้อยู่ภายในโครงสร้างเดียวกัน สำหรับการวิเคราะห์เพื่อหาคุณลักษณะของสายอากาศนั้น ได้นำวิธีของโมเมนต์มาใช้ในการคำนวณเพื่อหาคำตอบของสมการอินทิกรัล โดยใช้ค่าฟังก์ชันของไดแอดิกกรีน ซึ่งเป็นผลตอบสนองของสนามที่จุดสังเกตอันเนื่องมาจากจุดกำเนิดมาช่วยในการคำนวณ จะทำให้ได้คุณสมบัติของสายอากาศที่สำคัญ เช่น การกระจายของแรงดันที่แท้จริงที่กระจายอยู่ที่ปากร่อง และการกระจายของกระแสที่แท้จริงที่กระจายอยู่ตลอดความยาวของโพรบ แบบรูปการกระจายคลื่น ทิศชี้นำคลื่น ค่าอิมพีแดนซ์ของโพรบ และค่าการสูญเสียย้อนกลับ วัตถุประสงค์ของสายอากาศชนิดนี้ได้ถูกนำเสนอเพื่อใช้สำหรับสถานีฐานของระบบการสื่อสารเคลื่อนที่หรือเพื่อใช้สำหรับสถานีแพร่สัญญาณโทรทัศน์ จากผลเฉลยเชิงเลขที่ได้จากการคำนวณของสายอากาศชนิดนี้ จะสามารถหาคุณลักษณะอิมพีแดนซ์ของโพรบป้อนสัญญาณและแบบรูปการกระจายคลื่นได้เป็นอย่างดี ตลอดจนได้ทำการวัดทดสอบสายอากาศต้นแบบเพื่อยืนยันผลการคำนวณ พบว่าสายอากาศที่ออกแบบมีคุณลักษณะอิมพีแดนซ์และแบบรูปการกระจายคลื่นใกล้เคียงกับผลที่ได้จากการคำนวณ ซึ่งสามารถนำผลที่ได้ไปใช้ในการออกแบบสายอากาศตามวัตถุประสงค์ดังกล่าวต่อไป

Thesis Title	A Sectoral Cylindrical Cavity-Backed Slot Array Antenna
Student	Mr.Rangsan Wongsan
Student ID.	41060019
Degree	Doctor of Engineering
Programme	Electrical Engineering
Year	2003
Thesis Advisor	Assoc. Prof. Dr. Monai Krairiksh

ABSTRACT

This thesis presents the slot array antenna on a sectoral cylindrical cavity. The antenna structure is the slot array fed by the concentric cylindrical cavity. This cavity is enclosed by the conducting sector at specified angle and shorted at two ends of the sector. This structure is excited by a linear electric probe that is located at the center of the inner surface of the cavity. The advantage of this antenna is simple structure and not complicate since the power divider and feeding structure is integrated into single structure. For the antenna characteristics analysis, the Method of Moment is used to solve the integral equations. By using the dyadic Green's function, the response of field at the observation point due to the source, the antenna properties such as the actual voltage distribution along the slot, the current distribution on the probe, the radiation pattern, the directivity, the probe impedance and the return loss. The proposed antenna is aimed to use for base station of the mobile communication and broadcasting TV stations. From the numerical results of the antenna calculation, the input impedance of the probe and the radiation pattern can be determined. The antenna measurement is done to confirm the calculated results. It is obvious that the designed antenna provides the agreement with the calculated results. The results from the investigation can be applied for designing the antenna for further applications.

Acknowledgement

I would like to take this opportunity to express my gratitude to many individuals who concerned in the completion of this thesis.

First of all, I am so grateful to my advisor, Associate Professor Monai Krairiksh, who has been giving me helpful suggestion and stimulating the progress of this research since the first day I became his advisee. I also appreciate his kindness in accepting me as one of his advisees. I would also like to express my gratitude to Associate Professor Jun-ichi Takada of Tokyo Institute of Technology for his generous suggestions.

I would like to extend my sincere appreciation to Assistant Professor Sompol Kosulvit for his useful and warm suggestions. Also, I wish to thank Associate Professor Tawil Paungma, Dean of Faculty of Engineering and Associate Professor Kobchai Dejhan, Chair of Telecommunication Department who give me the encouragement along my Ph.D. student life in KMITL.

Special thanks for the fellow members of the Wireless Communication Laboratory, Dr. Chanchai Tongsopa, Dr. Komsak Meksamoot and Mr. Titipong Lertwiriyaprapa who gave me kind discussions. Many thanks to Dr. Chuwong Pongcharoenpanich for valuable discussions in every issue and reviewing all of my manuscripts. The assistances of Miss Nitikarn Pasri, Mr. Phairote Wounchoum, Mr. Phaisan Ngamjanyaporn , Mr. Duang-arthit Srimoon, Mr. Anat Mearnchu, Miss Suthasinee Lamultree and Mr. Sanya Amnartpluk have been much appreciated.

Finally, I am greatly indebted to all of my teachers in the past, my family, especially my mother, my wife, my daughter and son, who love me much and exactly understand my life throughout the study period.

Rangsan Wongsan

Table of Contents

Table of Contents (continued)

List of Tables

List of Figures

Fig. Page

Chapter 1

Introduction

This chapter introduces background of the sectoral cylindrical cavity-backed slot array antenna. It shows the cited literatures of the slot array antenna on the cylindrical surface and the feasible applications of this antenna. The purpose and the scope of the thesis including the outline of the remaining chapters that summarize the information of the succeeding chapters are addressed.

1.1 Background of the Sectoral Cylindrical Cavity-Backed Slot Array Antenna

1.1.1 Historical Notes

At present, wireless communication system has played a vital role and it has become an important part of daily life, especially the mobile communications and the broadcasting systems. The processes of launching the signal into space and receiving it are the functions of antenna that is a key device of the system. There have been various kinds of antennas extensively and continuously invented to accomplish the requirements for different features of the communications. The antenna applied for the base station of cellular system or the broadcasting station of the ultra high frequency television requires radiating either unidirectional or omnidirectional pattern in azimuthal plane with high gain and high power.

The slot cut on the conducting surface is one of many antenna types that are very useful for the application that the radiator is desirable to be flush-mounted with the conducting surface. There are many configurations of slots cut on the conductor; both flat and curved surfaces. The slot on the plane is

essential in case of the geometry of installation location is restricted to be flat in order to reduce the wind resistance.

There are many researches and developments on the slots on the conducting plane in literature [1-1]. Mostly, they are backed by the parallel plates [1-2], rectangular waveguide [1-3] and rectangular cavity [1-4]. However, for some particular applications of the curved surfaces [1-5] such as a portion of the vehicle, ship, aircraft and missile, the slot on the planar structure is inappropriately applied.

The conformal slot antenna is the most promising candidate for those requirements. Additionally, in case of the slot radiators located on the planar structure to form the planar slot antenna, the deterioration of gain or pattern occurs for wide-azimuthal angle. The conformal slot antennas such as slot antennas located on the cylindrical surface [1-6] is the attractive candidate to overcome the drawback of the planar slot antennas for the particular applications of the curved surface.

In historical literatures, most of substantial works relating to the conformal slot antennas have been paid to the analysis of the slots imposed on the cylindrical surface because the antenna can be steered in azimuthal plane without the degradation of radiation characteristics. This can be realized due to its rotationally symmetrical structure in circular cross section. This advantage of the slots on the circular cylinder surface can be used to be the antenna requires omnidirectional pattern in azimuthal plane. In addition, if we divided the circular cross section along the length of the cylinder to obtain the sectoral cylinders and cut the axial or circumferential slots on the surface of these sectors, they can be the elements of antenna which yield unidirectional pattern in azimuthal plane and obtain the wide beamwidth. However, when multiple of these elements are combined, they will be formed to be a compact circular array. Furthermore, if each element of antenna is excited by a probe, it has the

advantage of simple feeding system and high power handling. Therefore, the antenna structure will be designed to be a circular array of sectoral cylinder in order to use the back concave surface for installing an excitation probe.

Most of substantial works related to the sectoral cylindrical structure have been done about the sectoral cylindrical waveguide. Lin and Omar [1-7] determined the cutoff wavelength of this structure. The equivalent parameters for the slot on a sectoral waveguide were presented by Lue *et al* [1-8]. Fan and Jin [1-9] obtained radar cross section of cylindrically slotted waveguide array antenna. Besides these, Tam *et al* investigated annular sector dielectric resonator antenna geometry [1-10] and Richard *et al* [1-11] presented a theoretical and experimental investigation of annular, annular sector and circular sector microstrip antennas. As far as we know, there is no information about the cavity structure that is excited by probe which is necessary for the structure that requires the simple feeder and high power handling.

There are various kinds of antennas for the mobile base station and UHF-television broadcasting station, which can be used for radiating either unidirectional or omnidirectional pattern in azimuthal angle, such as the panel system [1-12]. This is another type of antenna contains elements of dipole or microstrip antennas as an array arrangement. The disadvantages of this antenna are large and not self-supporting. It requires an external spine to support which results in complex and bulky feed systems in addition to higher windload. The other popular one is superturnstile antenna that combines the omnidirectionality of the top-mounted slot antennas with the full UHF bandwidth of a panel antenna. The combination of features makes the superturnstile the best choice when both bandwidth and omnidirectional pattern are required. Its disadvantage is narrow band. Furthermore, mechanical structure is made of small radiating elements, therefore, it is not self supporting. This antenna must be enclosed by a structural radome that supports the antenna. The weight of a high power

superturnstile is about one third of an equivalent top-mounted slot antenna. However, because of the large radome diameter, this antenna will generate higher windload.

From these aforementioned literature review of the conventional antennas for the mobile base station and the UHF television broadcasting station, it is obvious that the antenna should possess simple feeding system, high power handling and low windload. Therefore, this thesis proposes to use a sectoral cylindrical cavity-backed slot array antenna, which the feeding structure is a linear electric probe excited at the inner surface of the cavity. This structure can be easily fed by a power divider. In addition, the sectoral structure is expected that it is simple to design rather than using annular cylinder structure. Accordingly, although we have to involve with the complicated mathematical functions, the considerable usefulness of the antenna for the specific applications is still being important. This fact has motivated the presentation of this thesis.

1.1.2 Possible Applications of the Sectoral Cylindrical Cavity-Backed Slot Array Antenna

A sectoral cylindrical cavity-backed slot array antenna designed to radiate the linearly polarized beam is proposed to serve as the antenna for the base station of the mobile communication and the broadcasting station of the UHF television, which can radiate either unidirectional or omnidirectional pattern in azimuthal angle.

1.1.2.1 UHF Television Broadcasting Station

Although the world's telecommunication trunk network are to all digital within the time frame of the 1990s, television, on the other hand, remains nearly all analog [1-13]. However, in the future, the trend to digitize television will be extensively used for transmitting over the public switching telecommunication

network and by using radio waves to direct to people via the broadcasting station. Our concern is the case of the broadcasting station antenna. International Telecommunication Union has extended the frequency band of television channel to UHF and EHF band for responding the increased demand of digital television. The proposed antenna, as shown in Fig.1.1,

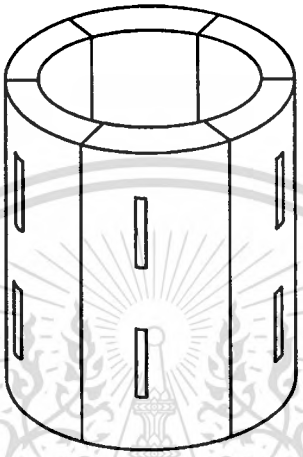

Fig. 1.1 The circular array of an axial slot array on the sectoral cylindrical cavity

has the following features:

(1) Configuration of the antenna is simple, which can be used for radiating either unidirectional or omnidirectional pattern. The antenna is designed to be multi-element, which can be combined to be the top-mounted compact circular array for yielding omnidirectional pattern in azimuth plane. When we use the single element to be the side-mounted antenna in a desired direction, unidirectional pattern will be obtained.

(2) The standard bandwidth of television transmission is based on 6 MHz RF assignments in most parts of the world. For the HDTV (High Definition Television), 30 MHz of video and sound can be digitized and compressed before transmitting in 6 MHz of this specific

bandwidth [1-13]. The proposed antenna has sufficiently wide bandwidth that can respond this standard.

(3) The azimuthal pattern of each element yields wider angle, which is appropriate to the requirements of the TV broadcasting.

(4) The feed system is an excitation probe, which does not result in complexity and bulkiness.

(5) The array of axial slots on the cylindrical surface yield horizontal polarized beam pattern.

1.1.2.2 Base Station Antennas in Mobile Radio Communication

The cellular/mobile radio communication system [1-14] is another application of interest for the linearly polarized beam of cylindrical cavity-backed slot array antenna. A linearly polarized beam cylindrical cavity-backed slot array antenna mentioned above is proposed for applying as the antenna for a base station. Features (1) through (4) of this antenna can be applied for this application. Merely, the difference of the antenna used in this system is linearly vertical polarization. It can be modified by cutting circumferential slot array on the outer surface instead of the axial slots array to yield the desired vertical polarization, as shown in Fig.1.2.

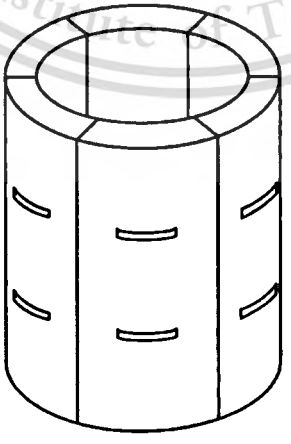

Fig. 1.2 The circular array of a circumferential slot array on the sectoral cylindrical cavity

1.2 Purpose and Scope of the Thesis

This thesis aims to propose a sectoral cylindrical cavity-backed slot array antenna excited by probe. The structure of the antenna is simple and suitable for mass production. This thesis is focused on the design of the sectoral cylindrical cavity-backed slot array antenna to radiate the horizontal linear polarized beam to meet the requirement of the UHF television broadcasting station antenna. The antenna characteristics such as input impedance, radiation pattern, directivity are consequently investigated by using Method of Moments with the aids of the dyadic Green's functions. Also, the design criteria of the further applications are provided. The antenna measurement is set up to confirm the proposed principle.

1.3 Outline of Remaining Chapters

As an introductory chapter, this chapter has mentioned about the overview of this thesis. The usefulness, objective, scope and organization of this thesis are summarized. As referred above that this thesis aims to propose a so-called sectoral cylindrical cavity-backed slot array antenna. The geometry of a sectoral cylindrical cavity-backed slot array antenna will be preliminarily studied in the next chapter, Chapter 2. The analysis model is divided into two canonical regions for introducing equivalent magnetic current density and equivalent electric current density by enforcing the boundary conditions at the slot aperture and the probe, respectively. The integral equations will be formulated, subsequently. They can be written in the form of the integration of the product between dyadic Green's functions and unknown currents to be determined.

In Chapter 3, the dyadic Green's functions are derived to complete the integral equations. The rigorous derivations for the dyadic Green's functions in electromagnetic theory for the sectoral cylindrical cavity are expressed.

Subsequently, the dyadic Green's functions for internal and external regions will be illustrated.

Chapter 4 investigates characteristics of a slot on the sectoral cylindrical cavity and its excitation. The basis function and weighting function are expanded to solve the integral equations by means of Method of Moments. The unknown currents are determined by solving the integral equations that the antenna characteristics are subsequently examined.

In Chapter 5, a slot array on the sectoral cylindrical cavity for the horizontal polarization will be formulated and the antenna characteristics are subsequently investigated.

Chapter 6 verifies the proposed principle and theory as presented in the preceding chapters by the measurements. The prototypes of the antenna were fabricated corresponding to the design parameters suggested in the previous chapters. The experimental results of radiation pattern, input impedance, return loss, and standing wave ratio are reported.

Chapter 7 summarizes the consequence of the material presented in the preceding chapters together with the discussions for further study.

Eventually, the expression of the special functions in cylindrical coordinates that are very useful for the study of the sectoral cylindrical slot array antenna as well as the components of the dyadic Green's functions for sectoral cylindrical cavity are summarized in the appendices.

References

[1-1] S.R.Rengarajarn and L.G.Josefsson, "Slotted waveguide array antenna technology," *IEEE AP-S and URSI National Radio Science Meeting*, California, June 1995.

[1-2] J.Hirokawa, M.Ando, and N.Goto, "Waveguide-fed parallel plate slot array antenna," *IEEE Trans. Antennas Propagat.*, vol.40, no.2, pp.218-223, Feb.1992.

[1-3] A.F.Stevenson, "Theory of slots in rectangular wave-guides," *J. Appl. Phys.*, vol. 19, no.1, pp.24-38, Jan.1948.

[1-4] J.Galejs, "Admittance of rectangular slot which is backed by a rectangular cavity," *IEEE Trans. Antennas Propagat.*, vol.11, no.3, pp.119-126, Mar.1963.

[1-5] A.Kumar and H.D.Hristov, *Microwave Cavity Antennas*, Sec.2.2, Artech House, Inc., Norwood, 1989.

[1-6] A.F.Peterson and R.Mittra, "Mutual Admittance between Slot in Cylinders of Arbitrary Shape," *IEEE Trans. Antennas Propagat.*, vol. 37, no.7, pp.858-864, July 1989.

[1-7] F.Lin and A.S.Omar, "Segment-sector waveguide," *1989 Antennas and Propagation Society International Symposium*, AP-S Digest, 1989.

[1-8] S.W.Lue, Y.Zhuang, and S.M.Cao, "The equivalent parameters for the radiating slot on a sectoral waveguide," *IEEE Trans. Antennas Propagat.*, vol.42, no.11,pp.1577-1581, Nov.1994.

[1-9] G.X.Fan and J.M.Jin, "Scattering from a cylindrically conformal slotted waveguide array antenna," *IEEE Antennas Propagat.*, vol.45, no.7, pp.1150-1159, July 1997.

[1-10] M.T.K.Tam and R.D.Murch, "Compact circular sector and annular sector dielectric resonator antennas," *IEEE Trans. Antennas Propagat.*, vol.47, no.5, pp.837-842, May 1999.

[1-11] W.F.Richards, J.D.Ou, and S.A.Long, "A theoretical and experimental investigation of annular, annular sector and circular sector microstrip antennas," *IEEE Trans. Antennas Propagat.*, vol.32, no.8, pp.864-867, Aug. 1984.

[1-12] D.Casciola, G.L.Miers, and R.A.Surette, "UHF antenna choices," *IEEE Trans. On Broadcasting*, vol.45, no.1, March 1999.

[1-13] R.L.Freeman, *Telecommunication Transmission Handbook*, Sec.13.2, John Wiley & Sons Inc., Toronto, 1996.

[1-14] J.D.Gibson,*The Mobile Communications Handbook*, Sec.16.2, CRC Press, Florida, 1996.

Chapter 2

A Sectoral Cylindrical Cavity-Backed Slot Antenna

2.1 Introduction

A sectoral cylindrical cavity-backed slot antenna is proposed in this chapter. The structure of the antenna is revealed. In order to meet the application of the television broadcasting station antennas, the sectoral cylindrical cavity-backed slot antenna is designed to generate linearly horizontal polarized beam pattern. The preliminarily geometry of a sectoral cylindrical cavity-backed slot array antenna will be described. The Method of Moments is used for the theoretical formulations of the antenna characteristics. The geometry will be divided into two canonical regions. The integral equations in the form of the integration of the product between dyadic Green's functions and two unknown currents, viz., a magnetic current sheet over the slot and an electric current at the probe can be formulated, subsequently.

2.2 Geometry of a Sectoral Cylindrical Cavity-Backed Slot Antenna

The structure of a sectoral cylindrical cavity-backed slot antenna is composed of a narrow axial slot cut on an outer surface of the sectoral cylindrical cavity as shown in Fig.2.1(a). The slot of the length l_s and the width w_s is aligned on z direction at which the center of this slot is located at (ρ_b, ϕ_s, z_s). The cavity is made of the concentric conducting circular cylindrical structure of the inner and outer radii of ρ_a and ρ_b, respectively. This structure is enclosed by the conducting surface at the angle of $\phi = 0$ and $\phi = \phi_c$ and shorted at the both ends ($z = 0$ and $z = z_d$). This cavity wall is considered to be a perfect electric conductor and the thickness is negligible. The cross-sectional view of the antenna is illustrated as shown in Fig.2.1(b). The excitation probe is located at the center of the inner surface of the cavity ($\rho_f = \rho_a$, $\phi_f = \phi_c/2$, $z_f = z_d/2$). The

length of the probe is l_f and it is assumed to be very thin so as to disregard the diameter.

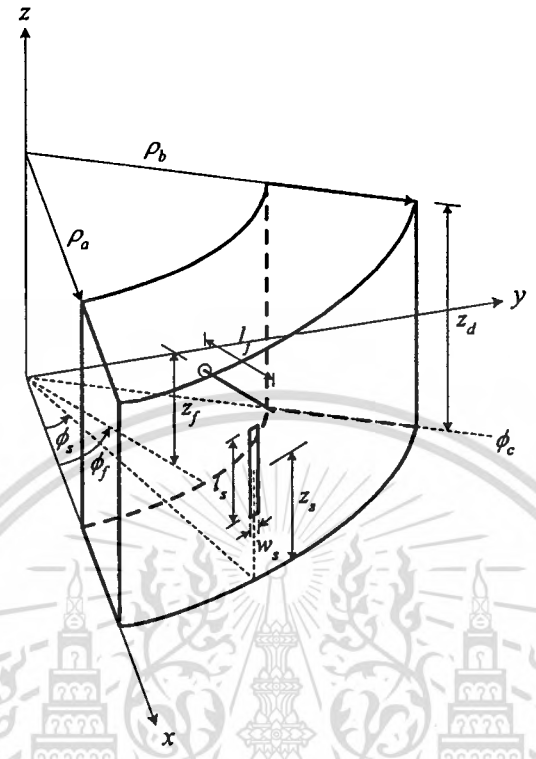

(a) Perspective view

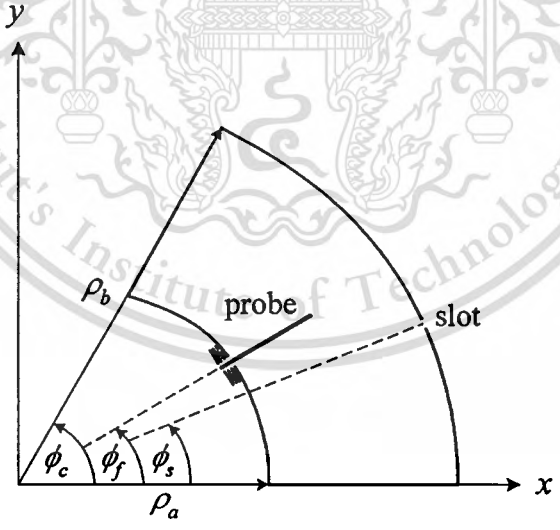

(b) Cross-sectional view

Fig.2.1 Configuration of a sectoral cylindrical cavity-backed slot antenna

2.3 Division of Analysis Model into Canonical Regions

The coupling of the energy from the excited probe and the subsequent radiation from the slot can be formulated by enforcing the boundary conditions on the slot aperture and the excited probe. The structure from Fig.2.1(b) is divided into two canonical regions: the region outside the sectoral cylinder (region I) and the region inside the cavity (region II), as illustrated in Fig.2.2. In accordance with the Field Equivalent Principle [2-1], the fields in the two regions can be decoupled by covering the aperture with a perfectly conducting surface and introducing equivalent magnetic current above and below the perfectly conducting surface. Denoting the equivalent magnetic current above aperture as $\overline{M}$ and that below one as $-\overline{M}$. For the excited probe, it is removed out and equivalent electric current is introduced. It is represented by $\overline{J}$. Therefore, the field in region I is due to $\overline{M}$, the field in region II is due to $-\overline{M}$ and $\overline{J}$ from the slot and the excited probe, respectively.

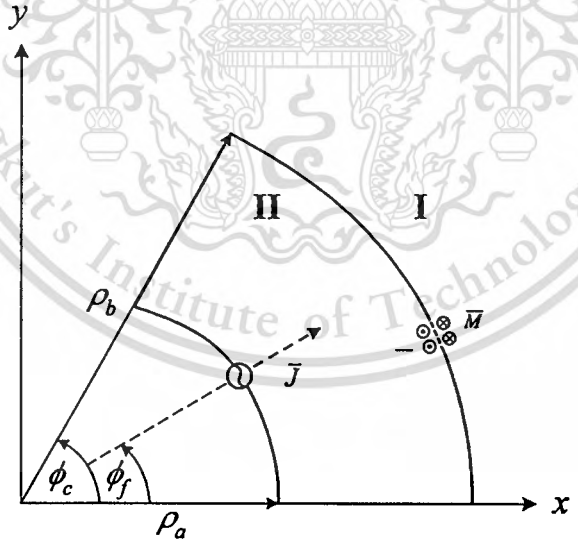

Fig.2.2 Equivalent analysis model of a sectoral cylindrical cavity-backed antenna

2.4 Integral Equations Formulations

From the analysis model as shown in Fig.2.2, the coupling of the energy and subsequent radiation of the slot can be formulated by enforcing the boundary conditions on the tangential magnetic fields in the upper and lower slot apertures and the tangential electric fields on the excited probe. These conditions are represented by using a coupled magnetic-field integral equation (MFIE) and electric-field integral equation (EFIE), referred to as the hybrid EFIE-MFIE (HEM), in terms of the sought-for current and the electric fields at the slot and on the probe, respectively;

$$\bar{H}_{tan}^{ext} = \bar{H}_{tan}^{int} \tag{2.1a}$$

$$\bar{H}_{tan}^{ext} = \bar{H}_{s}^{ext} \times \hat{\rho} \tag{2.1b}$$

$$\bar{H}_{tan}^{int} = \left(\bar{H}_{s}^{int} + \bar{H}_{p}^{int}\right) \times \hat{\rho} \tag{2.1c}$$

$$\bar{H}_{s}^{ext} = \bar{H}_{s}^{int} + \bar{H}_{p}^{int} \tag{2.1d}$$

where $\bar{H}_{tan}^{ext}$ and $\bar{H}_{tan}^{int}$ represent the external and internal tangential magnetic fields, respectively. $\bar{H}_{p}^{int}$ and $\bar{H}_{s}^{int}$ are the internal magnetic fields radiated from the linear electric probe and the slot aperture, respectively. $\bar{H}_{s}^{ext}$ denotes the external magnetic field radiated from the slot aperture. $\hat{\rho}$ is the unit normal vector to cylindrical surface.

In order to solve for the magnetic field, the dyadic Green's functions must be readily derived [2-2]-[2-3]. In this case, the scalar Green's function cannot be applied. The reason is that the field and source are vectors, and the Green's function that is the transformation between the field and the source must be dyadic Green's function. The magnetic field, therefore, can be immediately calculated, namely

$$\bar{H}_s^{ext}(\bar{R}) = j\omega\varepsilon_0 \iint_{S_s} \bar{\bar{G}}_{HM}^{ext}(\bar{R},\bar{R}') \cdot \left(\bar{E}(\bar{R}') \times \hat{\rho}\right) dS'$$

$$= j\omega\varepsilon_0 \iint_{S_s} \bar{\bar{G}}_{HM}^{ext}(\bar{R},\bar{R}') \cdot \bar{M}(\bar{R}') dS' \qquad (2.2)$$

and

$$\bar{H}_s^{int}(\bar{R}) = j\omega\varepsilon_0 \iint_{S_s} \bar{\bar{G}}_{HM}^{int}(\bar{R},\bar{R}') \cdot \left(\bar{E}(\bar{R}') \times (-\hat{\rho})\right) dS'$$

$$= -j\omega\varepsilon_0 \iint_{S_s} \bar{\bar{G}}_{HM}^{int}(\bar{R},\bar{R}') \cdot \bar{M}(\bar{R}') dS', \qquad (2.3)$$

$$\bar{H}_p^{int}(\bar{R}') = \iint_{L_f} \bar{\bar{G}}_{HJ}^{ext}(\bar{R},\bar{R}') \cdot \bar{J}(\bar{R}') dS' \qquad (2.4)$$

where $\bar{\bar{G}}_{HM}^{ext,int}(\bar{R},\bar{R}')$ and $\bar{\bar{G}}_{HJ}^{int}(\bar{R},\bar{R}')$ denote the magnetic dyadic Green's functions produced by a magnetic current sheet and electric current density, respectively. S_s and L_f are the limits of integration on the surface of slot aperture and on the length of probe, respectively. $\bar{R}$ and $\bar{R}'$ are the location coordinates of field and source points, respectively. In this thesis, the time function $e^{j\omega t}$ is used. Substituting (2.2), (2.3), and (2.4) into (2.1d), the simultaneous equation across the slot can be obtained as:

$$j\omega\varepsilon_0 \iint_{s_s} \left\{ \bar{\bar{G}}_{HM}^{in}(\bar{R},\bar{R}') + \bar{\bar{G}}_{HM}^{out}(\bar{R},\bar{R}') \right\} \cdot \bar{M}(\bar{R}') dS' + \int_{L_f} \bar{\bar{G}}_{HJ}^{in}(\bar{R},\bar{R}') \cdot \bar{J}(\bar{R}') dL' = 0 \qquad (2.5)$$

Alternatively, not only the boundary condition on the tangential electric field along the probe is considered, but the delta gap electric field at the bottom of the probe is also considered as the excitation. Therefore,

$$E_{tan}^{int} = 0 \tag{2.6a}$$

For the excitation by probe in ρ-direction , E_{tan}^{int} can be written as

$$E_{\tan}^{\text{int}} = \left(\bar{E}^{\text{int}} \cdot \hat{\rho}\right) + E_a \tag{2.6b}$$

where E_a is the applied field, which is defined by delta gap model as

$$E_a = \delta(\bar{R} - \bar{R}') \tag{2.6c}$$

and $\bar{E}^{int}$ denotes the internal scattering field, given as

$$\bar{E}^{int} = \bar{E}_s^{int} + \bar{E}_p^{int} \tag{2.6d}$$

Following (2.6a), (2.6b) can be rearranged as

$$\bar{E}^{int} \cdot \hat{\rho} = -E_a . \tag{2.7}$$

The complete condition can be stated by using delta gap model as (2.6c)

$$\left(\bar{E}_s^{int} + \bar{E}_p^{int}\right) \cdot \hat{\rho} = -\delta\left(\bar{R}'\right), \tag{2.8}$$

where $\bar{E}_s^{int}$ and $\bar{E}_p^{int}$ are the internal electric fields radiated from the slot aperture and the probe, respectively. $-\delta\left(\bar{R}'\right)$ is the assumed voltage source from the delta gap source model.

$$\bar{E}_s^{int}(\bar{R}) = \iint_{S_s} \bar{\bar{G}}_{EM}^{int}\left(\bar{R}, \bar{R}'\right) \cdot \left(\bar{E}\left(\bar{R}'\right) \times -\hat{\rho}\right) dS'$$

$$= -\iint_{L_f} \bar{\bar{G}}_{EM}^{int}\left(\bar{R}, \bar{R}'\right) \cdot \bar{M}\left(\bar{R}'\right) dS' \tag{2.9}$$

$$\bar{E}_p^{int}(\bar{R}) = -j\omega\mu_0 \iint_{L_f} \bar{\bar{G}}_{EJ}^{int}(\bar{R},\bar{R}') \cdot \bar{J}(\bar{R}')dS', \qquad (2.10)$$

where $\bar{\bar{G}}_{EM}^{int}(\bar{R},\bar{R}')$ and $\bar{\bar{G}}_{EJ}^{int}(\bar{R},\bar{R}')$ denote the electric dyadic Green's functions produced by magnetic current sheet and electric current density, respectively. Substituting (2.9) and (2.10) into (2.8), the simultaneous integral equation on the probe can be obtained as:

$$\iint_{S_s} \bar{\bar{G}}_{EM}^{in}(\bar{R},\bar{R}') \cdot \bar{M}(\bar{R}')dS' + j\omega\mu_0 \iint_{L_f} \bar{\bar{G}}_{EJ}^{in}(\bar{R},\bar{R}') \cdot \bar{J}(\bar{R}')dS' = \delta(\bar{R}'). \quad (2.11)$$

Now the integral equations have been obtained as shown in (2.5) and (2.11). The next step is the evaluation of the unknown magnetic current sheet and electric current density. This can be accomplished by using Method of Moments [2-3]-[2-5].

2.5 Conclusions

The expressions of the integral equations of two canonical regions of a sectoral cylindrical cavity-backed slot antenna that excited by a probe are formulated by applying the Field Equivalent Principle. The boundary condition in which the magnetic fields are continuous throughout the slot aperture and the delta gap source is modeled at the bottom of the cavity.

References

[2-1] A.F.Peterson, S.L.Ray, R.Mittra, *Computational Methods for Electromagnetics,* Sec.1.7-1.12, IEEE Press, 1998.

[2-2] R.Wongsan, C.Phongcharoenpanich, and M.Krairiksh, "Electromagnetic dyadic Green's functions of a sectoral cylindrical cavity," *Proceedings of the International Forum cum Conference on Information Technology and Communication at the Dawn of the New Millennium*, Bangkok, vol.2, pp.477-486, Aug. 2000.

[2-3] C.T.Tai, *Dyadic Green Function in Electromagnetic Theory*, 2nd Ed. Sec.4.3, New York: IEEE Press, 1993.

[2-4] R.F.Harrington, *Field Computation by Moment Methods*, Sec.7.3, Robert E.Krieger Publishing, Inc., 1968.

[2-5] A.R.Djordjevic and T.K.Sarkar "A theorem on the Moment Methods," *IEEE Trans. Antennas Propagat.*, vol. AP-35, no. 3, pp. 353-355, Mar. 1987.

Chapter 3

Dyadic Green's Functions Derivation

3.1 Introduction

This chapter presents various kinds of dyadic Green's functions of a sectoral cylindrical cavity, which is derived in series form to fulfill the requirement of the integral equations. The method of magnetic dyadic Green's function is applied to find the dyadic Green's functions of both electric and magnetic types. The Ohm-Rayleigh method is utilized to achieve the unknown coefficients of the Green's functions. Dirichlet and Neumann boundary conditions are applied corresponding to the source and the field of the wave functions. These Green's functions are essential to find the electromagnetic field inside this cavity.

3.2 Dyadic Green's Functions in Electromagnetic Theory

The dyadic Green's functions are direct transformation of the fields due to a specific electric or magnetic current source under specific boundary conditions [3-1]. Since dyadic Green's functions for our geometry are known, it is quite convenient and straightforward to formulate problems with boundaries for which dyadic Green's functions are known. For generalized Method of Moment, the basic approach to derive the integral equations has been discussed in section 2.4 and these dyadic Green's functions are applied in these integral equations.

From Maxwell equations, one immediately obtains the following equations in a region of a homogenous medium

$$\nabla \times \nabla \times \bar{E} - k^2 \bar{E} = -j\omega\mu \bar{J} - \nabla \times \bar{M} \tag{3.1}$$

$$\nabla\times\nabla\times\bar{H}-k^2\bar{H}=-j\omega\mu\bar{M}+\nabla\times\bar{J} \tag{3.2}$$

When $\bar{M}=0$, the above equations become

$$\nabla\times\nabla\times\bar{E}-k^2\bar{E}=-j\omega\mu\bar{J} \tag{3.3}$$

$$\nabla\times\nabla\times\bar{H}-k^2\bar{H}=\nabla\times\bar{J} \tag{3.4}$$

The solution of the above equations is ultimately related to the following dyadic equations

$$\nabla\times\nabla\times\bar{\bar{G}}_e\left(\bar{R},\bar{R}'\right)-k^2\bar{\bar{G}}_e\left(\bar{R},\bar{R}'\right)=\bar{\bar{I}}\delta\left(\bar{R}-\bar{R}'\right) \tag{3.5}$$

$$\nabla\times\nabla\times\bar{\bar{G}}_m\left(\bar{R},\bar{R}'\right)-k^2\bar{\bar{G}}_m\left(\bar{R},\bar{R}'\right)=\nabla\times\bar{\bar{I}}\delta\left(\bar{R}-\bar{R}'\right) \tag{3.6}$$

where $\bar{\bar{G}}_e$ and $\bar{\bar{G}}_m$ denote the electric and magnetic dyadic Green's functions respectively, $\bar{\bar{I}}$ is a unit dyad and δ is the Dirac delta function. These dyadic Green's functions are related to each other by the following relationships:

$$\bar{\bar{G}}_m\left(\bar{R},\bar{R}'\right)=\nabla\times\bar{\bar{G}}_e\left(\bar{R},\bar{R}'\right) \tag{3.7}$$

$$k^2\bar{\bar{G}}_e\left(\bar{R},\bar{R}'\right)=\nabla\times\bar{\bar{G}}_m\left(\bar{R},\bar{R}'\right)-\bar{\bar{I}}\delta\left(\bar{R}-\bar{R}'\right) \tag{3.8}$$

The following general relationships between sources and fields in term of dyadic Green's function can be shown as follows.

$$\bar{E}\left(\bar{R}\right)=-j\omega\mu\int_V\bar{\bar{G}}_e\left(\bar{R},\bar{R}'\right)\cdot\bar{J}\left(\bar{R}'\right)dv'-\int_V\bar{\bar{G}}_m\left(\bar{R},\bar{R}'\right)\cdot\bar{M}\left(\bar{R}'\right)dv' \tag{3.9}$$

$$\bar{H}\left(\bar{R}\right)=-j\omega\varepsilon\int_V\bar{\bar{G}}_e\left(\bar{R},\bar{R}'\right)\cdot\bar{M}\left(\bar{R}'\right)dv'+\int_V\bar{\bar{G}}_m\left(\bar{R},\bar{R}'\right)\cdot\bar{J}\left(\bar{R}'\right)dv' \tag{3.10}$$

3.3 Dyadic Green's Functions for Internal Region

The geometry of a sectoral cylindrical cavity is composed of the concentric conducting circular cylindrical structure with the inner and outer radii of ρ_a and ρ_b, respectively. This structure is enclosed by the conducting surface at an angle ϕ_c and is shorted at the both ends ($z = 0$ and $z = z_d$). This cavity wall is considered to be perfect electric conductor and the thickness is negligible.

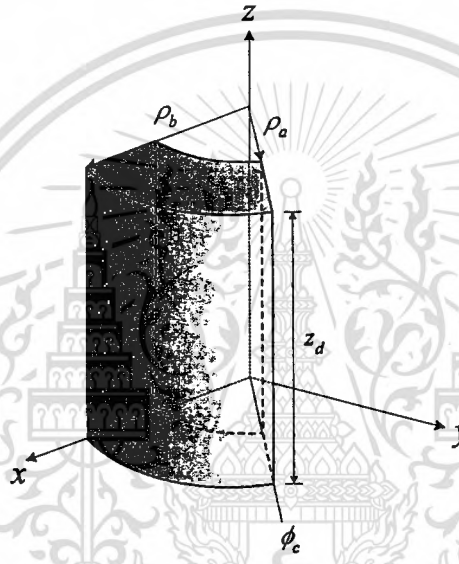

Fig.3.1 Geometry of a concentric sectoral cylindrical cavity

To derive the dyadic Green's functions of the sectoral cylindrical cavity, let us consider the structure of this cavity in Fig.3.1. The structure of the sectoral cylindrical cavity in the cylindrical coordinate system (ρ, ϕ, z) consists of two parts of the concentric sectoral cylindrical cavity which the inner and outer cylindrical radii are ρ_a and ρ_b, respectively.

The eigenfunction expansion method is used to derive the dyadic Green's functions. A lossless and homogeneous medium is considered to comply the real implementation that the antenna is filled with air. The $e^{j\omega t}$ time variation is

assumed and it is suppressed. The eigenfunction, $\varphi_{\substack{even \\ odd}\upsilon\xi}(k_g)$, which is a solution of the scalar wave equation [3-2]

$$\nabla^2\varphi + \kappa_\xi^2\varphi = 0, \tag{3.11}$$

in the cylindrical coordinate system is considered in the form

$$\varphi_{\substack{even \\ odd}\upsilon\xi}(k_g) = B_\upsilon(k_\xi\rho)\begin{Bmatrix}\cos \\ \sin\end{Bmatrix}\upsilon\phi\, e^{jk_g z}, \tag{3.12}$$

where k_g is the propagation constant. $B_\upsilon(k_\xi\rho)$ denotes the linear combination of the ordinary Bessel function of the first kind $J_\upsilon(k_\xi\rho)$ and the second kind $Y_\upsilon(k_\xi\rho)$ of order υ. It satisfies the ordinary Bessel differential equation

$$\frac{d^2B_\upsilon(x)}{dx^2} + \frac{1}{x}\frac{dB_\upsilon(x)}{dx} + \left[1 - \frac{\upsilon^2}{x^2}\right]B_\upsilon(x) = 0 \tag{3.13}$$

where x is $k_\xi\rho$, with the unknown normalized coefficient $A_\upsilon(k_\xi)$:

$$B_\upsilon(k_\xi\rho) = J_\upsilon(k_\xi\rho) + A_\upsilon(k_\xi)Y_\upsilon(k_\xi\rho). \tag{3.14}$$

By enforcing the boundary conditions that the tangential electric field in the radial direction vanishes, the unknown coefficient $A_\upsilon(k_\xi)$ can be determined from the characteristic equation.

The lower-order values of k_ξ in TE mode are given in Table 3.1. More details will be described in Appendix A.

Table 3.1 Roots of Bessel-Neumann boundary condition for TE modes:

Table values are $(\rho_b/\rho_a - 1)x_{vl}$

ρ_b / ρ_a	vl							
	01	11	21	31	02	12	22	32
1.0	*3.142*	*3.142*	*3.142*	*3.142*	*6.283*	*6.283*	*6.283*	*6.283*
1.1	*3.141*	*3.143*	*3.147*	*3.154*	*6.283*	*6.284*	*6.286*	*6.289*
1.2	*3.140*	*3.146*	*3.161*	*3.187*	*6.282*	*6.285*	*6.293*	*6.306*
1.3	*3.139*	*3.150*	*3.182*	*3.236*	*6.282*	*6.287*	*6.304*	*6.331*
1.4	*3.137*	*3.155*	*3.208*	*3.294*	*2.281*	*2.290*	*2.317*	*6.362*
1.5	*3.135*	*3.161*	*3.237*	*3.36*	*6.280*	*6.293*	*6.332*	*6.387*
1.6	*3.133*	*3.168*	*3.27*	*3.43*	*6.279*	*6.296*	*6.349*	*6.437*
1.8	*3.128*	*3.182*	*3.36*	*3.6*	*6.276*	*6.304*	*6.387*	*6.523*
2.0	*3.123*	*3.197*	*3.4*	*3.7*	*6.273*	*6.312*	*6.43*	*6.62*

ρ_b / ρ_a	vl							
	03	13	23	33	04	14	24	34
1.0	*9.425*	*9.425*	*9.425*	*9.425*	*12.566*	*12.566*	*12.566*	*12.566*
1.1	*9.425*	*9.425*	*9.427*	*9.429*	*12.566*	*12.567*	*12.568*	*12.569*
1.2	*9.424*	*9.426*	*9.431*	*9.440*	*12.566*	*12.567*	*12.571*	*12.578*
1.3	*9.424*	*9.427*	*9.438*	*9.457*	*12.566*	*12.568*	*12.577*	*12.590*
1.4	*9.423*	*9.429*	*9.447*	*9.478*	*12.565*	*12.570*	*12.583*	*12.606*
1.5	*9.423*	*9.431*	*9.458*	*9.502*	*12.565*	*12.571*	*12.591*	*12.624*
1.6	*9.422*	*9.434*	*9.469*	*9.528*	*12.564*	*12.573*	*12.600*	*12.644*
1.8	*9.420*	*9.439*	*9.495*	*9.587*	*12.563*	*12.577*	*12.619*	*12.689*
2.0	*9.418*	*9.444*	*9.523*	*9.652*	*12.561*	*12.581*	*12.640*	*12.738*

Once the value of k_ξ has been determined the value of $A_\upsilon(k_\xi)$ can be obtained [3-3]

$$A_\upsilon(k_\xi) = -\frac{J'_\upsilon(k_\xi\rho_a)}{Y'_\upsilon(k_\xi\rho_a)} = -\frac{J'_\upsilon(k_\xi\rho_b)}{Y'_\upsilon(k_\xi\rho_b)}, \tag{3.15}$$

where the prime denotes the differentiation with respect to the argument. This characteristic equation gives the solution

$$k_\xi\rho_a = x'_{\xi,\alpha} \tag{3.16}$$

and

$$k_\xi\rho_b = x'_{\xi,\beta} \tag{3.17}$$

such that

$$k_\xi(\rho_b - \rho_a) = x'_{\xi,\gamma} \tag{3.18}$$

where x' denotes the roots of zero of derivative of Bessel function ratio and γ is the interval between the roots α and β, the $\gamma = \alpha - \beta$ which corresponds to the order of the root interval. The lower-order values of k_ξ in TM mode are given in Table 3.2.

Table 3.2 Roots of Bessel-Neumann derivative boundary condition for TM modes: Table values are $(\rho_b/\rho_a - 1)x_{vl}$

ρ_b / ρ_a	vl							
	01	11	21	31	02	12	22	32
1.001	*3.141*	*3.141*	*3.141*	*3.141*	*6.283*	*6.283*	*6.283*	*6.283*
1.1	*3.142*	*0.095*	*0.190*	*0.285*	*6.283*	*3.144*	*3.148*	*3.155*
1.2	*4.145*	*0.182*	*0.364*	*0.546*	*6.285*	*3.150*	*3.166*	*3.193*
1.3	*3.149*	*0.261*	*0.523*	*0.784*	*6.287*	*3.160*	*3.194*	*3.248*
1.4	*3.154*	*0.334*	*0.669*	*1.002*	*6.289*	*3.173*	*3.228*	*3.318*
1.5	*3.160*	*0.402*	*0.804*	*1.203*	*6.293*	*3.188*	*3.269*	*3.400*
1.6	*3.167*	*0.465*	*0.928*	*1.387*	*6.296*	*3.204*	*3.314*	*3.490*
1.8	*3.181*	*0.578*	*1.150*	*1.710*	*6.304*	*3.241*	*3.416*	*3.694*
2.0	*3.196*	*0.677*	*1.340*	*1.978*	*6.312*	*3.282*	*3.531*	*3.920*

ρ_b / ρ_a	vl							
	03	13	23	33	04	14	24	34
1.001	*9.424*	*9.424*	*9.424*	*9.424*	*12.566*	*12.566*	*12.566*	*12.566*
1.1	*9.425*	*6.284*	*6.286*	*6.290*	*12.566*	*9.425*	*9.427*	*9.429*
1.2	*9.426*	*6.287*	*6.295*	*6.309*	*12.567*	*9.427*	*9.433*	*9.442*
1.3	*9.427*	*6.292*	*6.309*	*6.336*	*12.568*	*9.431*	*9.442*	*9.460*
1.4	*9.429*	*6.299*	*6.326*	*6.371*	*12.569*	*9.435*	*9.453*	*9.483*
1.5	*9.431*	*6.306*	*6.346*	*6.412*	*12.571*	*9.440*	*9.466*	*9.510*
1.6	*9.433*	*6.314*	*6.368*	*6.457*	*12.573*	*9.445*	*9.481*	*9.541*
1.8	*9.438*	*6.332*	*6.418*	*6.559*	*12.576*	*9.457*	*9.514*	*9.608*
2.0	*9.444*	*6.353*	*6.474*	*6.673*	*12.581*	*9.471*	*9.551*	*9.684*

When the value of k_ξ has been determined the value of $A_v(k_\xi)$ can be obtained

$$A_{\upsilon}(\xi) = -\frac{J_{\upsilon}(k_{\xi}\rho_a)}{Y_{\upsilon}(k_{\xi}\rho_a)} = -\frac{J_{\upsilon}(k_{\xi}\rho_b)}{Y_{\upsilon}(k_{\xi}\rho_b)} \tag{3.19}$$

the characteristic equation gives the solution

$$k_{\xi}\rho_a = x_{\xi,\alpha} \tag{3.20}$$

and

$$k_{\xi}\rho_b = x_{\xi,\beta} \tag{3.21}$$

such that

$$k_{\xi}(\rho_b - \rho_a) = x_{\xi,\gamma} \tag{3.22}$$

where x denotes the roots of zero of Bessel function ratio and α, β, γ are the same as declared before. The next step, we will use the cylindrical vector wave functions, which are the building blocks of the eigenfunction expansions of various kinds of dyadic Green functions, to describe the electric field inside a concentric sectoral cylindrical cavity. Therefore, ξ can be either e or h in case of TM mode and TE mode, respectively.

In the method of magnetic dyadic Green's function, $\overline{\overline{G}}_m$, for the configuration of the concentric sectoral cylindrical cavity, Tai [3-3] has specified the cavity to be waveguide. Therefore, the four sets of the solenoidal cylindrical vector wave functions with discrete eigenvalues must be functions for a concentric sectoral cylindrical waveguide. They are

$$\bar{M}_{\substack{even \\ odd}\upsilon\xi}(k_g) = \nabla \times \left[\varphi_{\substack{even \\ odd}\upsilon\xi}(k_g)\hat{z} \right], \tag{3.23}$$

$$\bar{N}_{\substack{even \\ odd}\upsilon\xi}(k_g) = \frac{1}{\kappa_{\xi}} \nabla \times \nabla \times \left[\varphi_{\substack{even \\ odd}\upsilon\xi}(k_g)\hat{z} \right]. \tag{3.24}$$

These vector wave functions, by definition, are the eigenfunctions or the characteristic functions, which are the solutions of the homogeneous vector wave equation

$$\nabla \times \nabla \times \bar{F} - \kappa_\xi^2 \bar{F} = 0, \tag{3.25}$$

where $\bar{F}$ is either $\bar{M}$ or $\bar{N}$ and satisfies the symmetrical relationships

$$\bar{N}_{\substack{even \\ odd}\upsilon\xi}(k_g) = \frac{1}{\kappa_\xi} \nabla \times \bar{M}_{\substack{even \\ odd}\upsilon\xi}(k_g) \tag{3.26}$$

and

$$\bar{M}_{\substack{even \\ odd}\upsilon\xi}(k_g) = \frac{1}{\kappa_\xi} \nabla \times \bar{N}_{\substack{even \\ odd}\upsilon\xi}(k_g). \tag{3.27}$$

By substituting the eigenfunction into (3.23) and (3.24), the complete expression of the vector wave function will be obtained and can be written in the form

$$\bar{M}_{\substack{even \\ odd}\upsilon h}(k_g) = \left[-\frac{\upsilon B_\upsilon(k_h\rho)}{\rho} \sin(\upsilon\phi)\hat{\rho} - \frac{\partial B_\upsilon(k_h\rho)}{\partial\rho} \cos(\upsilon\phi)\hat{\phi} \right] e^{jk_g z} \tag{3.28}$$

$$\bar{N}_{\substack{even \\ odd}\upsilon e}(k_g) = \frac{1}{k_e} \left[jk_g \frac{\partial B_\upsilon(k_e\rho)}{\partial\rho} \sin(\upsilon\phi)\hat{\rho} + \frac{jk_g\upsilon}{\rho} B_\upsilon(k_e\rho)\cos(\upsilon\phi)\hat{\phi} + k_e^2 B_\upsilon(k_e\rho)\sin(\upsilon\phi)\hat{z} \right] e^{jk_g z} \tag{3.29}$$

$$\bar{M}_{\substack{even \\ odd}\upsilon e}(k_g) = \left[\frac{\upsilon B_\upsilon(k_e\rho)}{\rho} \cos(\upsilon\phi)\hat{\rho} - \frac{\partial B_\upsilon(k_e\rho)}{\partial\rho} \sin(\upsilon\phi)\hat{\phi} \right] e^{jk_g z} \tag{3.30}$$

$$\bar{N}_{\substack{even \\ odd}\upsilon h}(k_g) = \frac{1}{\kappa_h} \left[jk_g \frac{\partial B_\upsilon(k_h\rho)}{\partial\rho} \cos(\upsilon\phi)\hat{\rho} - \frac{jk_g\upsilon}{\rho} B_\upsilon(k_h\rho)\sin(\upsilon\phi)\hat{\phi} + k_h^2 B_\upsilon(k_h\rho)\cos(\upsilon\phi)\hat{z} \right] e^{jk_g z} \tag{3.31}$$

where $\kappa_e^2 = k_e^2 + k_g^2$, $\kappa_h^2 = k_h^2 + k_g^2$.

The function $\bar{M}_{\substack{even \\ odd}\upsilon h}(k_g)$ can be used to describe the electric field of the TE mode in a concentric sectoral cylindrical waveguide with radius equals ρ_a through ρ_b. The function $\bar{N}_{\substack{even \\ odd}\upsilon e}(k_g)$ is used for the TM mode. The functions $\bar{M}_{\substack{even \\ odd}\upsilon e}(k_g)$ and $\bar{N}_{\substack{even \\ odd}\upsilon h}(k_g)$ can be used to describe the magnetic field in this waveguide of TM mode and TE mode, respectively.

To derive the dyadic Green's functions of the structure under consideration, the method of $\bar{\bar{G}}_m$ approach [3-2] will be applied. Applying the Neumann boundary condition [3-3], the magnetic dyadic Green's function of the second kind is first derived by using

$$\nabla \times \nabla \times \bar{\bar{G}}_{m2}(\bar{R}, \bar{R}') - k^2 \bar{\bar{G}}_{m2}(\bar{R}, \bar{R}') = \nabla \times \left(\bar{\bar{I}} \delta(\bar{R} - \bar{R}') \right), \tag{3.32}$$

where $\bar{\bar{G}}_{m2}$ denotes the magnetic dyadic Green's function of the second kind that satisfies the boundary condition

$$\hat{n} \times \nabla \times \bar{\bar{G}}_{m2}(\bar{R}, \bar{R}') = 0, \tag{3.33}$$

in domain $\rho_a \le \rho \le \rho_b$, $0 \le \phi \le \phi_c$ and $-\infty \le z \le \infty$, k is the wave number of the medium which is equal to $\omega\sqrt{\mu\varepsilon}$, ω is operating angular frequency, μ and ε are the permeability and permittivity of the medium, respectively. $\bar{\bar{I}}$ is the unit dyad and $\delta(\bar{R} - \bar{R}')$ is the three dimensional delta function.

According to Ohm-Rayleigh method [3-3], the source function is expanded in the form of solenoidal vector wave functions

$$\nabla\times\left(\bar{\bar{I}}\delta\left(\bar{R}-\bar{R}'\right)\right)=\int_{-\infty}^{\infty}dh\sum_{\upsilon=0}^{\infty}\sum_{l=1}^{\infty}\left(\bar{N}_{\substack{even\\odd}\upsilon h}\left(k_g\right)\bar{A}_{\substack{even\\odd}\upsilon h}\left(k_g\right)+\bar{M}_{\substack{even\\odd}\upsilon e}\left(k_g\right)\bar{B}_{\substack{even\\odd}\upsilon e}\left(k_g\right)\right),\tag{3.34}$$

when $\bar{A}_{\substack{even\\odd}\upsilon h}\left(k_g\right)$ and $\bar{B}_{\substack{even\\odd}\upsilon e}\left(k_g\right)$ are two unknown functions or vector coefficients to be determined. Index m is used to designate the ordinal number associated with p_{nm} and q_{nm}. By taking the anterior scalar product of (3.34) with $\bar{N}'_{\substack{even\\odd}\upsilon h}\left(-k_g'\right)$ and $\bar{M}'_{\substack{even\\odd}\upsilon e}\left(-k_g'\right)$, respectively, integrating the resultant equation throughout the entire volume of sectoral cylindrical waveguide and using the orthogonal relationship between the vector wave functions, the coefficients $\bar{A}_{\substack{even\\odd}\upsilon h}\left(k_g\right)$ and $\bar{B}_{\substack{even\\odd}\upsilon e}\left(k_g\right)$ are

$$\bar{A}_{\substack{even\\odd}\upsilon h}\left(k_g\right)=\frac{\left(2-\delta_o\right)\kappa_h}{2\pi\phi_c k_h{}^2 I_h}\bar{M}'_{\substack{even\\odd}\upsilon h}\left(-k_g\right)\tag{3.35}$$

and

$$\bar{B}_{\substack{even\\odd}\upsilon e}\left(k_g\right)=\frac{\left(2-\delta_o\right)\kappa_e}{2\pi\phi_c k_e{}^2 I_e}\bar{N}'_{\substack{even\\odd}\upsilon e}\left(-k_g\right)\tag{3.36}$$

where

$$I_e=\int_{\rho_a}^{\rho_b}B_\upsilon^2\left(k_e\rho\right)\rho d\rho=\frac{\left(\rho_a-\rho_b\right)^2}{2k_e{}^2}\left[\frac{\partial B_\upsilon\left(k_e\rho\right)}{\partial\rho}\right]_{\rho=\rho_a-\rho_b}^2\tag{3.37}$$

and

$$I_h=\int_{\rho_a}^{\rho_b}B_\upsilon^2\left(k_h\rho\right)\rho d\rho=\frac{\left(\rho_a-\rho_b\right)^2}{2k_h{}^2}\left[k_h{}^2-\frac{\upsilon^2}{\rho^2}\right]B_\upsilon^2\left(k_h\rho\right)\tag{3.38}$$

The primed functions in (3.35), (3.36) are defined with respect to the primed variables (ρ', ϕ', z'), corresponding to the location of $\bar{R}'$. δ is the Kronecker delta function. I_e and I_h are normalization factors.

To find $\bar{\bar{G}}_{m2}$, we will expand $\bar{\bar{G}}_{m2}$ by using the same expression of source function as shown in (3.34), but the two different scalar unknown coefficients $a(k_g)$ and $b(k_g)$ as

$$\bar{\bar{G}}_{m2}\left(\bar{R},\bar{R}'\right)=\int_{-\infty}^{\infty}dh\sum_{\upsilon=0}^{\infty}\sum_{l=1}^{\infty}\frac{(2-\delta_o)}{2\pi\phi_c}\left(\frac{\kappa_h}{k_h^{\,2}I_h}a\left(k_g\right)\bar{N}_{\substack{even\\odd}\upsilon h}\left(k_g\right)\bar{M}'_{\substack{even\\odd}\upsilon h}\left(-k_g\right)\right.$$
$$\left.+\frac{\kappa_e}{k_e^{\,2}I_e}b\left(k_g\right)\bar{M}_{\substack{even\\odd}\upsilon e}\left(k_g\right)\bar{N}'_{\substack{even\\odd}\upsilon e}\left(-k_g\right)\right),\qquad \begin{matrix} z>z' \\ z<z' \end{matrix} \tag{3.39}$$

By substituting (3.39) into (3.32), we can obtain the two of scalar coefficients

$$a\left(k_g\right)=\frac{1}{\kappa_h^2-k^2} \tag{3.40}$$

and

$$b\left(k_g\right)=\frac{1}{\kappa_e^2-k^2}\ , \tag{3.41}$$

therefore, $\bar{\bar{G}}_{m2}\left(\bar{R},\bar{R}'\right)$ is given by

$$\bar{\bar{G}}_{m2}\left(\bar{R},\bar{R}'\right)=\int_{-\infty}^{\infty}dk_g\sum_{\upsilon=0}^{\infty}\sum_{l=1}^{\infty}\frac{(2-\delta_o)}{2\pi\phi_c}\left\{\frac{\kappa_h}{k_h^{\,2}I_h\left(\kappa_h^2-k^2\right)}\bar{N}_{\substack{even\\odd}\upsilon h}\left(k_g\right)\bar{M}'_{\substack{even\\odd}\upsilon h}\left(-k_g\right)\right.$$
$$\left.+\frac{\kappa_e}{k_e^2I_e\left(\kappa_e^2-k^2\right)}\bar{M}_{\substack{even\\odd}\upsilon e}\left(k_g\right)\bar{N}'_{\substack{even\\odd}\upsilon e}\left(-k_g\right)\right\},\qquad \begin{matrix} z>z' \\ z<z' \end{matrix} \tag{3.42}$$

The Fourier integration in (3.42) can be evaluated by the method of contour integration. The poles of the integrand are different for the TE modes and TM modes; they are

$$k_g = \pm\left(k^2 - k_h^{\,2}\right)^{\frac{1}{2}} = \pm k_{gh}\,. \qquad \text{for the TE modes}$$

and

$$k_g = \pm\left(k^2 - k_e^{\,2}\right)^{\frac{1}{2}} = \pm k_{ge}\,. \qquad \text{for the TM modes}$$

where k_{gh} and k_{ge} represent the guided wave numbers. The final expression for $\overline{\overline{G}}_{m2}$ is given by

$$\overline{\overline{G}}^{\pm}_{m2}\left(\bar{R},\bar{R}'\right) = \sum_{\upsilon=0}^{\infty}\sum_{l=1}^{\infty}\Bigg(A_h \bar{N}_{\substack{even\\odd}\,\upsilon h}\left(\pm k_{gh}\right)\bar{M}'_{\substack{even\\odd}\,\upsilon h}\left(\mp k_{gh}\right) + A_e \bar{M}_{\substack{even\\odd}\,\upsilon e}\left(\pm k_{ge}\right)\bar{N}'_{\substack{even\\odd}\,\upsilon e}\left(\mp k_{ge}\right)\Bigg), \quad \begin{matrix} z > z' \\ z < z' \end{matrix} \tag{3.43}$$

where

$$A_h = \frac{j(2-\delta_o)}{2\phi_c k_h^{\,2} I_h k_{gh}} \tag{3.44}$$

$$A_e = \frac{j(2-\delta_o)}{2\phi_c k_e^{\,2} I_e k_{ge}} \tag{3.45}$$

The top line applies to $z > z'$ and the bottom line for $z < z'$. At $z = z'$, the function is discontinuous. For discontinuous magnetic dyadic Green's function, we have derived the equation

$$\hat{n}\times\left(\overline{\overline{G}}^{+}_{m} - \overline{\overline{G}}^{-}_{m}\right) = \overline{\overline{I}}_s\,\delta\left(\bar{\rho}-\bar{\rho}'\right), \tag{3.46}$$

where $\overline{\overline{I}}_s$ denotes the two dimensional idem factor defined by

$$\overline{\overline{I}}_s = \overline{\overline{I}} - \hat{n}\hat{n}\,. \tag{3.47}$$

For the present problem, it becomes

$$\hat{z}\times\left(\overline{\overline{G}}^{+}_{m2} - \overline{\overline{G}}^{-}_{m2}\right) = \left(\overline{\overline{I}} - \hat{z}\hat{z}\right)\delta\left(\bar{R}-\bar{R}'\right), \tag{3.48}$$

where $\overline{\overline{G}}_{m2}^{+}$ is for $z > z'$ and $\overline{\overline{G}}_{m2}^{-}$ is for $z < z'$. The point source is located at $\bar{R}'$. Knowing $\overline{\overline{G}}_{m2}$, we can find the electric dyadic Green's function of the first kind $\overline{\overline{G}}_{e1}$ by using the relation of Dirichlet and Neumann boundary condition and the singularities of the source point in form of the Maxwell's coupled differential equation in dyadic form,

$$\nabla \times \overline{\overline{G}}_{m2}\left(\bar{R},\bar{R}'\right) = \overline{\overline{I}}\delta\left(\bar{R}-\bar{R}'\right) + k^2 \overline{\overline{G}}_{e1}\left(\bar{R},\bar{R}'\right), \tag{3.49}$$

since $\overline{\overline{G}}_{m2}$ is discontinuous at $z = z'$, we can write

$$\overline{\overline{G}}_{m2}\left(\bar{R},\bar{R}'\right) = \overline{\overline{G}}_{m2}^{+}\left(\bar{R},\bar{R}'\right)U\left(z-z'\right) + \overline{\overline{G}}_{m2}^{-}\left(\bar{R},\bar{R}'\right)U\left(z'-z\right) \tag{3.50}$$

where the unit step functions are defined by

$$\begin{aligned} U\left(z-z'\right) &= \begin{cases} 1 & ,z > z' \\ 0 & ,z < z' \end{cases} \\ U\left(z'-z\right) &= \begin{cases} 1 & ,z < z' \\ 0 & ,z > z' \end{cases} \end{aligned} \tag{3.51}$$

By substituting (3.50) into (3.49) and using dyadic vector identity

$$\nabla \times \left(a\overline{\overline{b}}\right) = a\left(\nabla \times \overline{\overline{b}}\right) + \left(\nabla a\right) \times \overline{\overline{b}}, \tag{3.52}$$

we can write (3.49) in the form

$$\begin{aligned} \nabla \times \overline{\overline{G}}_{m2}\left(\bar{R},\bar{R}'\right) = &\left[\nabla \times \overline{\overline{G}}_{m2}^{+}\left(\bar{R},\bar{R}'\right)\right]U\left(z-z'\right) + \left[\nabla \times \overline{\overline{G}}_{m2}^{-}\left(\bar{R},\bar{R}'\right)\right]U\left(z'-z\right) \\ &+ \left(\overline{\overline{I}} - \hat{z}\hat{z}\right)\delta\left(\bar{R}-\bar{R}'\right) \end{aligned} \tag{3.53}$$

where $\left(\overline{\overline{I}} - \hat{z}\hat{z}\right)\delta\left(\bar{R}-\bar{R}'\right) = -\hat{z}\hat{z}\delta\left(\rho-\rho'\right)\delta\left(\phi-\phi'\right)\delta\left(z-z'\right)$. Substituting (3.53) into (3.49) yields

$$\overline{\overline{G}}^{\pm}_{e1}\left(\bar{R},\bar{R}'\right)=-\frac{1}{k^2}\hat{z}\hat{z}\delta\left(\bar{R}-\bar{R}'\right)+\sum_{\upsilon}^{\infty}\sum_{l=1}^{\infty}\Bigg(A_h\bar{M}_{\substack{even\\odd}\upsilon h}\left(\pm k_{gh}\right)\bar{M}'_{\substack{even\\odd}\upsilon h}\left(\mp k_{gh}\right)$$

$$+A_e\bar{N}_{\substack{even\\odd}\upsilon e}\left(\pm k_{ge}\right)\bar{N}'_{\substack{even\\odd}\upsilon e}\left(\mp k_{ge}\right)\Bigg),\qquad \begin{matrix} z>z' \\ z<z' \end{matrix}. \quad (3.54)$$

The function $\overline{\overline{G}}_{e2}\left(\bar{R},\bar{R}'\right)$ for the concentric sectoral cylindrical waveguide can be found by using the symmetrical relations between $\overline{\overline{G}}_{e1}$ and $\overline{\overline{G}}_{e2}$ without going through a lengthy derivation. The result is given by

$$\overline{\overline{G}}^{\pm}_{e2}\left(\bar{R},\bar{R}'\right)=-\frac{1}{k^2}\hat{z}\hat{z}\delta\left(\bar{R}-\bar{R}'\right)+\sum_{\upsilon=0}^{\infty}\sum_{l=1}^{\infty}\Bigg(A_h\bar{N}_{\substack{even\\odd}\upsilon h}\left(\pm k_{gh}\right)\bar{N}'_{\substack{even\\odd}\upsilon h}\left(\mp k_{gh}\right)$$

$$+A_e\bar{M}_{\substack{even\\odd}\upsilon e}\left(\pm k_{ge}\right)\bar{M}'_{\substack{even\\odd}\upsilon e}\left(\mp k_{ge}\right)\Bigg),\qquad \begin{matrix} z>z' \\ z<z' \end{matrix}. \quad (3.55)$$

By definition $\nabla\times\overline{\overline{G}}_{e2}=\overline{\overline{G}}_{m1}$, thus, we can apply the same method used in deriving $\overline{\overline{G}}_{m2}$ to find

$$\overline{\overline{G}}^{\pm}_{m1}\left(\bar{R},\bar{R}'\right)=\sum_{\upsilon=0}^{\infty}\sum_{l=1}^{\infty}k\Bigg(A_h\bar{M}_{\substack{even\\odd}\upsilon h}\left(\pm k_{gh}\right)\bar{N}'_{\substack{even\\odd}\upsilon h}\left(\mp k_{gh}\right)$$

$$+A_e\bar{N}_{\substack{even\\odd}\upsilon e}\left(\pm k_{ge}\right)\bar{M}'_{\substack{even\\odd}\upsilon e}\left(\mp k_{ge}\right)\Bigg),\qquad \begin{matrix} z>z' \\ z<z' \end{matrix}. \quad (3.56)$$

The approach to derive the dyadic Green's functions for a sectoral cylindrical cavity is to start with the functions available for a sectoral cylindrical waveguide, in (3.43), (3.54), (3.55) and (3.56), with the same cross-sectional dimension and apply the method of scattering superposition to find all kinds of electric and magnetic dyadic Green's function. The procedure to accomplish it can be carried out in two steps. We consider first the functions for a semi-

infinite waveguide defined in a region $0 \le z < \infty$, terminated at $z = 0$ with a conducting wall.

To find the electric dyadic Green's function of the first kind for the semi-infinite waveguide, denoted by $\overline{\overline{G}}_{E1}$, we let

$$\overline{\overline{G}}_{E1}\left(\bar{R},\bar{R}'\right)=\overline{\overline{G}}_{e1}\left(\bar{R},\bar{R}'\right)+\overline{\overline{G}}_{es}\left(\bar{R},\bar{R}'\right), \tag{3.57}$$

where

$$\overline{\overline{G}}_{es}\left(\bar{R},\bar{R}'\right)=\sum_{\upsilon=0}^{\infty}\sum_{l=1}^{\infty}\left(-A_h\bar{M}_{\substack{even\\odd}\,\upsilon h}\left(k_{gh}\right)\bar{M}'_{\substack{even\\odd}\,\upsilon h}\left(k_{gh}\right)+A_e\bar{N}_{\substack{even\\odd}\,\upsilon e}\left(k_{ge}\right)\bar{N}'_{\substack{even\\odd}\,\upsilon e}\left(k_{ge}\right)\right),\quad \begin{matrix} z>z' \\ z<z' \end{matrix}. \tag{3.58}$$

By substituting (3.58) into (3.57), we obtain

$$\overline{\overline{G}}_{E1}\left(\bar{R},\bar{R}'\right)=-\frac{1}{k^2}\hat{z}\hat{z}\delta\left(\bar{R}-\bar{R}'\right)+\sum_{\upsilon=0}^{\infty}\sum_{l=1}^{\hbar}(-2j)\begin{cases}A_h\bar{M}_h\left(k_{gh}\right)\bar{M}'_{h,odd}\left(z\right)+jA_e\bar{N}_e\left(k_{ge}\right)\bar{N}'_{e,even}\left(z\right) & z>z'\\ A_h\bar{M}_{h,odd}\left(z\right)\bar{M}'_h\left(k_{gh}\right)+jA_e\bar{N}_{e,even}\left(z\right)\bar{N}'_e\left(k_{ge}\right) & z<z'\end{cases}, \tag{3.59}$$

where we have used a condensed notation for the functions in (3.59); they are

$$\bar{M}_h\left(k_{gh}\right)=\bar{M}_{\substack{even\\odd}\,\upsilon h}\left(k_{gh}\right) \tag{3.59a}$$

$$\bar{N}_e\left(k_{ge}\right)=\bar{N}_{\substack{even\\odd}\,\upsilon e}\left(k_{ge}\right) \tag{3.59b}$$

$$\bar{M}_{h,odd}\left(z\right)=\bar{M}_{\substack{even\\odd}\,\upsilon h,odd}\left(z\right)=\nabla\times\left[B_\upsilon\left(k_h\rho\right)\cos\left(\upsilon\phi\right)\sin\left(k_{gh}z\right)\hat{z}\right] \tag{3.59c}$$

$$\bar{N}_{e,even}(z)=\bar{N}_{\substack{even\\odd}\upsilon e,even}(z)$$

$$=\frac{1}{k}\nabla\times\nabla\times\left[B_{\upsilon}(k_e\rho)\sin(\upsilon\phi)\cos(k_{ge}z)\hat{z}\right] \quad (3.59d)$$

The functions $\bar{M}_{h,odd}(z)$ and $\bar{N}_{e,even}(z)$ are two standing wave vector wave functions for the semi-finite concentric sectoral cylindrical waveguide. Applying once more the method of scattering superposition for the sectoral cylindrical cavity of length z_d, we obtain the electrical dyadic Green's function of the first kind for the cavity given by

$$\bar{\bar{G}}_{E1}(\bar{R},\bar{R}')=-\frac{1}{k^2}\hat{z}\hat{z}\delta(\bar{R}-\bar{R}')$$
$$+\sum_{\upsilon=0}^{\infty}\sum_{l=1}^{\infty}\frac{(2-\delta_o)}{\phi_c}\left\{\frac{1}{k_h^{\,2}I_h k_{gh}\sin(k_{gh}z_d)}\begin{bmatrix}\bar{M}_{h,odd}(z_d-z)\bar{M}'_{h,odd}(z)\\ \bar{M}_{h,odd}(z)\bar{M}'_{h,odd}(z_d-z)\end{bmatrix}\right.$$
$$\left.-\frac{1}{k_e^{\,2}I_e k_{ge}\sin(k_{ge}z_d)}\begin{bmatrix}\bar{N}_{e,even}(z_d-z)\bar{N}'_{e,even}(z)\\ \bar{N}_{e,even}(z)\bar{N}'_{e,even}(z_d-z)\end{bmatrix}\right\},\quad \begin{matrix}z>z'\\ z<z'\end{matrix} \quad (3.60)$$

where the functions $\bar{M}_{h,odd}(z_d-z)$ and $\bar{N}_{e,even}(z_d-z)$ are two standing wave vector wave functions for the concentric sectoral cylindrical cavity and z_d is the length of cavity, which are given by

$$\bar{M}_{h,odd}(z_d-z)=\nabla\times\left[B_{\upsilon}(k_h\rho)\cos(\upsilon\phi)\sin k_{gh}(z_d-z)\hat{z}\right] \quad (3.61)$$

and

$$\bar{N}_{e,even}(z_d-z)=\frac{1}{k}\nabla\times\nabla\times\left[B_{\upsilon}(k_e\rho)\sin(\upsilon\phi)\cos k_{ge}(z_d-z)\hat{z}\right]. \quad (3.62)$$

In the same manner for derivation of dyadic Green's functions of concentric sectoral cylindrical waveguide, we will obtain [3-4]

$$\overline{\overline{G}}_{E'2}\left(\bar{R},\bar{R}'\right)=-\frac{1}{k^2}\hat{z}\hat{z}\delta\left(\bar{R}-\bar{R}'\right)$$
$$+\sum_{\upsilon=0}^{\infty}\sum_{l=1}^{\infty}\frac{\left(2-\delta_o\right)}{\phi_c}\left\{\frac{1}{k_h{}^2 I_h k_{gh}\sin\left(k_{gh}z_d\right)}\begin{bmatrix}\bar{N}_{h,odd}\left(z_d-z\right)\bar{N}'_{h,odd}\left(z\right)\\ \bar{N}_{h,odd}\left(z\right)\bar{N}'_{h,odd}\left(z_d-z\right)\end{bmatrix}\right.$$
$$\left.-\frac{1}{k_e{}^2 I_e k_{ge}\sin\left(k_{ge}z_d\right)}\begin{bmatrix}\bar{M}_{e,even}\left(z_d-z\right)\bar{M}'_{e,even}\left(z\right)\\ \bar{M}_{e,even}\left(z\right)\bar{M}'_{e,even}\left(z_d-z\right)\end{bmatrix}\right\}\qquad\begin{matrix},z>z'\\,z<z'\end{matrix}$$

(3.63)

$$\overline{\overline{G}}_{M'1}\left(\bar{R},\bar{R}'\right)=\sum_{\upsilon=0}^{\infty}\sum_{l=1}^{\infty}\frac{\left(2-\delta_o\right)k}{\phi_c}\left\{\frac{1}{k_h{}^2 I_h k_{gh}\sin\left(k_{gh}z_d\right)}\begin{bmatrix}\bar{M}_{h,odd}\left(z_d-z\right)\bar{N}'_{h,odd}\left(z\right)\\ \bar{M}_{h,odd}\left(z\right)\bar{N}_{h,odd}\left(z_d-z\right)\end{bmatrix}\right.$$
$$\left.-\frac{1}{k_e{}^2 I_e k_{ge}\sin\left(k_{ge}z_d\right)}\begin{bmatrix}\bar{N}_{e,even}\left(z_d-z\right)\bar{M}'_{e,even}\left(z\right)\\ \bar{N}_{e,even}\left(z\right)\bar{M}'_{e,even}\left(z_d-z\right)\end{bmatrix}\right\},\qquad\begin{matrix}z>z'\\z<z'\end{matrix}$$

(3.64)

$$\overline{\overline{G}}_{M'2}\left(\bar{R},\bar{R}'\right)=\sum_{\upsilon=0}^{\infty}\sum_{l=1}^{\infty}\frac{\left(2-\delta_o\right)k}{\phi_c}\left\{\frac{1}{k_h{}^2 I_h k_{gh}\sin\left(k_{gh}z_d\right)}\begin{bmatrix}\bar{N}_{h,odd}\left(z_d-z\right)\bar{M}'_{h,odd}\left(z\right)\\ \bar{N}_{h,odd}\left(z\right)\bar{M}_{h,odd}\left(c-z\right)\end{bmatrix}\right.$$
$$\left.-\frac{1}{k_e{}^2 I_e k_{ge}\sin\left(k_{ge}z_d\right)}\begin{bmatrix}\bar{M}_{e,even}\left(z_d-z\right)\bar{N}'_{e,even}\left(z\right)\\ \bar{M}_{e,even}\left(z\right)\bar{N}'_{e,even}\left(z_d-z\right)\end{bmatrix}\right\},\qquad\begin{matrix}z>z'\\z<z'\end{matrix}$$

(3.65)

The notations of dyadic Green's functions for general use to find electromagnetic field are $\overline{\overline{G}}_{EJ}$, $\overline{\overline{G}}_{HM}$, $\overline{\overline{G}}_{HJ}$ and $\overline{\overline{G}}_{EM}$, but solutions of dyadic Green's functions inside a concentric sectoral cylindrical cavity, which we obtain in (3.60), (3.63), (3.64) and (3.65) are $\overline{\overline{G}}_{E'1}$, $\overline{\overline{G}}_{E'2}$, $\overline{\overline{G}}_{M'1}$ and $\overline{\overline{G}}_{M'2}$, respectively. Actually, they are identical and the same meaning, $\overline{\overline{G}}_{E'1}$ is $\overline{\overline{G}}^{int}_{EJ}$, $\overline{\overline{G}}_{E'2}$ is $\overline{\overline{G}}^{int}_{HM}$, $\overline{\overline{G}}_{M'1}$ is $\overline{\overline{G}}^{int}_{EM}$ and $\overline{\overline{G}}_{M'2}$ is $\overline{\overline{G}}^{int}_{HJ}$. The first notation group is based

on the source/field components, but the second notation groups are of Tai is based on the boundary condition.

To check the convergence of the calculation, the internal dyadic Green's function of this cavity is calculated using various modes υ and l. The calculated results of four kinds of dyadic Green's function are shown in Table 3.3 where υ is obtained by $\upsilon = m\pi/\phi_c$ with the angle of sector ϕ_c equals 60°. It is found that $\overline{\overline{G}}_{HM}^{in}$ for the sectoral cylindrical cavity converges at υ = 18 and l = 6 (m =6). For $\overline{\overline{G}}_{HJ}^{in}$, its convergence is also at υ = 24 and l = 5. Next, the $\overline{\overline{G}}_{EM}^{in}$ converges at υ = 30 and l = 6. Finally, the convergence of $\overline{\overline{G}}_{EJ}^{in}$ is at υ = 39 and l = 18. However, as mentioned above, it can be shown graphically in Fig. 3.2.

Table 3.3 The calculated results of the dyadic Green's functions of the sectoral cylindrical cavity

m	$\overline{\overline{G}}_{HM}^{in}$	$\overline{\overline{G}}_{HJ}^{in}$	$\overline{\overline{G}}_{EM}^{in}$	$\overline{\overline{G}}_{EJ}^{in}$
1	1.64E-01	4097.549	-2189.07	-16002.2
2	-4.22E-05	5.36E-11	-1.23E-11	6.656114
3	4.10E-01	19066.2	-2424.2	-26495.8
4	4.013505	-7.96E-03	6.69E-04	-6.74E-01
5	-6.44E-01	-44339.1	3276.288	100417
6	-4.22E-05	-9.02E-10	2.49E-10	90.57536
7	-4.22E-05	-8.69E-10	2.47E-10	18.52563
8	-4.22E-05	-8.21E-10	2.44E-10	9.353178
9	-4.22E-05	-8.21E-10	2.43E-10	5.771267
10	-4.22E-05	-8.21E-10	2.41E-10	3.869608
11	-4.22E-05	-8.21E-10	2.41E-10	2.696299
12	-4.22E-05	-8.21E-10	2.41E-10	1.902432
13	-4.22E-05	-8.21E-10	2.41E-10	1.330931
14	-4.22E-05	-8.21E-10	2.41E-10	1.330924
15	-4.22E-05	-8.21E-10	2.41E-10	1.330922
	l = 6	l = 5	l = 6	l = 18

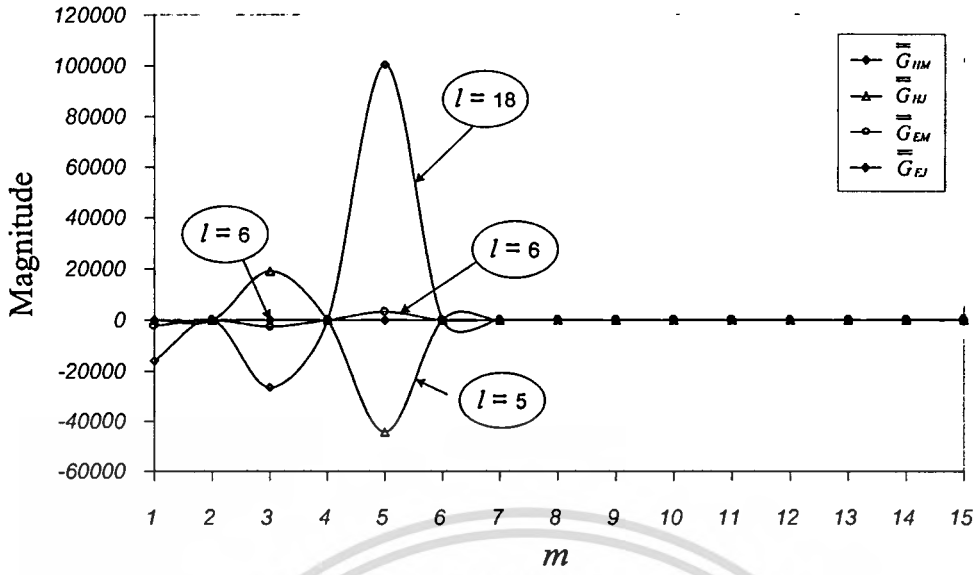

Fig.3.2 Graphical result of four kinds of dyadic Green's functions for a sectoral cylindrical cavity

3.4 Dyadic Green's Functions for External Region

Determining the electric field at P due to P' on the infinite cylindrical cavity for the outer radius, ρ_b as shown in Fig.3.2. The path of the electric field from source point presents by path t and angle θ.

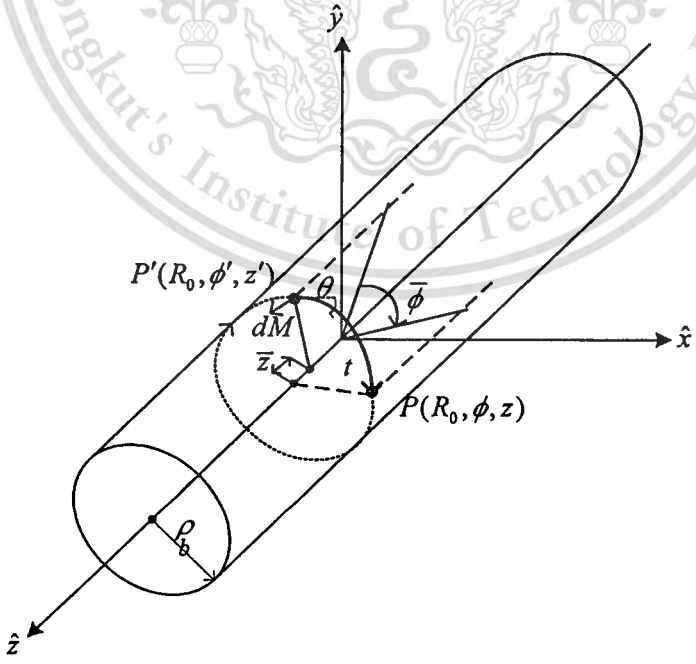

Fig.3.3 Geometry of the circular cylinder

T.S.Bird [3-5] presented the tangential magnetic field on the conducting surface of the circular cylinder at (ρ_b, ϕ, z) as follows

$$dH_s(\phi, z \mid \phi', z') = \overline{\overline{T}}(\phi, z \mid \phi', z') \cdot dM \tag{3.66}$$

where H_s denotes the tangential magnetic field at (ρ_b, ϕ, z), $\overline{\overline{T}}$ is dyadic Green's function for the magnetic field due to magnetic source. M presents the magnetic current on the conducting surface of circular cylinder.

The notations of the external electromagnetic-field magnetic-source dyadic Green's functions for general use in this thesis is $\overline{\overline{G}}_{HM}^{out}$. It is actually identical and the same meaning with $\overline{\overline{T}}$. Therefore, it can be written as

$$\overline{\overline{G}}_{HM}^{out}(\phi, z \mid \phi', z') = \left[\hat{\phi}\hat{\phi}G_{HM,\phi\phi}^{out} + \hat{\phi}\hat{z}G_{HM,\phi z}^{out} + \hat{z}\hat{\phi}G_{HM,z\phi}^{out} + \hat{z}\hat{z}G_{HM,zz}^{out}\right] = \overline{\overline{T}}(\phi, z \mid \phi', z') \tag{3.67}$$

Therefore the representation of the dyadic components, known as the modal solution, are given below:

$$\hat{\phi}\hat{\phi}G_{HM,\phi\phi}^{out} = -\hat{\phi}\hat{\phi}c_h \int_{-\infty}^{\infty} d\xi \sum_{n=-\infty}^{\infty} e^{j(n\bar{\phi}-\xi\bar{z})} \frac{k_0}{h}\left[\frac{H_n^{(2)'}(h\rho_b)}{H_n^{(2)}(h\rho_b)} - \left(\frac{n\xi}{k_0 h\rho_b}\right)^2 \cdot \frac{H_n^{(2)}(h\rho_b)}{H_n^{(2)'}(h\rho_b)}\right] \tag{3.68}$$

$$\hat{\phi}\hat{z}G_{HM,\phi z}^{out} = \hat{\phi}\hat{z}c_h \int_{-\infty}^{\infty} d\xi \sum_{n=-\infty}^{\infty} e^{j(n\bar{\phi}-\xi\bar{z})} \cdot \frac{n\xi}{k_0 h\rho_b} \frac{H_n^{(2)}(h\rho_b)}{H_n^{(2)'}(h\rho_b)} \tag{3.69}$$

$$\hat{z}\hat{\phi}G_{HM,z\phi}^{out} = \hat{\phi}\hat{z}G_{HM,\phi z}^{out} \tag{3.70}$$

$$\hat{z}\hat{z}G_{HM,zz}^{out} = \hat{z}\hat{z}c_h \int_{-\infty}^{\infty} d\xi \sum_{n=-\infty}^{\infty} e^{j(n\bar{\phi}-\xi\bar{z})} \cdot \frac{h}{k_0} \frac{H_n^{(2)}(h\rho_b)}{H_n^{(2)'}(h\rho_b)} \tag{3.71}$$

where

$$h = \begin{cases} |h| & ;|\xi| < k_0 \\ -j|h| & ;|\xi| > k_0 \end{cases}, \tag{3.72}$$

$$|h| = \sqrt{|k_0^2 - \xi^2|} \quad , \tag{3.73}$$

$$c_h = \frac{jY_0}{(2\pi)^2 \rho_b} \quad , \tag{3.74}$$

$$\overline{\phi} = \phi - \phi' \quad , \tag{3.75}$$

$$\overline{z} = z - z' \quad , \tag{3.76}$$

and $k_0 = 2\pi/\lambda_0$; $H_n^{(2)}$ is the Hankel function of second kind order n. A prime on this function denotes the first derivative with respect to the argument; λ_o and Y_o are the free-space wavelength and wave admittance, respectively.

3.5 Conclusions

The various kinds of dyadic Green's functions of a sectoral cylindrical cavity are essential to find the electromagnetic field inside this cavity, which is derived in series form, by using the eigenfunction expansions. First step, the method of magnetic dyadic Green's function is applied to find the dyadic Green's functions of both electric and magnetic types of a concentric cylindrical waveguide because the irrotational vector wave function is not necessary. The Ohm-Rayleigh method is utilized to achieve the unknown coefficients of the Green's functions. Dirichlet and Neumann boundary conditions are applied corresponding to the source and the field of the wave functions. Next step, the dyadic Green's functions for a semi-infinite waveguide were considered by modifying the original structure by terminating at z=0 with a conducting wall. Finally, the dyadic Green's functions for a concentric cylindrical cavity were obtained by terminating the remaining end of semi-infinite waveguide at z=z_d with a conducting wall.

References

[3-1] JH.Wang, *Generalized Moment Methods in Electromagnetics*, Sec.8.2, New York: Wiley and Sons. 1991.

[3-2] C.T.Tai, *Dyadic Green Function in Electromagnetic Theory*, 2nd Ed., Sec.6.2, New York: IEEE Press, 1993.

[3-3] C.A. Balanis, *Advanced Engineering Electromagnetics*, Sec.9.2, New York: Wiley and Sons. 1989.

[3-4] R.Wongsan, C.Phongcharoenpanich, and M.Krairiksh, "Electromagnetic dyadic Green's functions of a sectoral cylindrical cavity," *Proceedings of the International Forum cum Conference on Information Technology and Communication at the Dawn of the New Millennium*, Bangkok, vol.2, pp.477-486, Aug. 2000.

[3-5] T.S.Bird, "Accurate assymptotic solution for the structure field due to apertures in a conducting cylinder," *IEEE Trans Antennas Propagat.*, vol.33, no.10, pp.1108-1117, Oct.1985.

Chapter 4

Characteristics of a Slot on the Sectoral Cylindrical Cavity and its Excitation Probe by using Method of Moments

4.1 Introduction

The radiation characteristics such as radiation pattern and directivity of a slot on the sectoral cylindrical cavity and impedance characteristics of its excitation probe are investigated in this chapter. Method of Moments technique has been used to compute the magnetic current and the electric current at the aperture and the probe, respectively. Using Galerkin's technique to form simultaneous equations across the slot and on the probe, the electric field is solved. The electric field hence obtained is used to compute the radiation characteristics and impedance characteristics of the antenna.

4.2 Basis Function and Weighting Function

From the analysis model as shown in Fig.2.2, we obtain the simultaneous integral equations across the slot (2.5), and on the probe (2.11). The next step is the evaluation of the unknown magnetic current sheet and electric current density. This can be accomplished by using Method of Moments [4-1]-[4-3].

Next, by following the Method of Moments the basis and weighting functions must be appropriately selected. The basis functions are determined by taking the nature of electric field on a slot aperture. Therefore,

- The behavior of aperture electric field distribution is cosinusoidal with respect to the direction of slot length.
- The width of slot is considered because of it affects to field distribution.

In order to deal with the natures of a slot aperture, the sinusoidal entire domain basis function is appropriate because it is continuous and smooth function throughout a slot aperture. It is easy to include the higher order mode functions into the analysis. Only a few expansion terms are usually adequate to obtain the required accuracy. Accordingly, the expansion of magnetic current can be expressed as following

$$\bar{M}(\bar{R}') = \sum_{s=1}^{N_s} a_s \bar{m}_s(\bar{R}') \tag{4.1}$$

where $\bar{m}_s(\bar{R}')$ is a basis function for the slot aperture and a_s is the unknown coefficients.

For a linear excitation probe, the basis function can be written as

$$\bar{J}(\bar{R}') = \sum_{f=1}^{N_f} b_f \bar{j}_f(\bar{R}') \tag{4.2}$$

where $\bar{j}_f(\bar{R}')$ is a basis function for the probe and b_f is the unknown coefficients.

The following basis/testing functions on the slots $\hat{m}_s$ and on the feeding probe $\hat{j}_f$ are used, assuming that the slots are narrow and the probe is thin [4-4]:

$$\hat{m}_s = \hat{z}\frac{1}{w_s}\sin\frac{s\pi}{l_s}\left(z' - \frac{l_s}{2}\right), \quad s = 1,2,3,.... \tag{4.3}$$

$$\hat{j}_f = \hat{\rho}\sin\frac{f\pi}{2l_f}\left(\rho' - \rho_a + l_f\right), \quad f = 1,2,3,.... \tag{4.4}$$

where l_s and w_s, are the length and the width of slot and l_f is the length of excitation probe.

It is important to select the appropriate weighting function to obtain the high accurate result, ease of evaluation of matrix elements analytically. There are many ways to select the weighting function. However, the Galerkin's technique can be effectively responsible for these requirements. This procedure is to select the weighting function to be the same as the basis function.

4.3 Matrix Solution of the Unknown Currents

After applying the Galerkin's Method of Moments, the following linear equations for unknown coefficients a_s and b_f are obtained [4-4].

$$j\omega\varepsilon_o\sum_{s=1}^{N_s}a_s\left\{\iint_s\iint_s\hat{m}_s\cdot\left(\overline{\overline{G}}_{HM}^{in}+\overline{\overline{G}}_{HM}^{out}\right)\cdot\hat{m}_s dS_s dS_s\right\}+\sum_{f=1}^{N_f}b_f\iint_s\int_f\bar{m}_s\cdot\overline{\overline{G}}_{HJ}^{in}\cdot\bar{j}_f dL_f dS_s=0 \quad (4.5)$$

$$\sum_{s=1}^{N_s}a_s\int_f\iint_s\hat{j}_f\cdot\overline{\overline{G}}_{EM}^{in}\cdot\hat{m}_s dS_s dL_f+j\omega\mu_o\sum_{f=1}^{N_f}b_f\int_f\int_f\hat{j}_f\cdot\overline{\overline{G}}_{EJ}^{in}\cdot\hat{j}_f dL_f dL_f=1. \quad (4.6)$$

To fulfill the requirement of the integral equations for electric and magnetic fields due to the electric and magnetic current sources, we have to choose each component of dyadic Green's functions, inside and outside the sectoral cylindrical cavity described in Chapter 3, according to the positions and directions of the slot and the probe located on the cavity. These components of the dyadic Green's functions inside the cavity are

$$\hat{z}\hat{z}G_{HM,zz}^{in}=-\frac{1}{k^2\rho_b}\delta(\rho-\rho')\delta(\phi-\phi')\delta(z-z')+\hat{z}\hat{z}2j\sum_{m=1}^{\infty}\sum_{n=0}^{\infty}\frac{A_h k_h^2}{\sin(k_{gh}z_d)}B_\upsilon(k_h\rho)B_\upsilon(k_h\rho')$$
$$\times\cos(\upsilon\phi)\cos(\upsilon\phi')\begin{cases}\cos k_{gh}(z_d-z)\cos(k_{gh}z'), & z>z'\\ \cos(k_{gh}z)\cos k_{gh}(z_d-z'), & z<z'\end{cases} \quad (4.7)$$

$$\hat{z}\hat{\rho}G^{in}_{HJ,z\rho} = -\hat{z}\hat{\rho}2j\sum_{m=1}^{\infty}\sum_{n=0}^{\infty}\frac{A_h k_h^2 k\upsilon}{\rho_b' \sin\left(k_{gh}z_d\right)}B_\upsilon\left(k_h\rho\right)B_\upsilon\left(k_h\rho'\right)$$
$$\times\cos\left(\upsilon\phi\right)\sin\left(\upsilon\phi'\right)\begin{cases}\sin k_{gh}\left(z_d - z\right)\cos\left(k_{gh}z'\right), & z > z'\\ \sin\left(k_{gh}z\right)\cos k_{gh}\left(z_d - z'\right), & z < z'\end{cases} \tag{4.8}$$

$$\hat{\rho}\hat{z}G^{in}_{EM,\rho z} = -\hat{\rho}\hat{z}2j\sum_{m=1}^{\infty}\sum_{n=0}^{\infty}\frac{A_h k_h^2 k\upsilon}{\rho_b \sin\left(k_{gh}z_d\right)}B_\upsilon\left(k_h\rho\right)B_\upsilon\left(k_h\rho'\right)$$
$$\times\sin\left(\upsilon\phi\right)\cos\left(\upsilon\phi'\right)\begin{cases}\cos k_{gh}\left(z_d - z\right)\sin\left(k_{gh}z'\right), & z > z'\\ \cos\left(k_{gh}z\right)\sin k_{gh}\left(z_d - z'\right), & z < z'\end{cases} \tag{4.9}$$

$$\hat{\rho}\hat{\rho}G^{in}_{EJ,\rho\rho} = \hat{\rho}\hat{\rho}2j\sum_{m=1}^{\infty}\sum_{n=0}^{\infty}\frac{A_h \upsilon^2}{\rho_b\rho_b' \sin\left(k_{gh}z_d\right)}B_\upsilon\left(k_h\rho\right)B_\upsilon\left(k_h\rho'\right)$$
$$\times\sin\left(\upsilon\phi\right)\sin\left(\upsilon\phi'\right)\begin{cases}\sin k_{gh}\left(z_d - z\right)\sin\left(k_{gh}z'\right)\\ \sin\left(k_{gh}z\right)\sin k_{gh}\left(z_d - z'\right)\end{cases}$$
$$+\hat{\rho}\hat{\rho}2j\frac{A_e k_{ge}^2}{k^2\sin\left(k_{ge}z_d\right)}\frac{\partial B_\upsilon\left(k_e\rho\right)}{\partial\rho}\frac{\partial B_\upsilon\left(k_e\rho'\right)}{\partial\rho}$$
$$\times\sin\left(\upsilon\phi\right)\sin\left(\upsilon\phi'\right)\begin{cases}\sin k_{ge}\left(z_d - z\right)\sin\left(k_{ge}z'\right), & z > z'\\ \sin\left(k_{ge}z\right)\sin k_{ge}\left(z_d - z'\right), & z < z'\end{cases} \tag{4.10}$$

The component of dyadic Green's functions outside the sectoral cylindrical cavity is given by

$$\hat{z}\hat{z}G^{out}_{HM,zz} = \hat{z}\hat{z}c_h\int_{-\infty}^{\infty}d\xi\sum_{n=-\infty}^{\infty}e^{j(n\vec{\phi}-\xi\vec{z})}\cdot\frac{h}{k_0}\frac{H_n^{(2)}(h\rho_b)}{H_n^{(2)'}(h\rho_b)} \tag{4.11}$$

where the common parameters have been defined in Chapter 3.

The integral equations are solved by using Method of Moments and basis function with the Galerkin's method in (4.5) and (4.6), which can be converted into the matrix equation given by

$$\begin{bmatrix} Y_{ss}^{out} + Y_{ss}^{in} & \alpha_{sf}^{in} \\ \beta_{fs}^{in} & Z_{ff}^{in} \end{bmatrix} \times \begin{bmatrix} a_s \\ b_f \end{bmatrix} = \begin{bmatrix} 0 \\ 1 \end{bmatrix} \tag{4.12}$$

where $Y_{ss}^{out}, Y_{ss}^{in}, \alpha_{sf}^{in}, \beta_{fs}^{in}$, and Z_{ff}^{in} are reaction coefficients, given by

$$Y_{ss}^{out} = j\omega\varepsilon_o \iint_s \iint_s \hat{m}_s \cdot \overline{\overline{G}}_{HM}^{out} \cdot \hat{m}_s dS_s dS_s \tag{4.13}$$

$$Y_{ss}^{in} = j\omega\varepsilon_o \iint_s \iint_s \hat{m}_s \cdot \overline{\overline{G}}_{HM}^{in} \cdot \hat{m}_s dS_s dS_s \tag{4.14}$$

$$\alpha_{sf}^{in} = \iint_s \int_f \bar{m}_s \cdot \overline{\overline{G}}_{HJ}^{in} \cdot \bar{j}_f dL_f dS_s \tag{4.15}$$

$$\beta_{fs}^{in} = \int_f \iint_s \hat{j}_f \cdot \overline{\overline{G}}_{EM}^{in} \cdot \hat{m}_s dS_s dL_f \tag{4.16}$$

$$Z_{ff}^{in} = j\omega\mu_o \int_f \int_f \hat{j}_f \cdot \overline{\overline{G}}_{EJ}^{in} \cdot \hat{j}_f dL_f dL_f \tag{4.17}$$

By inverting matrix in (4.12), the unknown coefficients a_s and b_f can be obtained, then unknown currents will be solved. The antenna characteristics can be subsequently determined by using these currents.

4.4 Aperture Current Distribution of the Slot and Current Distribution on the Excitation Probe

The current on the configuration of the antenna will be divided into two parts, namely, the magnetic current across the slot and the electric current on the

probe. In case of slot, the magnetic field distribution along the length of the slot is determined to be cosine function and constant along the width, as expressed in (4.3). When the unknown coefficient, a_s, is obtained by inverting the matrix form in (4.12), the magnetic current distribution across the slot can be shown in Fig.4.1.

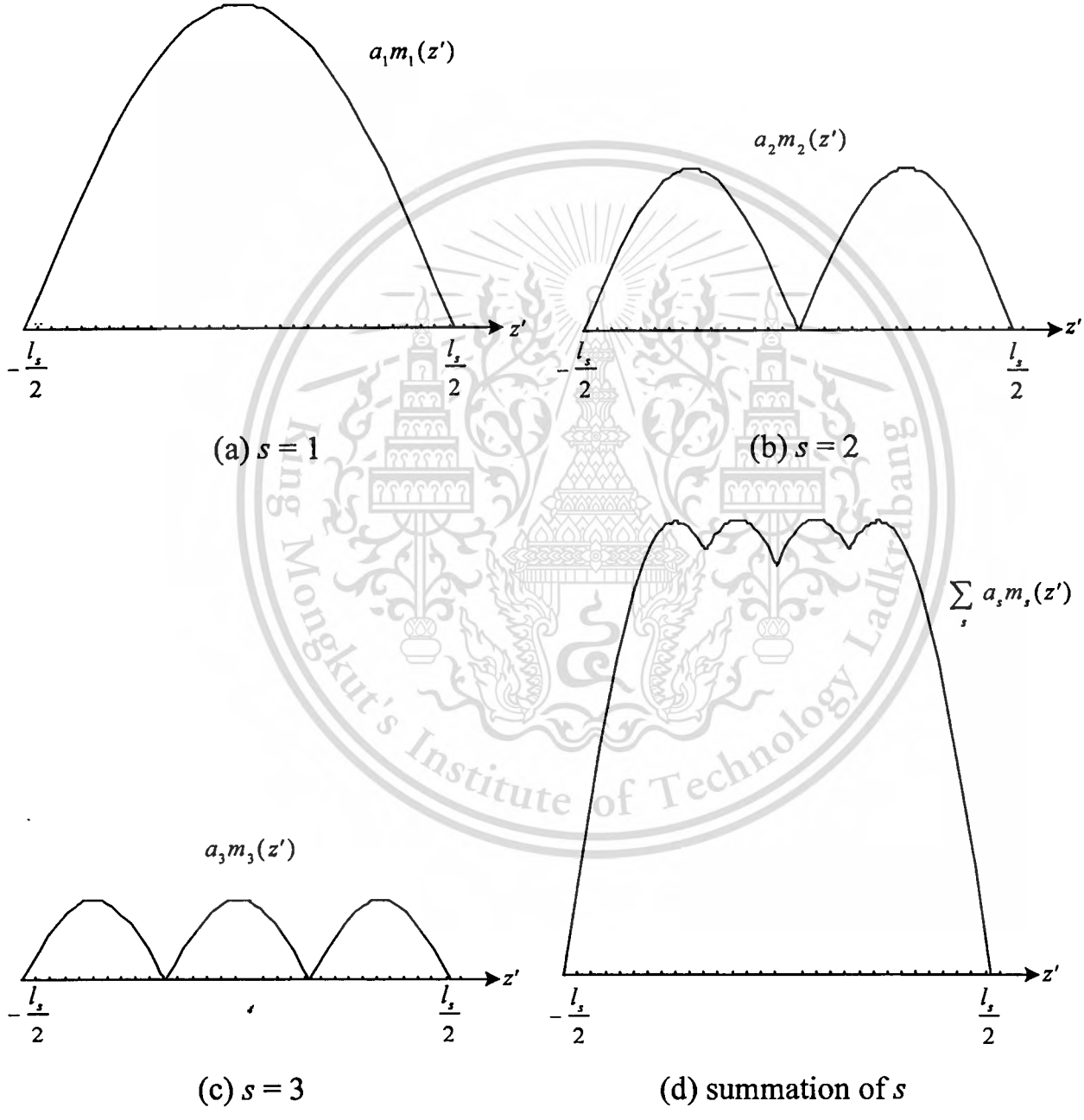

Fig.4.1 Magnetic current distributions by utilizing the basis function $\bar{m}_s(\bar{R}')$

As shown in Fig. 4.1, evidently, the basis function, which is obtained from (4.3), according to the nature of electric field on a slot aperture, that is the major term of aperture electric field distribution is cosinusoidal with respect to the z-axis [4-5]. Moreover the small numbers of basis functions yield the magnetic current density within the required accuracy [4-6].

The second part of current on antenna is the electric current density on the probe. The probe is assumed to be very thin so that the electric current distributes on the probe is sinusoidal [4-7]. Substituting unknown coefficient, b_f, into (4.2), electric current distribution on the probe can be plotted as shown in Fig.4.2.

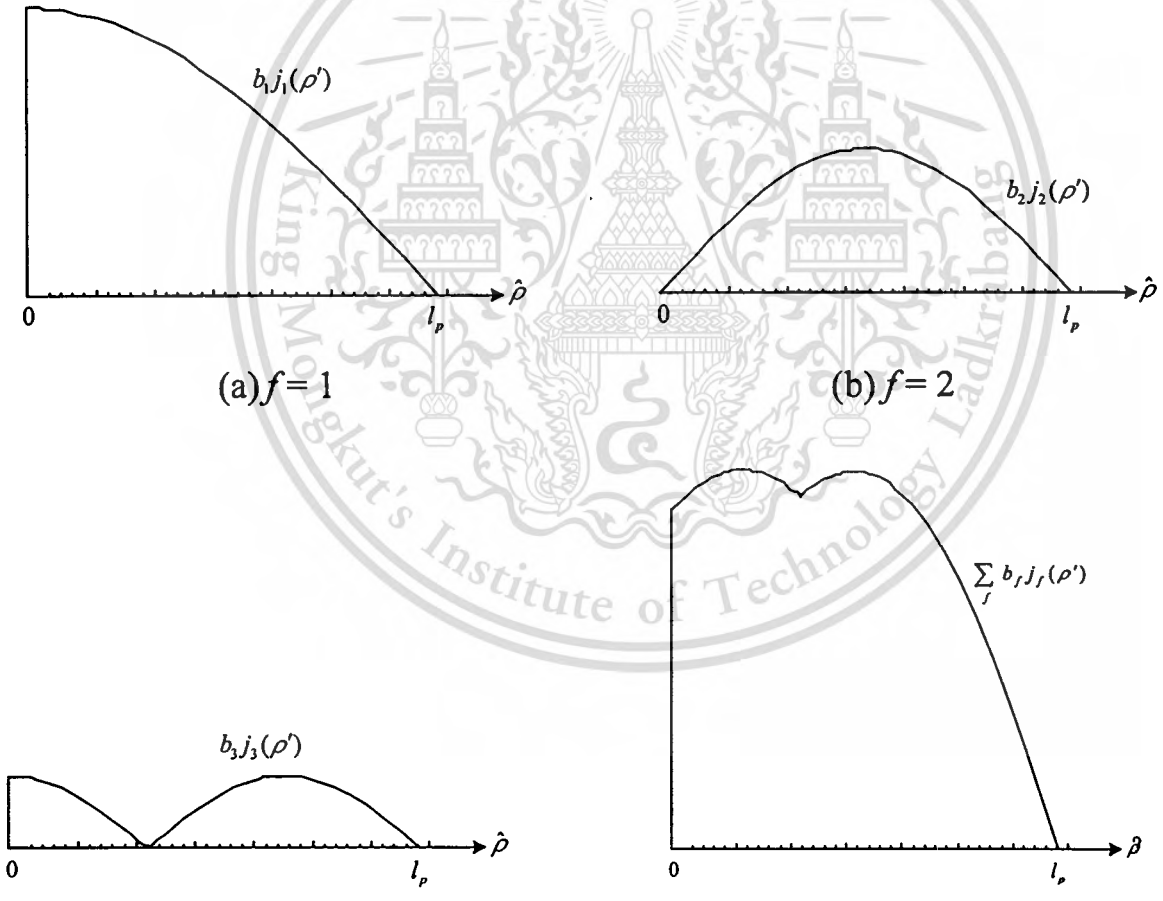

Fig.4.2 Electric current distributions by utilizing the basis function $\overline{j}_f(\overline{R}')$

From Fig.4.2, we can see that electric current density on open-end excited probe is sinusoidal with respect to the ρ-axis according to the nature of electric field on a probe. Especially, the single term basis function yields electric current distribution similar to the case of the quarter-wavelength monopole antenna. That is its electric current distribution at the end of probe is zero and electric current distribution at the feed point of probe is maximum.

4.5 Radiation Pattern, Directivity, and Impedance Characteristics of the Antenna

4.5.1 Radiation Pattern

By applying Method of Moments to solve the integral equations, the unknown coefficients of the current distribution are examined. Subsequently, the electromagnetic fields outside the sectoral cylindrical cavity-backed slot antenna can be determined by integrating the Green's functions outside the cavity, from (3.66) in Chapter 3, and the magnetic current sheet along the slot in (4.1). Therefore the actual electric field with aperture field source can be found by using the formula [4-1]

$$\overline{E}(\overline{R}) = -\iint_{S_a} \nabla \times \overline{\overline{G}}_{HM}^{out}(\overline{R},\overline{R'}) \cdot \left[\hat{n}' \times \overline{E}(\overline{R'})\right] dS' \tag{4.18}$$

or

$$\overline{E}(\overline{R}) = \iint_{S_a} \overline{\overline{G}}_{EM}^{out}(\overline{R},\overline{R'}) \cdot \overline{M}(\overline{R'}) dS' \tag{4.19}$$

In this work, the far-field expression of the actual electric fields are carried out by using (4.19) and utilizing the first kind of external magnetic dyadic Green's function $\overline{\overline{G}}_{EM}^{out}$, which can be derived from section 3.4, Chapter 3. We obtain

$$\bar{\bar{G}}_{EM}^{out}(\bar{R},\bar{R}') = \frac{e^{-jkR}}{4\pi R\sin\theta}\sum_{n=0}^{\infty}(2-\delta_0)(j)^{n+1}\begin{pmatrix}\cos\\ \sin\end{pmatrix} n\phi\Bigg\{\hat{\phi}\Bigg[\bar{N}'_{\substack{e\\ o}ns}(-k\cos\theta)+a_{\substack{e\\ o}n}\bar{N}'^{(1)}_{\substack{e\\ o}ns}(-k\cos\theta)\Bigg]$$

$$+j\hat{\theta}\Bigg[\bar{M}'_{\substack{e\\ o}ns}(-k\cos\theta)+b_{\substack{e\\ o}n}\bar{M}'^{(1)}_{\substack{e\\ o}ns}(-k\cos\theta)\Bigg]\Bigg\}. \quad (4.20)$$

Assuming the kR is large compared to unity, the Hankel function in $\bar{M}^{(1)}$ and $\bar{N}^{(1)}$, as shown in Appendix A, can be approximated by its asymptotic expression; that is,

$$H_n^{(1)}(kR) \simeq \left(\frac{2}{\pi kR}\right)^{\frac{1}{2}}(j)^{n+\frac{1}{2}}e^{-jkR}. \quad (4.21)$$

The components of electric-field magnetic-source dyadic Green's function $\bar{\bar{G}}_{EM}^{out}$ of the cylindrical cavity, in which an axial slot cut on the outer surface, are the $\hat{\phi}\hat{z}$ and $\hat{\theta}\hat{z}$ components expressed in form of the dyadic Green's function involving infinite series in (4.20), as follow

$$\hat{\phi}\hat{z}G_{EM,\phi z} = \hat{\phi}\hat{z}\frac{ke^{-jk(R-\cos\theta R'\cos\theta')}}{4\pi R}\sum_{n=1}^{\infty}(2-\delta_0)(j)^{n+1}(\cos n\phi+\sin n\phi)$$

$$\times\Bigg\{j\frac{\cos\theta}{2}(\cos\theta+\sin\theta)\Big[\big(J_{n-1}(k\sin\theta R'\sin\theta')\big)-\big(J_{n+1}(k\sin\theta R'\sin\theta')\big)$$

$$+a_{\substack{e\\ o}n}\big(H_{n-1}^{(1)}(k\sin\theta R'\sin\theta')-H_{n+1}^{(1)}(k\sin\theta R'\sin\theta')\big)\Big]$$

$$+(\cos n\phi'+\sin n\phi')(\cos\theta-\sin\theta)\Big[J_n(k\sin\theta R'\sin\theta')+a_{\substack{e\\ o}n}H_n^{(1)}(k\sin\theta R'\sin\theta')\Big]\Bigg\}$$

(4.22)

and

$$\hat{\theta}\hat{z}G_{EM,\theta z} = \hat{\theta}\hat{z}\frac{e^{-jk(R-\cos\theta R'\cos\theta')}}{4\pi R\sin\theta R'\sin\theta'}\sum_{n=1}^{\infty} n(2-\delta_0)(j)^{n+1}(\cos n\phi+\sin n\phi)$$

$$\times(\cos n\phi'-\sin n\phi')(\cos\theta+\sin\theta)\left[J_n(k\sin\theta R'\sin\theta')+b_{\substack{e\\o}n}H_n^{(1)}(k\sin\theta R'\sin\theta')\right]$$

(4.23)

Therefore, the electric field radiated from the axial slot on the sectoral cylindrical cavity as expressed in (4.19) can be written as

$$\bar{E}(\bar{R}) = \iint[G_{EM,\theta\phi'}\hat{\theta}+G_{EM,\phi\phi'}\hat{\phi}]\cdot[M_{\phi'}\hat{\phi}][\sin\theta'(R')^2]d\theta' d\phi' \tag{4.24}$$

$$\bar{E}(\bar{R}) = \bar{E}(\theta,\phi) = E_\theta\hat{\theta}+E_\phi\hat{\phi} \tag{4.25}$$

The far zone expression of radiated magnetic field, $\bar{H}(\theta,\phi)$, can also be found by using the relation of the far zone electric field, $\bar{E}(\theta,\phi)$in (4.19), that is

$$\bar{H}(\theta,\phi) = \frac{1}{\eta}\bar{E}(\theta,\phi) \tag{4.26}$$

Because of the preliminary investigations of the radiation pattern of an axial slot on the cylindrical cavity are determined by utilizing the dyadic Green's function for infinite length circular cylinder as mentioned above. Therefore, the radiation pattern is investigated as a function of the outer radius of infinite circular cylinder. The results are shown in Fig. 4.3.

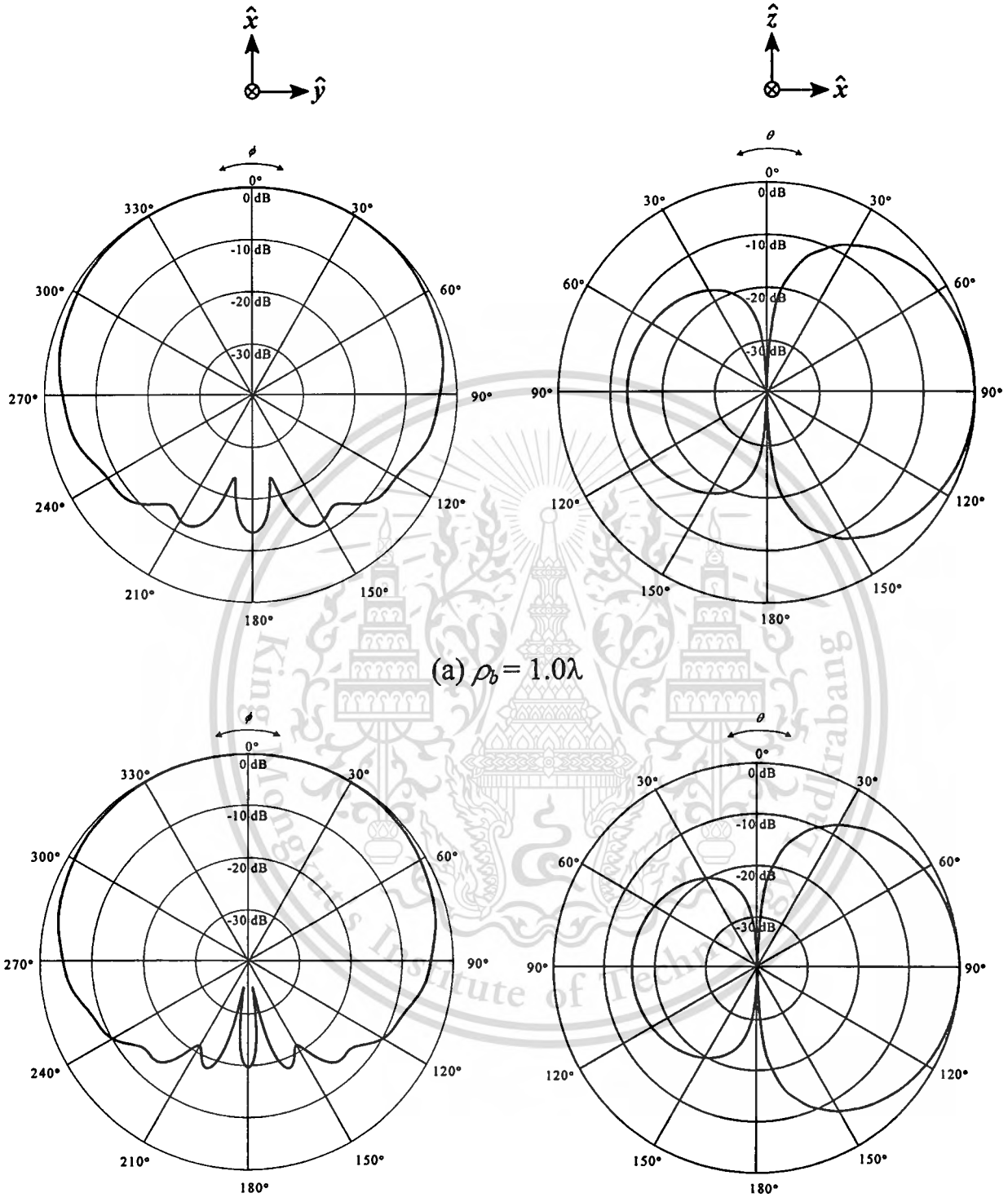

(a) $\rho_b = 1.0\lambda$

(b) $\rho_b = 1.25\lambda$

Fig. 4.3 Radiation patterns in azimuthal and elevational plane of an axial slot as a function of the outer radius

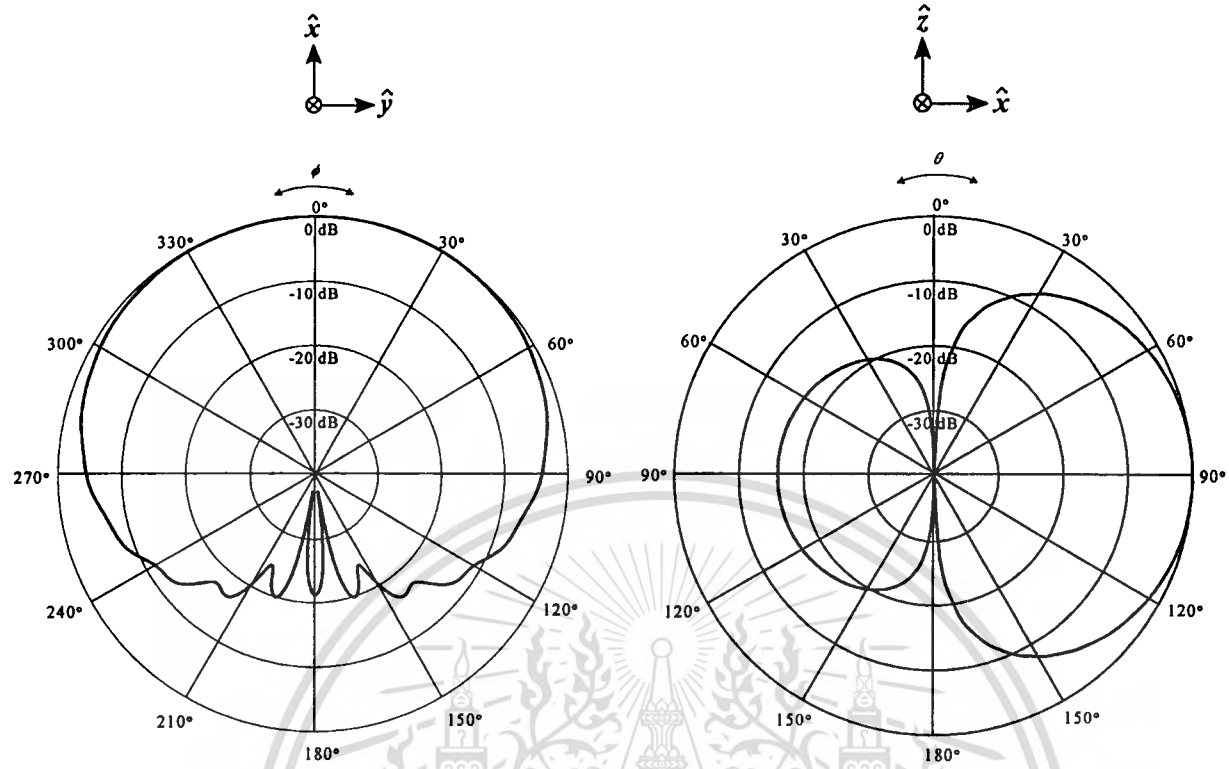

(c) $\rho_b = 1.50\lambda$

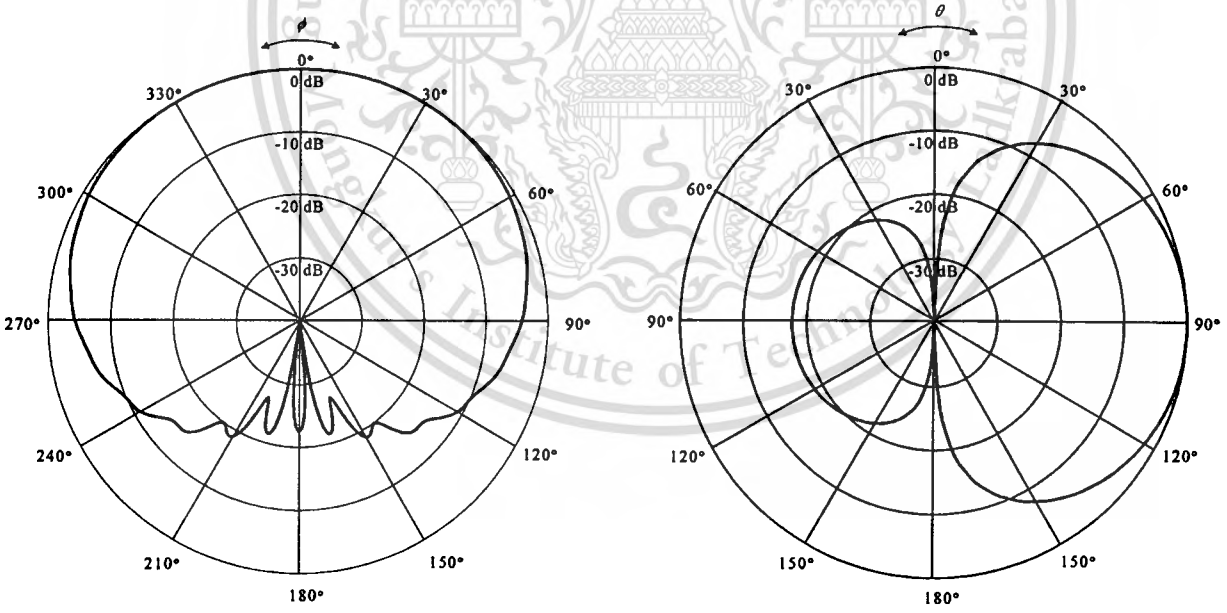

(d) $\rho_b = 1.75\lambda$

Fig. 4.3 Continued. Radiation patterns in azimuthal and elevational plane of an axial slot as a function of the outer radius

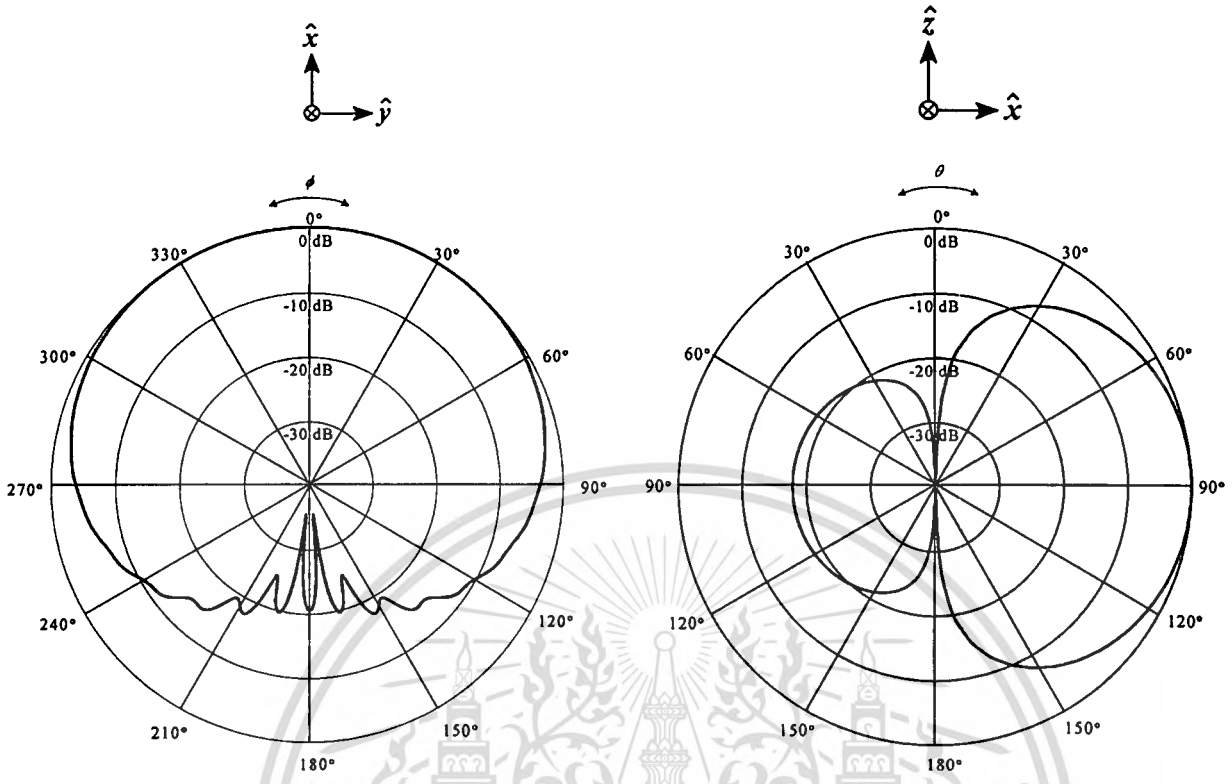

(e) $\rho_b = 2.0\lambda$

Fig. 4.3 Continued. Radiation patterns in azimuthal and elevational plane of an axial slot as a function of the outer radius

In Fig. 4.3, It is found that the back lobe is appeared in the radiation pattern with various sizes of outer radius in both azimuthal (xy) plane and elevational (xz) plane. Since the radiation patterns of the antenna are calculated by using the external dyadic Green's function for the infinite cylinder and the equivalent magnetic current. This magnetic current is calculated by using the combination of the internal dyadic Green's functions of the sectoral cylindrical cavity and the external dyadic Green's function of the infinite cylinder in the integral equations. However, it is apparent that the larger outer radius the smaller back lobe. Since the electrical characteristics of slot on the curved surface will be similar to the characteristics of slot on the plane, which cause the value of back lobe is declined.

The 3-dB beamwidth (HPBW) are also observed from these radiation patterns. We found that the 3-dB beamwidth of radiated fields, which radiated by an axial slot on the circular cylinder with various sizes of outer radius, are also slightly similar in each plane. For *xy*-plane, the HPBW is varied from 174° to 178° when outer radius is increased, while first nulls beamwidth (FNBW) is narrower. However, the HPBW for *xz*-plane with various sizes of outer radius is almost constant at about 78°, while its FNBW is constant at 180°.

4.5.2 Directivity

Directivity is another characteristic that is used to evaluate the merit of the antenna. It can be calculated as the ratio of the radiation intensity of the antenna to the radiation intensity of isotropic source [4-8]. The directivity of an axial slot on a cylindrical cavity can be estimated by using

$$\text{Directivity(dBi)} = 10\log\left|\frac{4\pi\left(\bar{E}(\theta,\phi)\big|_{\max}\right)^2}{\int_0^{2\pi}\int_0^{\pi}\left|\bar{E}(\theta,\phi)\right|^2\sin\theta\,\mathrm{d}\theta\,\mathrm{d}\phi}\right|. \tag{4.27}$$

Fig.4.4 shows the directivity of an axial slot on a sectoral cylindrical cavity as a function of various outer cylindrical radii. We found that when we adjust the radius of the cylinder the directivity is alternately changed for ρ_b = 1.0λ through 1.2λ. After that the directivity will be arisen to the maximum value at 5.277 dB for ρ_b = 1.3λ and then its values are declined and alternately changed for ρ_b = 1.4λ through 2.0λ. However, the variation of directivity for ρ_b = 1.0λ to 2.0λ has the difference of 0.078 dB or 7.8%.

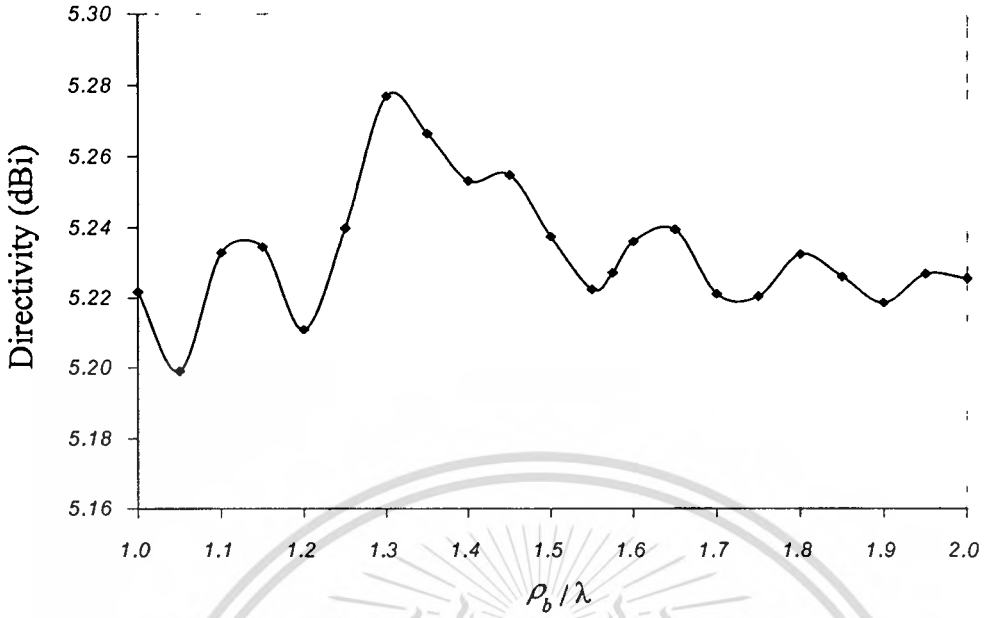

Fig. 4.4 Directivity as a function of the outer radius

4.5.3 Gain

Gain is the important performance of an antenna, which is closely related to the directivity, it is a measure that takes into account the efficiency of the antenna as well as its directional capabilities. In most case we deal with relative gain, which is defined as the ratio of the power gain in a given direction and the power gain of a reference antenna in its referenced direction. In most case, however, the reference antenna is a lossless isotropic source. Thus

$$G(\theta,\phi) = e_{cd}\left[4\pi\frac{U(\theta,\phi)}{P_{rad\partial}}\right] \tag{4.28}$$

where P_{rad} and e_{cd} are the total radiated power and the antenna radiation efficiency of a lossless isotropic source. From calculated results, the relative gain as a function of frequency is plotted in Fig. 4.5. It is found that when the frequency is increased, the gain is higher. The reason is that the dimension of the slot seems to be larger when the frequency is increased.

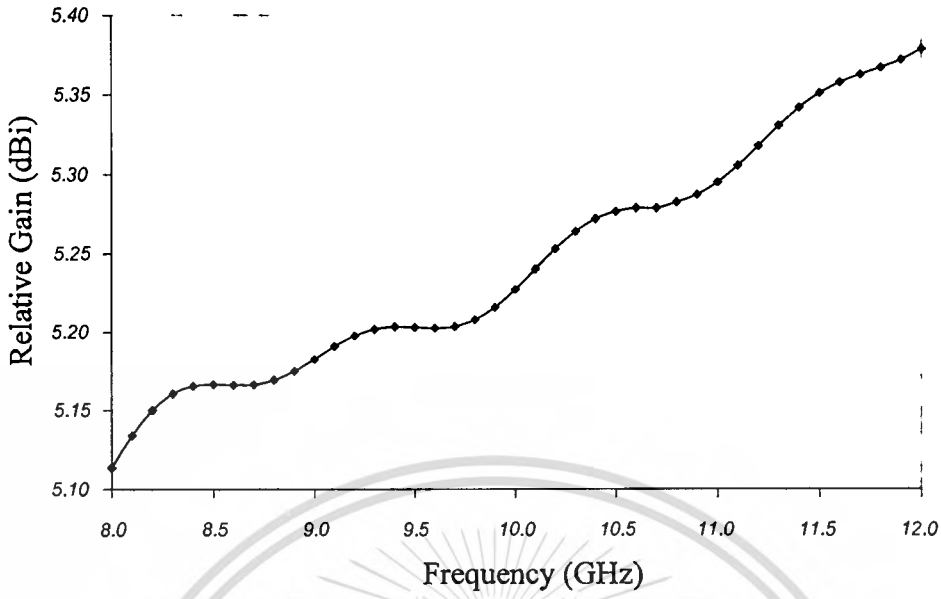

Fig. 4.5 Gain of one slot on the cavity for various frequencies

4.5.4 Front-to-Back Ratio

Front-to-back ratio is defined as the ratio of the maximum field radiated in the front side of the antenna to the maximum field radiated in the rear side of the antenna. It is desirable for the antenna to posses the high front-to-back ratio since it should radiate as less as possible in the backside. However, this circumstance is difficult to avoid since the cylindrical cavity has the finite radius. The front-to-back ratio will be infinity or there is not back lobe only if the radius of the cylinder is infinite extent that the cylindrical surface becomes the plane. The front-to-back ratio are shown with various outer radius of infinite cylinder in Fig.4.6

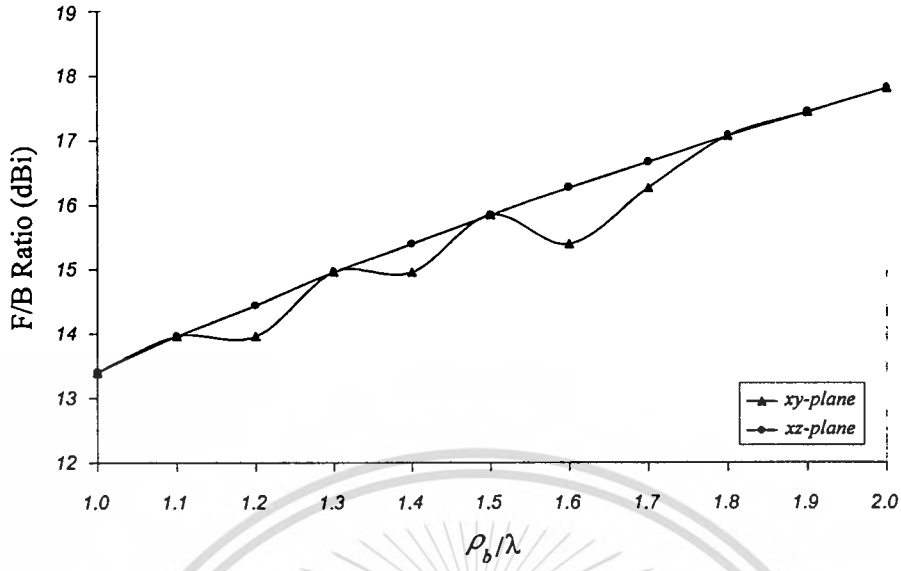

Fig.4.6 Front-to-back ratio as a function of the outer radius

From calculated results, we found that in azimuthal plane, front-to-back ratio for $\rho_b = 1.0\lambda$ through 2.0λ is not monotonic increasing. There is a fluctuation for instance, for $\rho_b = 1.1\lambda$ and 1.2λ, the values of front-to-back ratio are identical at 13.955 dB and for $\rho_b = 1.3\lambda$ and 1.4λ, their values are increased and identical at 14.958 dB. After that its value is arisen at 15.852 dB for $\rho_b = 1.5\lambda$, then declined at 15.396 dB for $\rho_b = 1.6\lambda$. Finally, front-to-back ratios for $\rho_b = 1.7\lambda$ through 2.0λ are increased continuously at 16.271, 17.072, 17.437 and 17.809 dB. In elevational plane, their values at the same conditions are gradually increased at 13.395 dB until to 17.809 dB.

4.5.5 Impedance Characteristics

The input impedance of the excited probe is obtained by using the relation of the electric voltage and current at the input terminal of antenna. That is

$$Z_{in} = \frac{V_{in}}{I_{in}} \tag{4.29}$$

where V_{in} and I_{in} present the electric voltage and current at the input terminal of antenna, respectively. By assuming the input voltage at the feed point is the delta gap, therefore, V_{in} is given to be unity.

From the electric current expansion along the probe $\bar{J}(\bar{R}')$ in term of sinusoidal basis function in (4.2) and the coefficient b_f that obtained from (4.12), the electric current distribution along the probe can be known. By choosing $\hat{j}_f$ at $\rho' = \rho_a$, the sinusoidal basis function can be written as

$$\begin{aligned}\bar{j}_f(\bar{R}') = \hat{j}_f(\rho') &= \sin\frac{f\pi}{2l_f}\left(\rho' - \rho_a + l_f\right)\Big|_{\rho'=\rho_a} \\ &= \sin\frac{f\pi}{2}\end{aligned} \tag{4.30}$$

Therefore, input current at the feed point is given by

$$I_{in} = \hat{j}_f(\rho') = \sum_{f=1}^{N_f} b_f \sin\frac{f\pi}{2} \tag{4.31}$$

Substituting (4.31) into (4.29), input impedance can be obtained as

$$Z_{in} = \frac{1}{I_{in}} = \frac{1}{\sum_{f=1}^{N_f} b_f \sin\frac{f\pi}{2}} \tag{4.32}$$

The other impedance characteristic, which is also necessary to be specified, is the reflection coefficient and the standing wave ratio. The formulations to determine the reflection coefficient and the return loss can be written as [4-8]

$$\Gamma(\text{dimensionless}) = \frac{Z_{in} - Z_o}{Z_{in} + Z_o} \tag{4.33}$$

and

$$\text{Return Loss (dB)} = -20\log\left|\Gamma(\text{dimensionless})\right|, \tag{4.34}$$

respectively, where Γ is the reflection coefficient, Z_{in} is the input impedance of the antenna and Z_o is the characteristic impedance of the transmission line.

The numerical results of impedance characteristics for various antenna parameters are obtained in this section. Since the purpose of this thesis is to realize the single element of antenna, which can be used for radiating either unidirectional or omnidirectional pattern. This antenna is designed to be multi-element, which can be combined to be the top-mounted compact circular array for yielding omnidirectional pattern in azimuthal plane. When we use the single element to be the side-mounted antenna in a desired direction, unidirectional pattern will be obtained.

Therefore, the antenna parameters that yield the desired horizontal pattern as mentioned above with the acceptable impedance characteristics are first designed. From the preliminary study [4-9]-[4-10], it is evident that the outer radius and the number of the sectors that includes a slot element are significant parameters that influence the achievable radiation pattern. Ultimately, the outer radius is selected to be 1.575λ and it is necessary to fix to this value throughout this thesis in order to accomplish the omnidirectional pattern. The number of sectors that correspond to that radius should be six. Therefore, the angle of each sector must be certainly 60°. The location of the probe excitation is at $\rho_f = \rho_a$, $\phi_f = \phi_c/2$ and $z_f = z_d/2$ that is at the center of the sectoral cylindrical cavity to accomplish the dominant propagation mode for transverse electric (TE_{10}) and symmetrical coupling. The radiated slot is initially located at 15° and assumed to be half-wavelength slot. The operating

frequency of 10 GHz is selected corresponding to the available equipment in the Wireless Communication Laboratory. Therefore, the numerical results are carried out at this frequency that is coincided with the experiment in the succeeding section. The frequency is also varied from 8.0 to 12.0 GHz to observe the frequency response of the input impedance characteristics. Not only the input impedance are illustrated, but also the return loss is also calculated to express the matching condition between the antenna and the 50Ω-transmission line.

a) Cavity length

The length of the sectoral cylindrical cavity is the first parameter to characterize the impedance characteristics. The cavity length is varied from 1.1λ to 1.5λ while other parameters are fixed at ρ_a=1.050λ, ρ_b=1.575λ, ϕ_c=60°, ϕ_s=15°, z_s=$0.5z_d$, ϕ_f=30°, z_f=$0.5z_d$, l_s=0.5λ, w_s=0.03λ and l_f=0.25λ. The numerical results of the input impedance and the return loss as a function of the frequency are plotted as shown in Fig. 4.7(a) and Fig. 4.7(b), respectively. From Fig. 4.7(a), it is obvious that the larger the cavity, the larger the resistance and the reactance. For the resonant frequency observed from the zero reactance, it can be seen that the resonant frequency will be higher when the cavity length is shortened. The resonant frequency of 10 GHz is realized when cavity length is 1.3λ, which yields the values of resistance and reactance are around 42 Ω and ±20 Ω, respectively. Furthermore, the return loss for different cavity lengths is illustrated in Fig. 4.7(b). The minimum level of the return loss of –46 dB is accomplished with the desired frequency of 10 GHz. It is shown that the antenna is matched to transmission line when the cavity length is 1.3λ. Therefore, this value of cavity length will be used as the designed parameter.

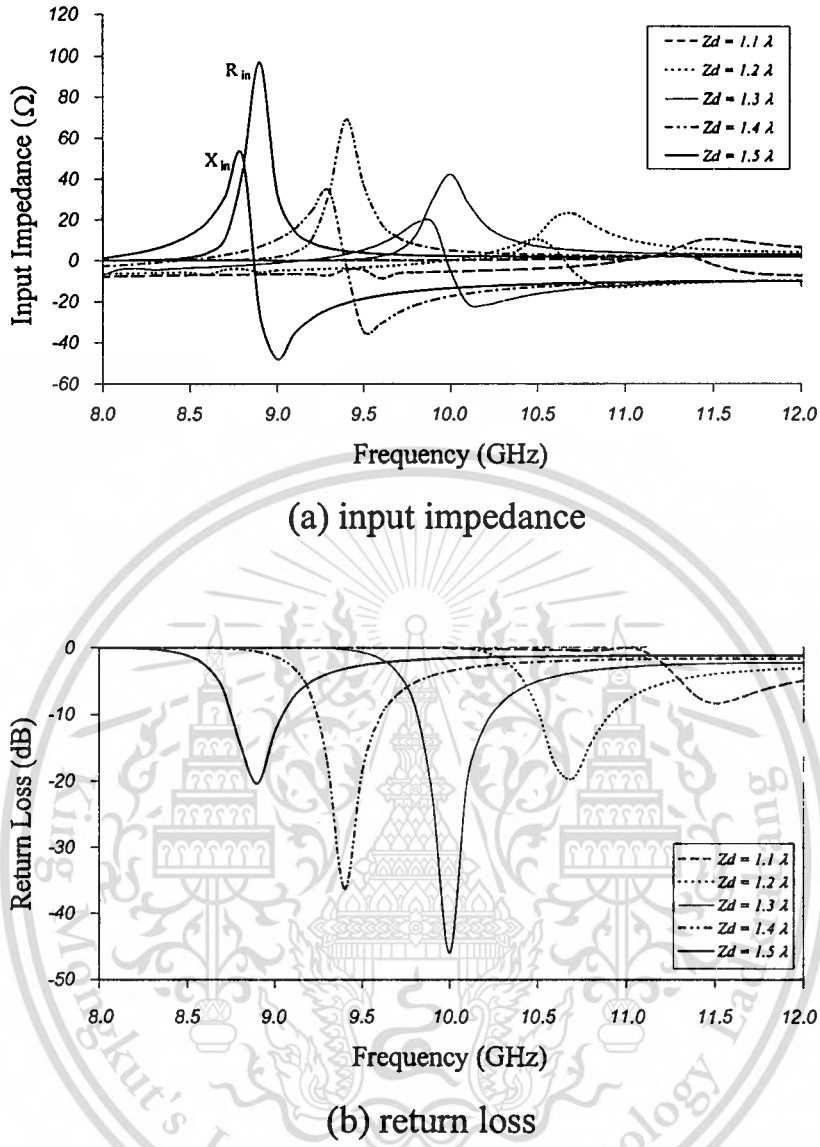

Fig. 4.7 Impedance characteristics for various cavity lengths

b) Cavity radius ratio

The ratio of the outer to inner sectoral cylindrical radii is another parameter to investigate the impedance characteristics. Since the outer radius of the cavity has to be fixed to be 1.575λ due to the achievable radiation characteristics, the inner radius will be changed to vary the ratio of the radius between 1.3 to 1.6. The cavity length of 1.3λ is chosen. The other parameters are the same as previously mentioned in the preceding section. The numerical results of the input impedance

and the return loss for the different ratios are displayed in Fig.4.8(a) through Fig.4.8(c). It is apparent that value of the nominal resistance and reactance is larger and the resonant frequency is higher when the ratio is lessen. The values of the input resistance are closed to 50 Ω when the ratio of the radius equal to 1.4 and 1.5,which their input resistance are 42 Ω and 52.4 Ω, respectively. However, the variation of the resonant frequency is little when adjusting the ratio of the sectoral cylindrical cavity. For the return loss, the frequency that gives the well matching condition is almost identical for different ratios. However, the level of the return loss is minimum at the expense of the bandwidth degradation when the ratio is 1.4. To compromise between the level of the return loss and the frequency bandwidth, the ratio of 1.5 is appropriately chosen, which also yields the values of resistance and reactance are around 42 Ω and ±20 Ω, respectively.

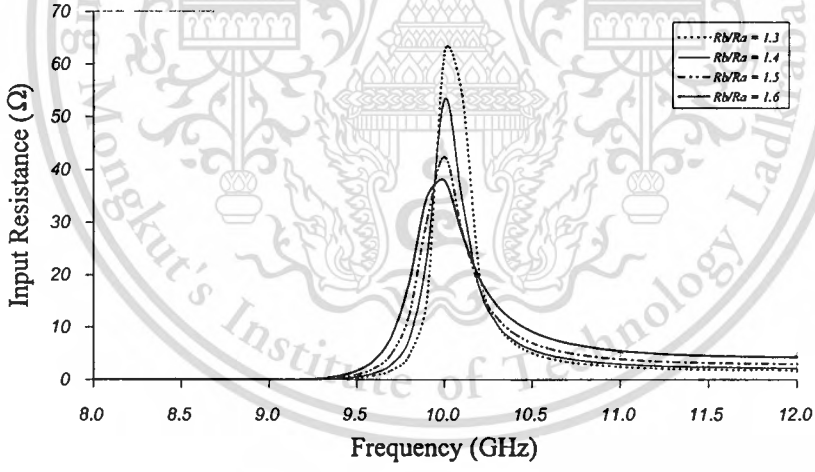

(a) input resistance

Fig. 4.8 Impedance characteristics for various cavity radius ratios

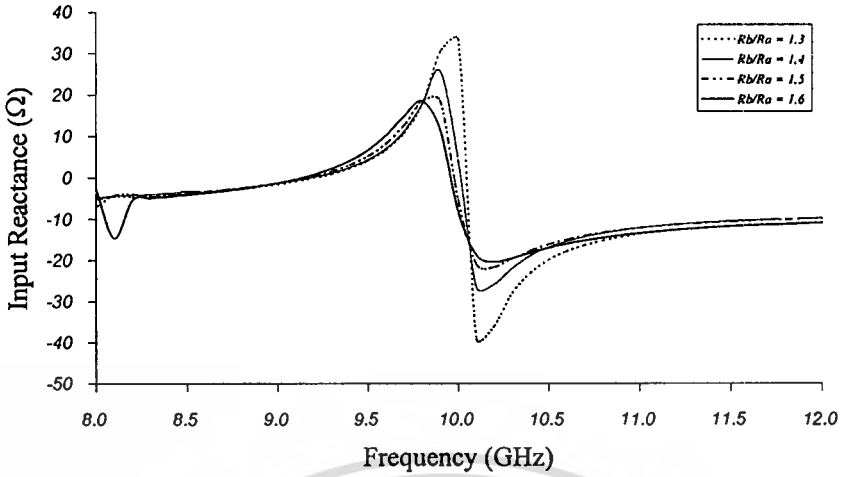

(b) input reactance

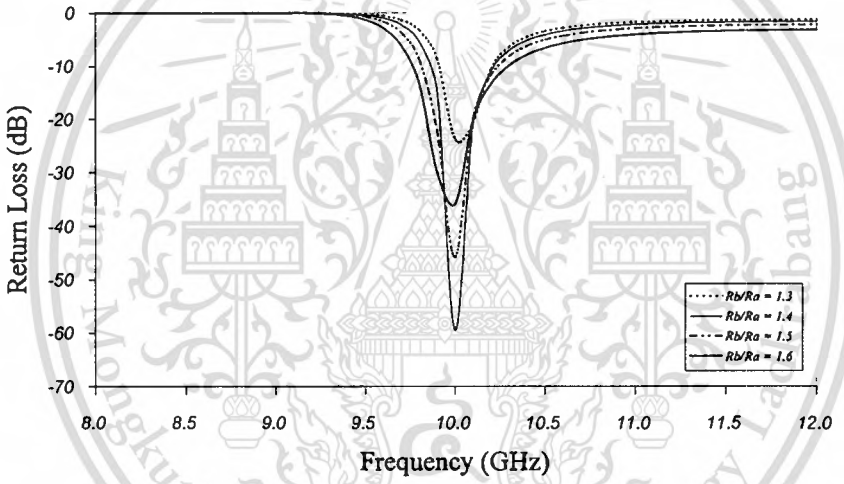

(c) return loss

Fig. 4.8 Continued. Impedance characteristics for various cavity radius ratios

c) Slot location in ϕ direction

The location of the slot on the sectoral cylindrical cavity is an important parameter to be considered in the antenna design. The slot is cut at the outer surface of the sectoral cylindrical cavity. The orientation in z direction is fixed at the center in order to obtain the symmetrically vertical pattern. The parameter that

c) Slot location in ϕ direction

The location of the slot on the sectoral cylindrical cavity is an important parameter to be considered in the antenna design. The slot is cut at the outer surface of the sectoral cylindrical cavity. The orientation in z direction is fixed at the center in order to obtain the symmetrically vertical pattern. The parameter that can be varied is the angle of the slot in azimuth (ϕ direction). Fig. 4.9(a) through Fig. 4.9(c) shows the input impedance and return loss as the function of the frequency for various slot angles. It is noted that the configuration of the sectoral cylindrical cavity is similar to the configuration of the rectangular cavity and we found that the equivalent magnetic current density is zero when the slot is at the centerline of the cavity. Therefore, the slot at the centerline (ϕ_s=30°) of the cavity is non-radiating slot. To realize the radiating slot, the location of each slot should be offset from this centerline. The location of the slot in ϕ direction is varied at 7.5°, 15.0° and 22.5°. For the slot orientation between 30° and 60°, the locations are symmetrical with the slot between 0° and 30°. Thus, the impedance are identical. From Fig.4.9, it is evident that when the angle is further increased with respect to the centerline, the resonant frequency is higher. The positions of the slot that give very good matching condition at frequency 10 GHz, are located at the angles of 7.5° and 15.0° offset from centerline. To compromise between the level of the return loss and the frequency bandwidth, the acceptable bandwidth at–10 dB-return loss will be considered. It is obvious that the slot at the angle of 15° gives the wider bandwidth than the slot at the angle of 7.5°. Therefore, the ϕ_s=15° is selected, which also yields the values of resistance and reactance are around 42 Ω and ±20 Ω, respectively.

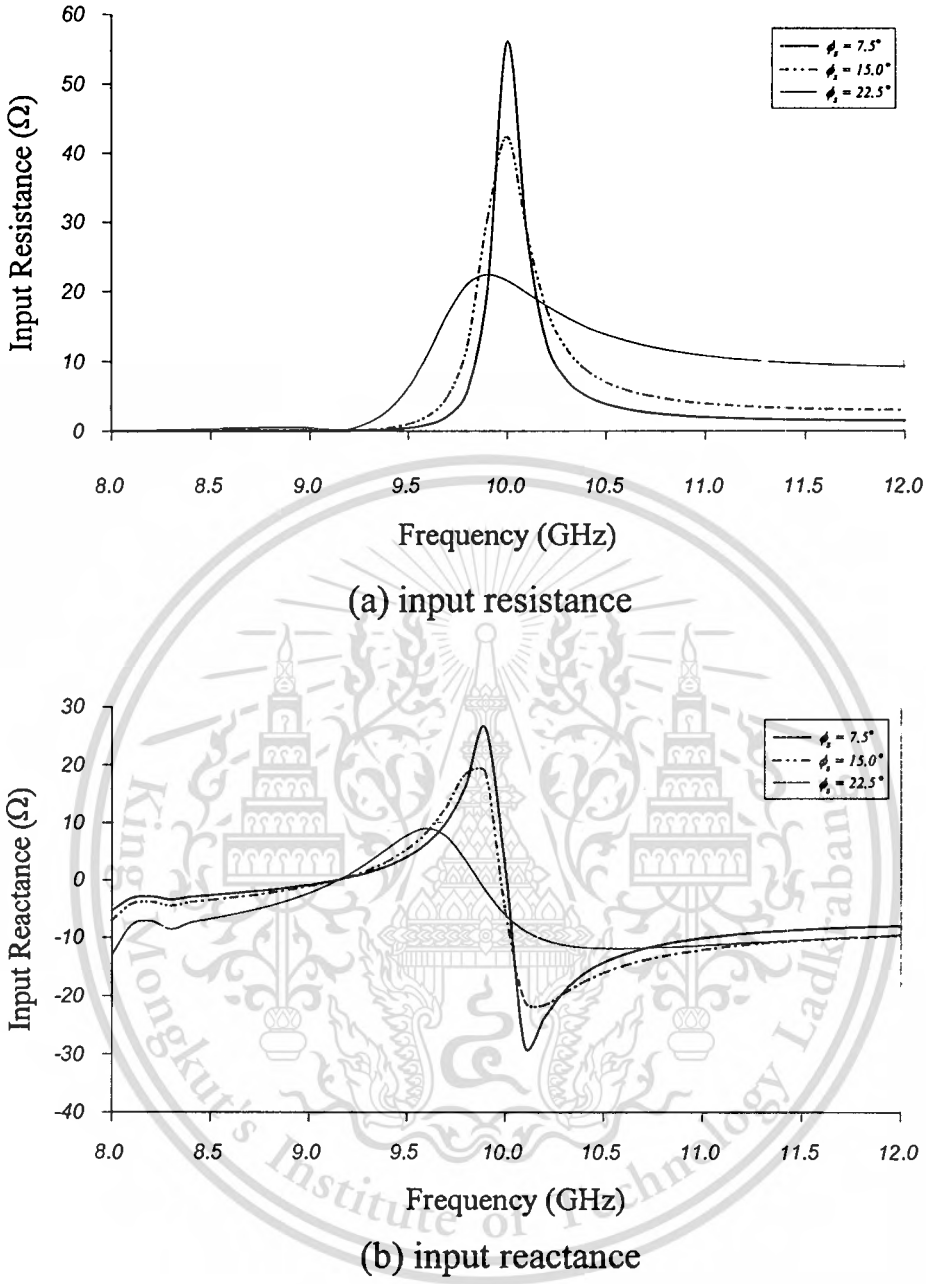

Fig.4.9 Impedance characteristics for various slot angles

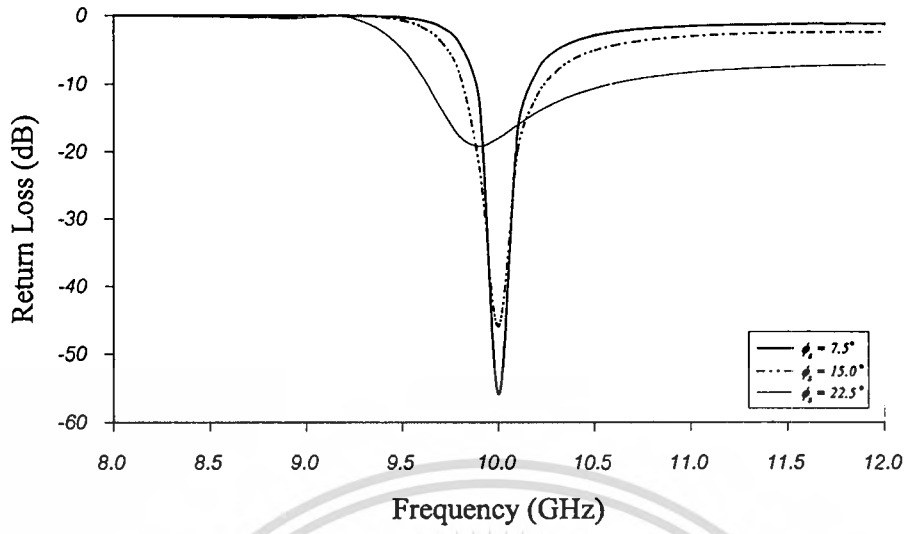

(c) return loss

Fig.4.9 Continued. Impedance characteristics for various slot angles

d) Slot length

Fig. 4.10(a) through Fig. 4.10(c) illustrates the input impedance and return loss for slot length variation. It can be inspected that when the slot length is longer the results of resistance and reactance are smaller. In each slot length, the resonant frequencies occur twice. When the slot length is longer, the lower resonant frequency will be higher whereas the upper resonant frequency will be lower. However, the frequency of the good matching condition is increased by decreasing the length of the slot. It is found that the slot length that yields the best matching situation is 0.50λ, which also yields the values of resistance and reactance are around 42 Ω and $\pm 20\,\Omega$, respectively. This parameter is used as the design parameter.

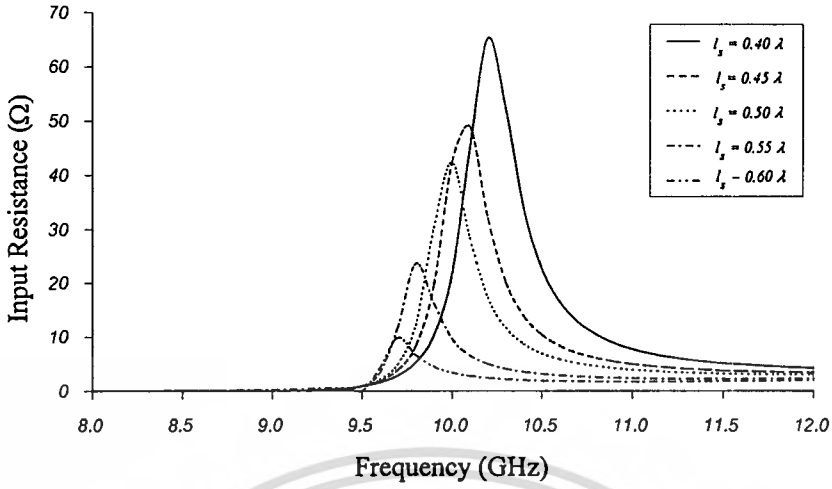

(a) input resistance

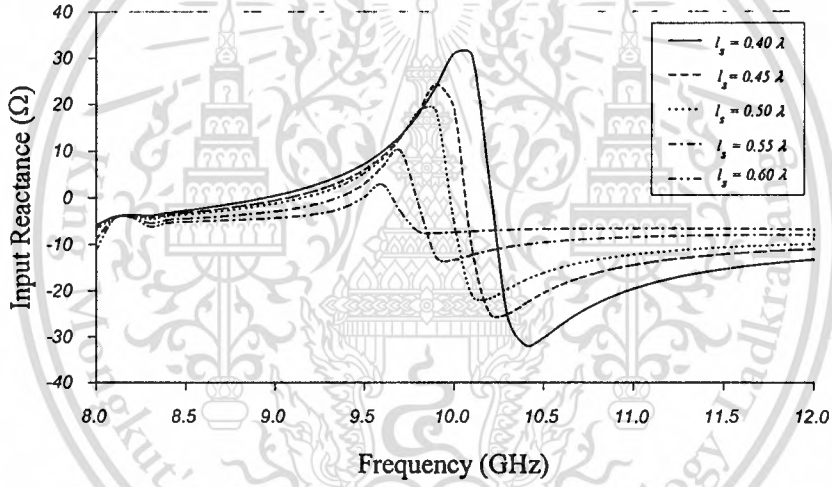

(b) input reactance

Fig.4.10 Impedance characteristics for various slot lengths

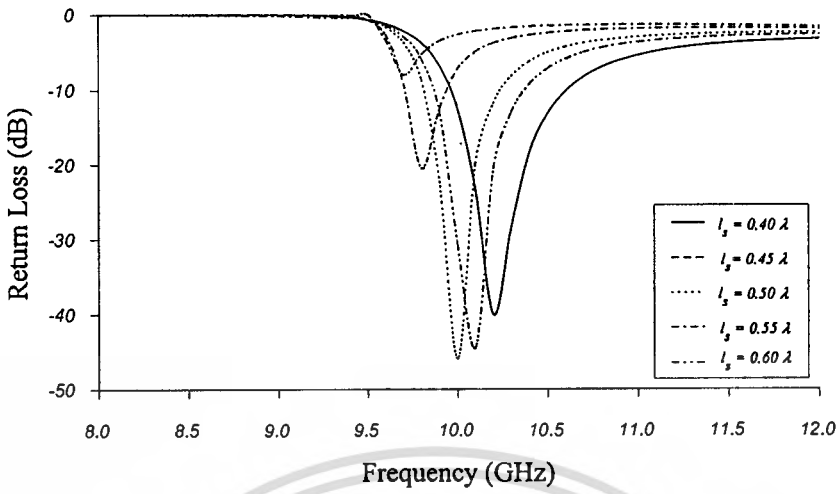

(c) return loss

Fig.4.10 Continued. Impedance characteristics for various slot lengths

e) Probe length

The length of the probe is varied from 0.24λ to 0.30λ. The impedance and the return loss are shown in Fig. 4.11(a) and Fig. 4.11(b), respectively. The longer the probe length, the larger the impedance both resistance and reactance. The frequencies of the minimum return loss for different probe lengths are slightly different. The best return loss is occurred at –54 dB when the probe length is 0.28λ, which yields the best values of resistance and reactance are around 52 Ω and ±12 Ω, respectively. Thus, this probe length is used for optimum design parameter.

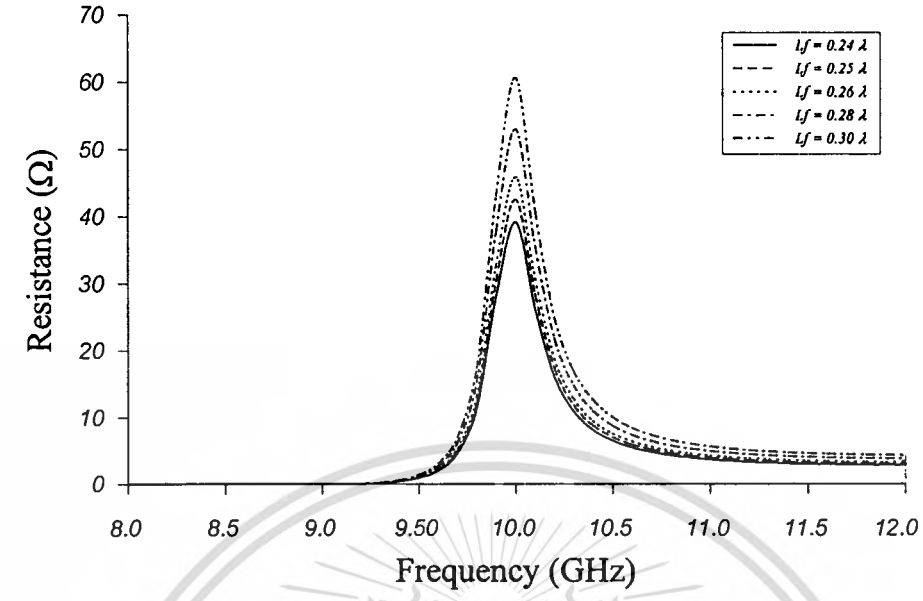

(a) input resistance

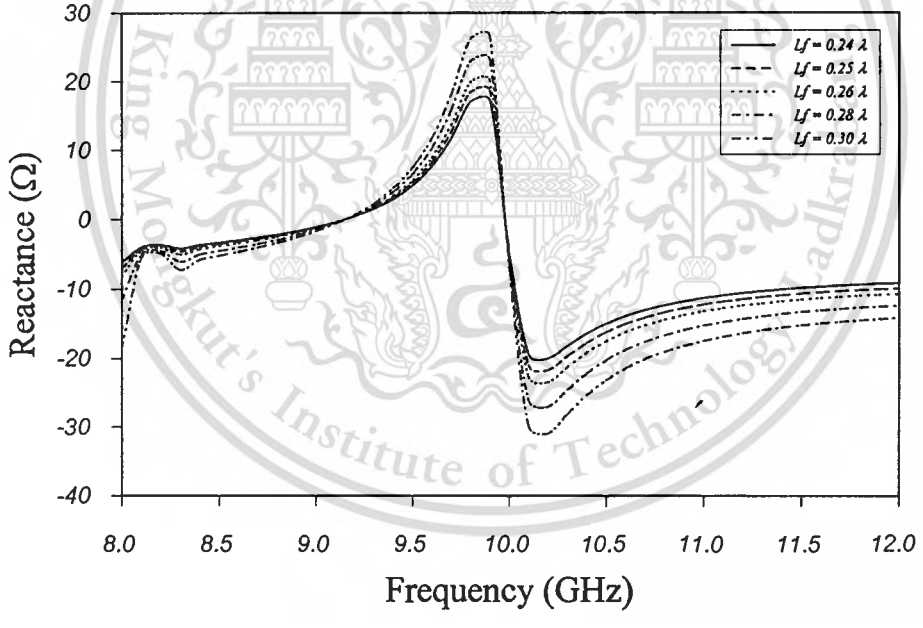

(b) input reactance

Fig.4.11 Impedance characteristics for various probe lengths

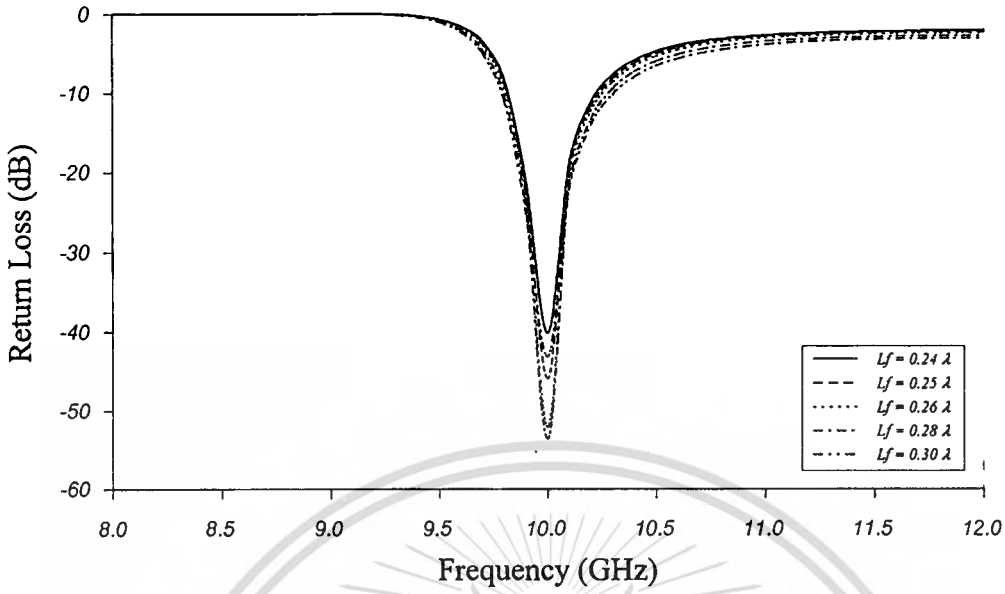

(c) return loss

Fig.4.11 Continued. Impedance characteristics for various probe lengths

4.6 Conclusions

Aperture current distribution of the slot and current distribution on the excitation probe is calculated by using Method of Moments with Galerkin's technique. Subsequently, the radiation pattern of an axial half-wavelength slot on infinite cylindrical cavity with various sizes of outer radius can be obtained. From the results, we found both in azimuthal (*xy*) plane and elevational (*xz*) plane, the radiation patterns with various sizes of outer radius are slightly different and its back lobe can be adjusted by varying the outer radius of the cavity. The directivity of the antenna is determined to fulfill the specification of the actual applications. The directivity are plotted as the functions of the outer radius of the infinite circular cylinder. Finally, the impedance characteristics of the antenna at desired resonant frequency are analyzed to clarify matching condition of the antenna when connected to the 50 Ω-transmission line. The matching condition can be improved by adjusting the cavity length, cavity radius ratio, slot location, slot length, and

probe length. According to the results of the analysis, the antenna with the acceptable properties can be designed. The experimental verification will be presented in Chapter 6.

References

[4-1] C.T.Tai, *Dyadic Green Function in Electromagnetic Theory*, 2nd., Sec.4.3, New York: IEEE Press, 1993.

[4-2] R.F.Harrington, *Field Computation by Moment Methods*, Sec.7.2, Robert E.Krieger Publishing, Inc., 1968.

[4-3] A.R.Djordjevic and T.K.Sarkar "A theorem on the Moment Methods," *IEEE Trans. Antennas Propagat.*, vol. AP-35, no. 3, pp. 353-355, Mar. 1987.

[4-4] J.Takada, " A study of the slot design for Radial Line Slot Antennas," Sec.2.2, Doctoral Dissertation of Tokyo Institute of Technology, Dec. 1991.

[4-5] A.F.Stevenson, "Theory of Slots in Rectangular Wave-guide," J.Appl. Phys., vol.19, pp.24-38, Jan.1948.

[4-6] H.Seki, "Moment and Variational Analysis is of Slotted Waveguide Arrays and its Applications," Sec.2.4, Doctor Dissertation of Tokyo Institute of Technology, Dec.1981.

[4-7] C.A. Balanis, *Antenna Theory*, Sec.8.5, New York: John Wiley & Sons, Inc., 1997.

[4-8] *IEEE Standard Definitions Terms for Antennas*, IEEE Std 149 - 1979, published by IEEE, Inc., 1993, distributed by Wiley-Interscience.

[4-9] C.Phongcharoenpanich, P.Wounchoum, S.Kosulvit and M.Krairiksh, "A Horizontally Polarized Omnidirectional Beam Antenna using Array of Axial Slot on Cylindrical Surface," Proceedings of the 3rd International Conference on Microwave and Millimeter Wave Technology, Beijing, pp.576-579, Aug. 2002.

[4-10]R.Wongsan, C.Phongcharoenpanich, M.Krairiksh and J.Takada, "Impedance Characteristic Analysis of an Axial Slot Antenna on a Sectoral Cylindrical Cavity Excited by a Probe using Method of Moments," *IEICE Trans. Fundamentals*, vol. E85-A, No.6, June 2003.

Chapter 5

Analysis of a Slot Array on the Sectoral Cylindrical Cavity

5.1 Introduction

In the previous chapter, the characteristics of a single slot on the sectoral cylindrical cavity were discussed and analyzed. Usually the radiation pattern of a single slot is relatively wide, and each slot provides low values of directivity (gain). In many applications it is necessary to design antennas with very directive characteristics to meet the demands of long distance communication. This can only be accomplished by assembling of radiating slots in an electrical and geometrical configuration, which is referred to as an array. In this case, the slots of an array are identical because of convenience, simple and more practical. The total fields of the array for vertical and horizontal polarization are determined by using the scattering vector superposition of the fields radiated by the individual slots. Finally, the another radiation characteristics and impedance characteristics of antenna can be found by using the procedures as described in Chapter 4.

5.2 Formulation of a Slot Array on the Sectoral Cylindrical Cavity

This section generally presents the formulation of a slot array on the sectoral cylindrical cavity, which can be used for either an axial slot array or a circumferential slot array on the sectoral cylindrical cavity. For the ith slot, the equivalent magnetic currents above and below aperture are denoted as $\bar{M}_i$ and $-\bar{M}_i$, respectively. By enforcing the continuity of the tangential magnetic fields across all slots on outer radius of cavity and tangential electric fields on an excited probe inside the cavity, which can be represented by $\bar{J}$ we obtain the integral equations satisfied by the equivalent magnetic current $\bar{M}_i$ and electric current $\bar{J}$ as

$$\sum_{i=1}^{n}\left[j\omega\varepsilon_0 \iint_{s_s}\left\{\bar{\bar{G}}_{HM}^{in}(\bar{R},\bar{R}')+\bar{\bar{G}}_{HM}^{out}(\bar{R},\bar{R}')\right\}\cdot\bar{M}_i(\bar{R}')dS' + \int_{L_f}\bar{\bar{G}}_{HJ}^{in}(\bar{R},\bar{R}')\cdot\bar{J}(\bar{R}')dL' \right]=0 \tag{5.1}$$

$$\sum_{i=1}^{n}\left[\iint_{S_s}\bar{\bar{G}}_{EM}^{in}\left(\bar{R},\bar{R}'\right)\cdot\bar{M}_i\left(\bar{R}'\right)dS' + j\omega\mu_0 \iint_{L_f}\bar{\bar{G}}_{EJ}^{in}\left(\bar{R},\bar{R}'\right)\cdot\bar{J}\left(\bar{R}'\right)dS' \right]=\delta\left(\bar{R}'\right). \tag{5.2}$$

To seek a numerical solution of (5.1) and (5.2), each equivalent magnetic current is expanded by using the sinusoidal entire domain basis functions.

$$\bar{M}_j\left(\bar{R}'\right)=\sum_{s=1}^{N_j}a_{sj}\bar{m}_{sj}\left(\bar{R}'\right) \tag{5.3}$$

where subscript j denotes the jth slot and $\bar{m}_{sj}\left(\bar{R}'\right)$ can be written in form

$$\hat{m}_{sj}=\hat{\zeta}_{sj}\frac{1}{w_{sj}}\sin\frac{s\pi}{l_{sj}}\left(\zeta_{sj}'+\frac{l_{sj}}{2}\right), \qquad \begin{matrix} s=1,2,3,...,N_j \\ j=1,2,3,...,n \end{matrix}, \tag{5.4}$$

where $\hat{\zeta}_{sj}$ is unit vector in direction of the slot length. While w_{sj} and l_{sj} present the width and the length, respectively.

Applying Galerkin's procedure, the integral equations can be converted into the matrix equation given by

$$\begin{bmatrix} Y_{sisj}^{out,ij}+Y_{sisj}^{in,ij} & \alpha_{sif}^{in,i} \\ \beta_{fsj}^{in,j} & Z_{ff}^{in} \end{bmatrix}\times\begin{bmatrix} a_{sj} \\ b_f \end{bmatrix}=\begin{bmatrix} 0 \\ 1 \end{bmatrix}, \tag{5.5}$$

where $Y_{sisj}^{out,ij}$, $Y_{sisj}^{in,ij}$, $\alpha_{sif}^{in,i}$, $\beta_{fsj}^{in,j}$, and Z_{ff}^{in} are the general reaction coefficients, given by

$$Y_{sisj}^{out,ij}=j\omega\varepsilon_o\iint_{si}\iint_{sj}\hat{m}_{si}\cdot\bar{\bar{G}}_{HM}^{out}\cdot\hat{m}_{sj}dS_{si}dS_{sj} \tag{5.6}$$

$$Y_{sisj}^{in,ij} = j\omega\varepsilon_o \iint_{si} \iint_{sj} \hat{m}_{si} \cdot \overline{\overline{G}}_{HM}^{in} \cdot \hat{m}_{sj} dS_{si} dS_{sj} \tag{5.7}$$

$$\alpha_{sif}^{in,i} = \iint_{si} \int_{f} \overline{m}_{si} \cdot \overline{\overline{G}}_{HJ}^{in} \cdot \overline{j}_f dL_f dS_{si} \tag{5.8}$$

$$\beta_{fsj}^{in,j} = \int_{f} \iint_{sj} \hat{j}_f \cdot \overline{\overline{G}}_{EM}^{in} \cdot \hat{m}_{sj} dS_{sj} dL_f \tag{5.9}$$

$$Z_{ff}^{in} = j\omega\mu_o \int_{f} \int_{f} \hat{j}_f \cdot \overline{\overline{G}}_{EJ}^{in} \cdot \hat{j}_f dL_f dL_f \tag{5.10}$$

By solving the system of linear equations (5.1) and (5.2) into the matrix form (5.5), the expansion coefficients a_{sj} and b_f are obtained, then the currents across the slots and at the probe will be solved. The antenna characteristics can be subsequently determined by using such currents.

The electric fields on each slot aperture are obtained by using the procedures from subsection 4.6.1 in Chapter 4. The total field of an array is calculated as the superposition of the radiation from all the slots. The directivity of an array can be also calculated.

The electric field expressed in (4.17) can be written in form of the electric field due to the *i*th slot as

$$\overline{E}^{i}(\overline{R}) = \int_{S_a} \overline{\overline{G}}_{EM}^{out,i}(\overline{R}_i, \overline{R}_i') \cdot \overline{M}(\overline{R}_i') dV' \qquad ,i = 1,2,3,.... \tag{5.11}$$

Therefore, the total field of array *n* slots is given by

$$\overline{E}(\overline{R}) = \sum_{i=1}^{n} \overline{E}^{i}(\overline{R}) \tag{5.12}$$

By considering the component of electric-field magnetic-source dyadic Green's function $\overline{\overline{G}}_{EM}^{out}$ of the infinite circular cylinder, in which the slots cut on the outer surface, each component is expressed in form of the dyadic Green's

function involve infinite series of Hankel's functions. Therefore, the radiation pattern of an axial slot array or a circumferential slot array, which is cut on the cylindrical cavity, will be determined as a function of the outer radius of infinite cylinder.

5.3 Analysis of a Slot Array for the Vertical Polarization

The vertical polarization can be realized by cutting slots on the outer surface of the sectoral cylindrical cavity in circumferential direction [5-1] as shown in Fig.5.1.

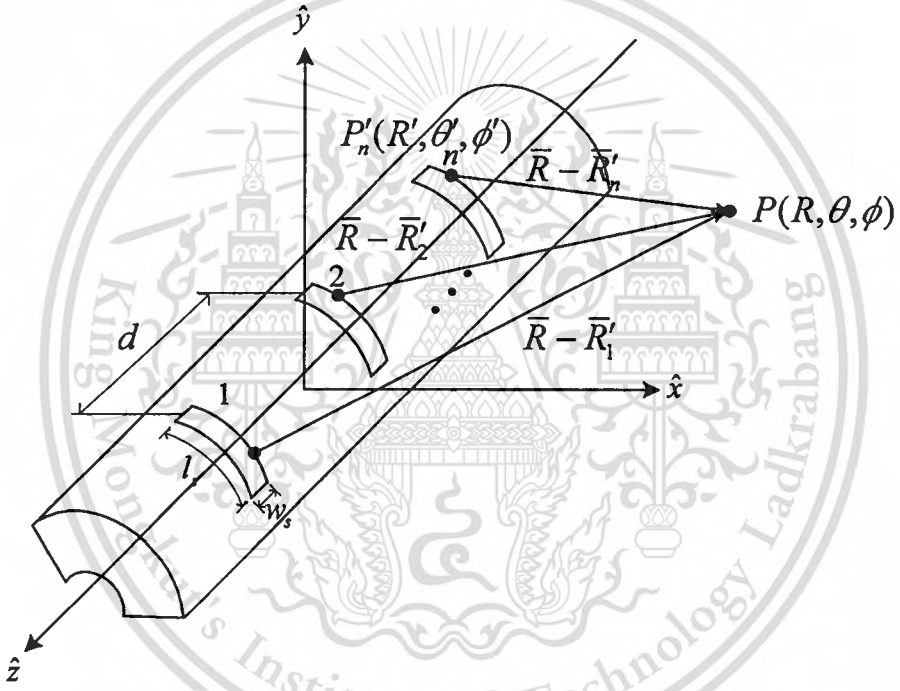

Fig.5.1 The circumferential slot array on the sectoral cylindrical cavity

The basis function for magnetic current distribution across the slots in (5.4) is modified according to the direction of slots in Fig.5.1, given by

$$\hat{m}_{sj} = \hat{\phi}_{sj} \frac{1}{w_{sj}} \sin \frac{s\pi}{l_{sj}} \left(\rho_b \phi'_{sj} + \frac{l_{sj}}{2} \right), \qquad \begin{matrix} s = 1,2,3,...,N_j \\ j = 1,2,3,...,n \end{matrix}. \tag{5.13}$$

The components of electric-field magnetic-source dyadic Green's function $\overline{\overline{G}}_{EM}^{out}$ of the cylindrical cavity, in which the circumferential slots cut on

the outer surface, are the $\hat{\theta}\hat{\phi}$ and $\hat{\phi}\hat{\phi}$ components are expressed in form of the dyadic Green's function involve infinite series, as follow

$$\hat{\theta}\hat{\phi}G^{i}_{EM,\theta\phi} = \hat{\theta}\hat{\phi}\frac{ke^{-jk(R-\cos\theta R'\cos\theta')}}{8\pi R}\sum_{n=0}^{\infty}(2-\delta_0)(j^{n+2})[\cos(n\phi)\cos(n\phi')+\sin(n\phi)\sin(n\phi')]$$
$$\left\{[J_{n-1}(kR'\sin\theta\sin\theta')-J_{n+1}(kR'\sin\theta\sin\theta')]\right.$$
$$\left.+b_{\substack{e\\o}n}[H^{(1)}_{n-1}(kR'\sin\theta\sin\theta')-H^{(1)}_{n+1}(kR'\sin\theta\sin\theta')]\right\}, \quad (5.14)$$

and

$$\hat{\phi}\hat{\phi}G^{i}_{EM,\phi\phi} = \hat{\phi}\hat{\phi}\frac{e^{-jk(R-\cos\theta R'\cos\theta')}}{4\pi RR'\tan\theta\sin\theta'}\sum_{n=0}^{\infty}(2-\delta_0)(j^{n+2})[\cos(n\phi)\sin(n\phi')-\sin(n\phi)\cos(n\phi')]$$
$$\times[J_n(kR'\sin\theta\sin\theta')+a_{\substack{e\\o}n}H^{(1)}_n(kR'\sin\theta\sin\theta')], \quad (5.15)$$

By inverting matrix in (5.5), the unknown coefficients, a_{sj} and b_f are obtained then unknown currents $\bar{M}(\bar{R}'_i)$ and $\bar{J}(\bar{R}')$ will be solved. The antenna characteristics can be subsequently determined by using these currents as described in Chapter 4.

5.3.1 Radiation Pattern of a Circumferential Slot Array

The electric field radiates from the *i*th circumferential slot on the sectoral cylindrical cavity consist of components of electric field in θ and ϕ directions, are given by

$$\bar{E}^{i}(\bar{R}) = E^{i}_{\theta}\hat{\theta}+E^{i}_{\phi}\hat{\phi} \quad . \quad (5.16)$$

which is written as

$$\bar{E}^{i}(\bar{R}) = \iint_{s_i}\left[G^{i}_{EM,\theta\phi'}\hat{\theta}+G^{i}_{EM,\phi\phi'}\hat{\phi}\right]\cdot[M''^{i}_{\phi}\hat{\phi}][\sin\theta'(R')^2]d\theta' d\phi' \quad . \quad (5.17)$$

Finally, the total electric field can be obtained by

$$E(\bar{R}) = \sum_{i=1}^{n} E^{i}(\bar{R}). \tag{5.18}$$

From the preliminary study [5.1], it was evident that the outer radius is a significant parameter that influences to the achievable radiation pattern. Therefore, the optimum value of outer radius as described in chapter 4 is selected to be 1.575λ. The radiation pattern of two circumferential slots array on the infinite circular cylinder is preliminary investigated as a function of element spacing (d) between slots of 0.233λ, 0.466λ, 0.7λ, and 0.933λ, respectively. The results have been shown in Fig. 5.2.

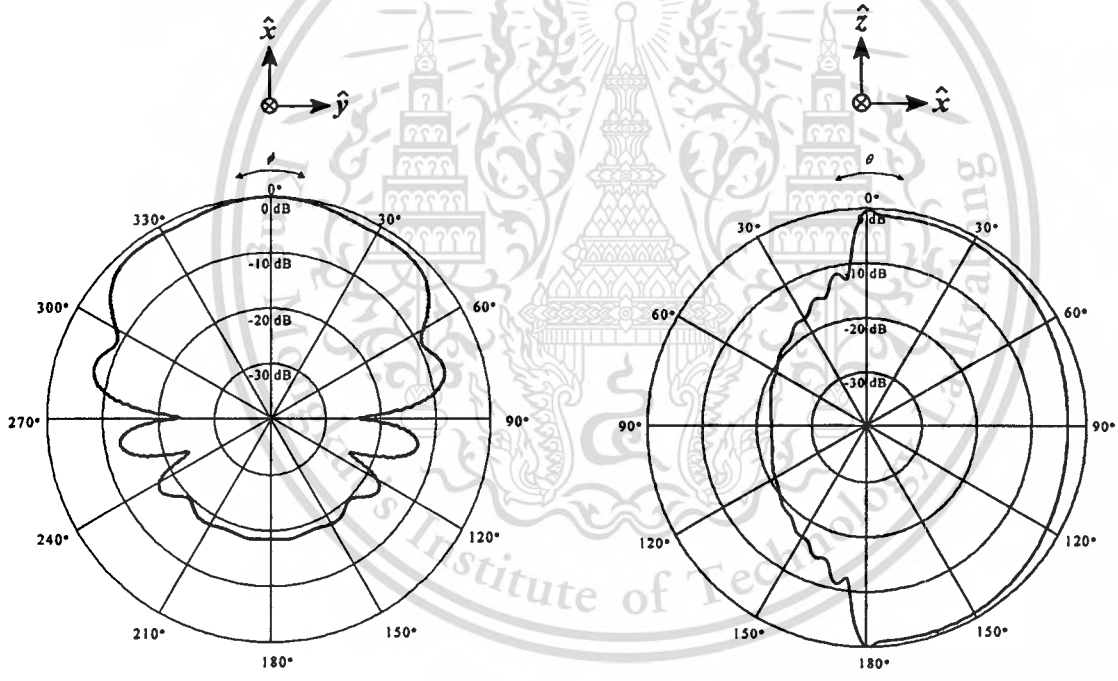

(a) d= 0.233λ

Fig.5.2 Radiation patterns of two circumferential slots array as a function of the element spacing between two slots

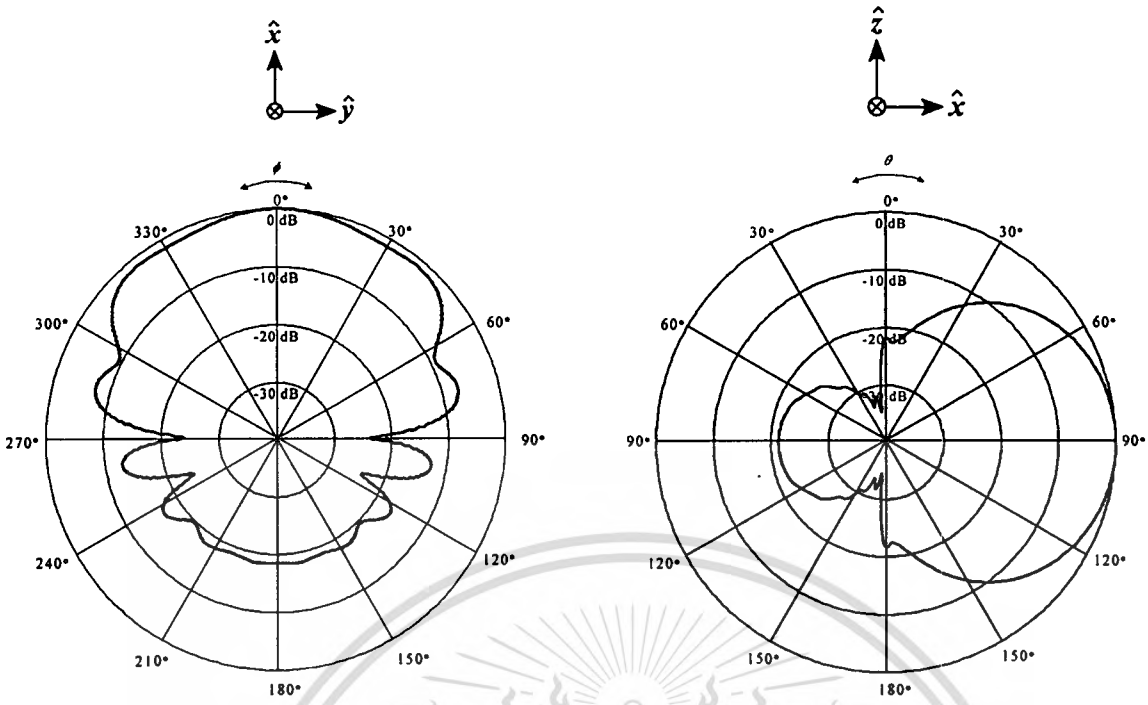

(b) $d = 0.466\lambda$

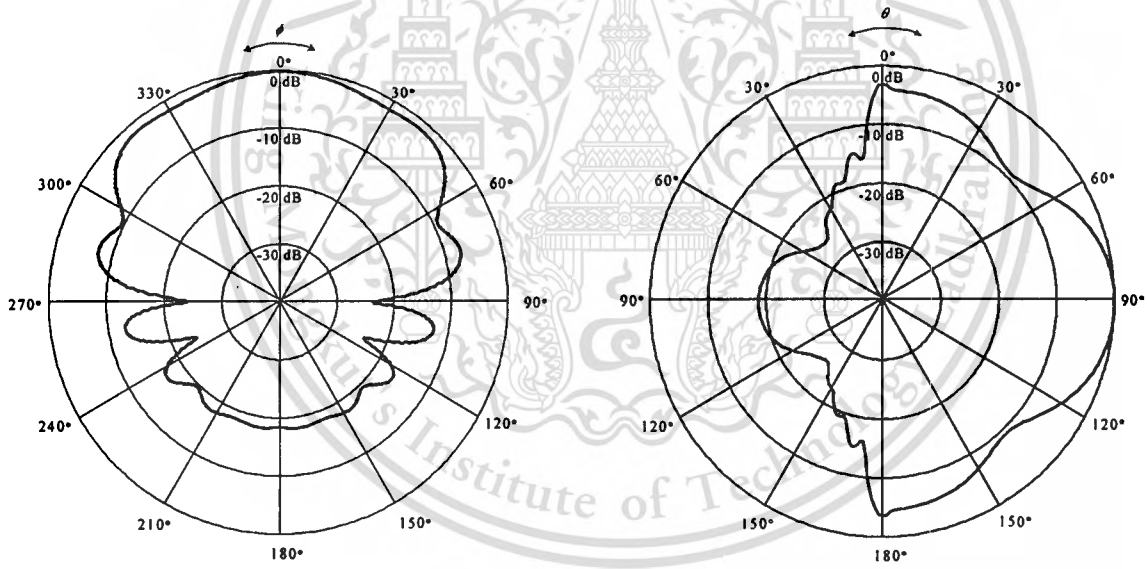

(c) $d = 0.7\lambda$

Fig.5.2 Continued. Radiation patterns of two circumferential slots array as a function of the element spacing between two slots

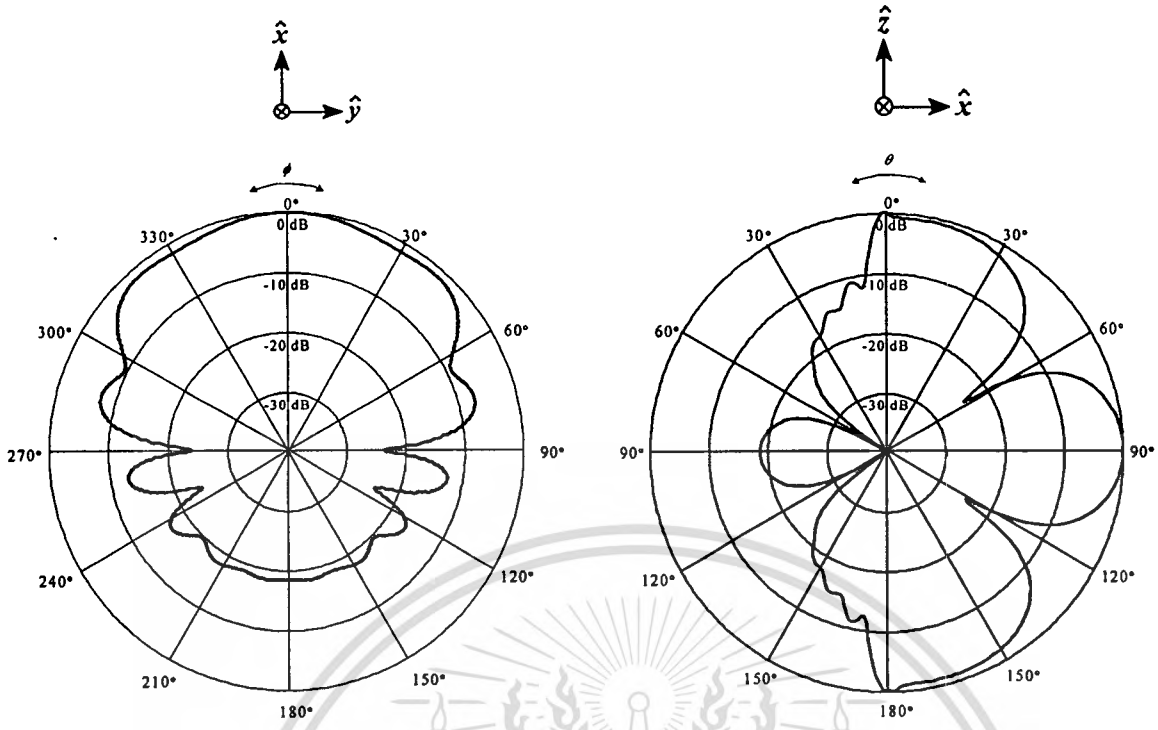

(d) $d = 0.933\lambda$

Fig.5.2 Continued. Radiation patterns of two circumferential slots array as a function of the element spacing between two slots

From the radiation patterns of Fig.5.2, it is evident that each element spacing between two slots, $d = 0.233\lambda$, 0.466λ, 0.7λ, and 0.933λ, does not have impact to the radiation pattern in azimuthal (xy) plane. The shape of radiation patterns are obtained by varying element spacings are not changed. The 3-dB beamwidth of each pattern in xy-plane is about 106°. Nevertheless, spacing of slots will influence to the radiation pattern in elevational (xz) plane as shown in Fig.5.2. It is observed that there are no minor lobes for the arrays with element spacing less than $\lambda/2$, as shown in Fig.5.2 (a) and (b). While minor lobes of arrays with spacing between elements larger than $\lambda/2$ will be risen and more increased when spacing approaches to one wavelength, as shown in Fig.5.2 (c) and (d), respectively. However, it is evident that when spacing of slots is further increased with respect to the centerline on the outer surface and along z-direction, then 3-dB beamwidth of radiation pattern is narrower, while its back

lobe is higher (HPBW are about 180°, 63.64°, 48.22°, 35.38° and back lobe levels are -22,5, -21.25, -18.80, -17.82 dB at d = 0.233λ, 0.466λ, 0.7λ, 0.933λ, respectively). Practically, we can compromise between side lobe level and beamwidth by controlling element spacing between slots for optimization.

5.3.2 Impedance Characteristics of a Circumferntial Slot Array

In the previous section, it is evident that element spacing between slots influences to the radiation pattern of the antenna. Beside that such element spacing also effects the impedance characteristics of antenna. Therefore, these parameters will be considered by varying various elements spacing similar to considering its radiation pattern as shown in Fig. 5.3.

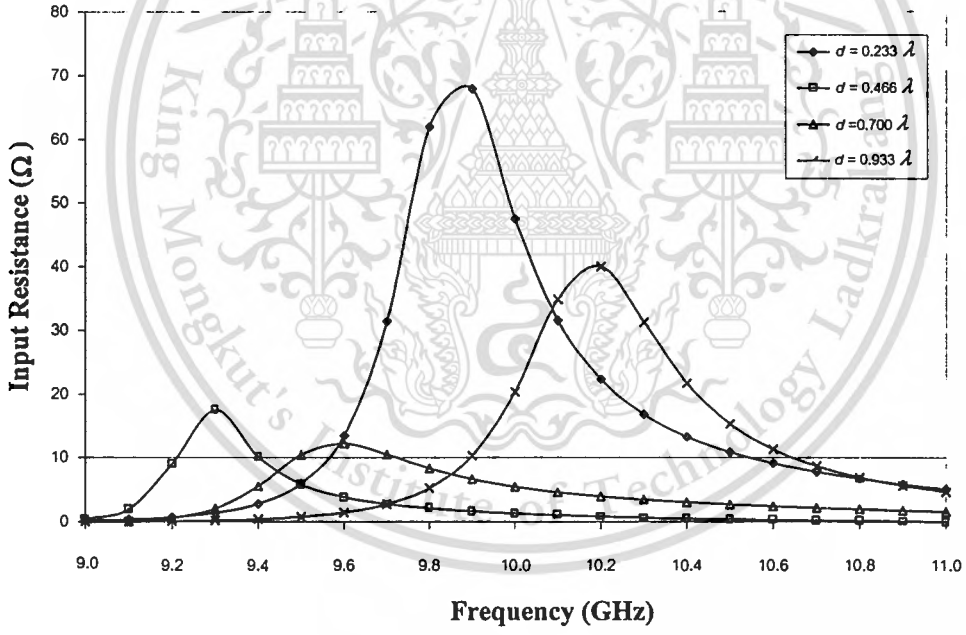

(a) input resistance

Fig. 5.3 Impedance characteristics of a circumferential two-slot for various element spacings

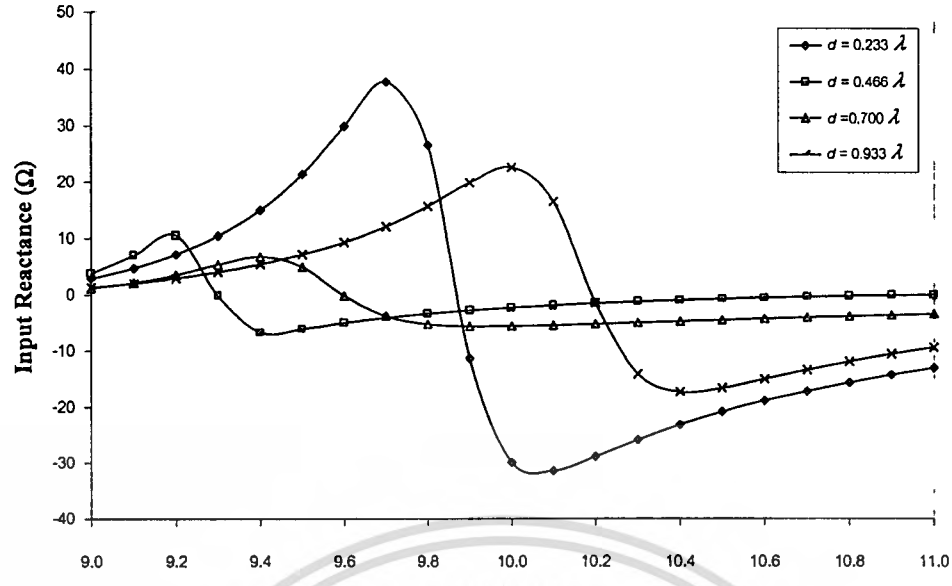

(b) input reactance

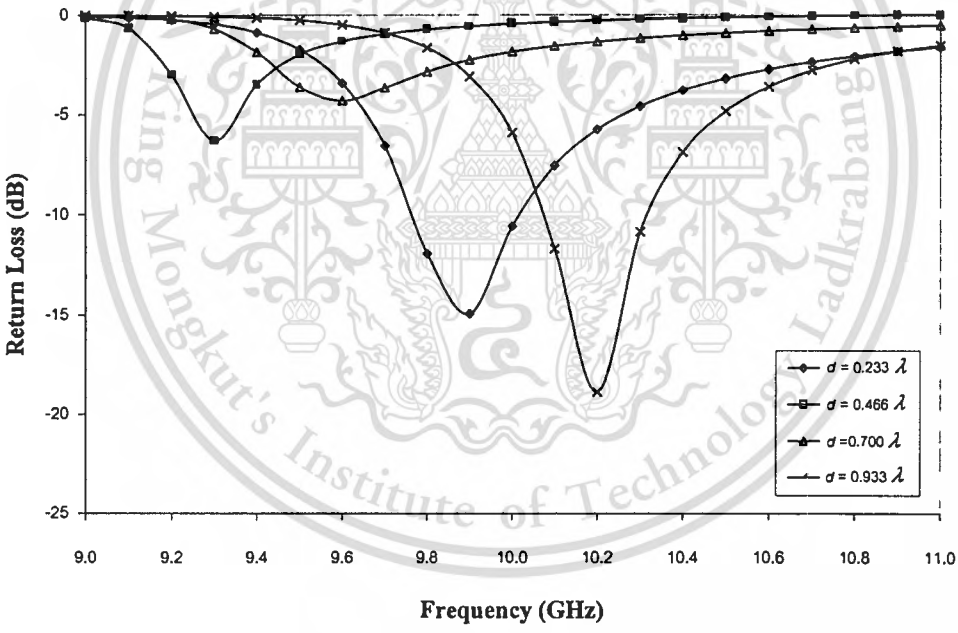

(c) return loss

Fig. 5.3 Continued. Impedance characteristics of a circumferential two-slot for various element spacings

Impedance characteristics of circumferential two slots array on the surface of a sectoral cylindrical cavity excited by probe are shown in Fig.5.3. It

is apparent that element spacing between slots is a significant parameter which considerably effects to impedance characteristics of the antenna. From Fig.5.3 (a)-(c), element spacing of two slots is varied with d = 0.233λ, 0.466λ, 0.7λ, and 0.933λ, respectively. These correspond to 0.7 cm, 1.4 cm, 2.1 cm and 2.8 cm. Another parameters of the antenna structure are specified at the optimized values as described in chapter 4. Input resistance of excited probe is largest when element spacing is closest (d = 0.233λ) and its value is gradually decreased when element spacing is increased. While this spacing is approached to one wavelength (d = 0.933λ), input resistance of excited probe will be gradually increased again as shown in Fig.5.3 (a). From Fig. 5.3(b), it is obvious that the larger element spacing, the smaller the reactance. For the resonant frequency observed from the zero reactance, it can be seen that the resonant frequency will be lower when the element spacing is extended. However, it will be higher again when spacing between two slots is closed to one wavelength. Furthermore, the return loss for different element spacing is illustrated in Fig. 5.3(c). The optimum matching frequency increases when element spacing is widened. The optimum level of the return loss of –19 dB is accomplished at the frequency of 10.2 GHz when element spacing of two slots is 0.933λ. I should be noted that these parameters must be optimized to provide desirable pattern and matching at the operating frequency.

5.4 Analysis of a Slot Array for the Horizontal Polarization

In case of horizontal polarization, the position of slots will be changed from circumferential direction to axial direction. A linear array of n slot elements is positioned by a distance d, as shown in Fig.5.4. The positions of each slot are located along the z-direction respect to the centerline on the outer surface of the sectoral cylindrical cavity, while the R- and ϕ- directions are identical.

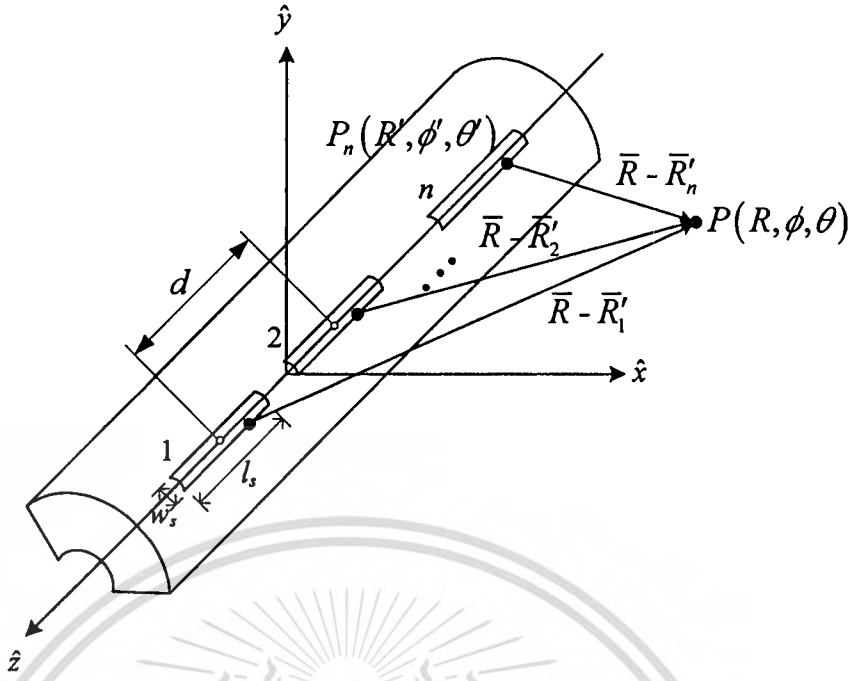

Fig.5.4 The axial slot array on the sectoral cylindrical cavity

The basis function for magnetic current distribution above and below the n-slots in (5.4) is modified according to the direction of slots in Fig.5.4, given by

$$\hat{m}_{sj} = \hat{z}\frac{1}{w_{sj}}\sin\frac{s\pi}{l_{sj}}\left(z'-\frac{l_{sj}}{2}\right), \quad \begin{matrix} s=1,2,3,...,N_j \\ j=1,2,3,...,n \end{matrix} \tag{5.19}$$

where $z' = R'\cos\theta$

and $\hat{z} = \hat{R}\cos\theta - \hat{\theta}\sin\theta$.

For the axial slot, the components of electric-field magnetic-source dyadic Green's function $\overline{\overline{G}}_{EM}^{out}$ of the cylindrical cavity are changed to be the $\hat{\theta}\hat{z}$ and $\hat{\phi}\hat{z}$ that are expressed in form of the dyadic Green's function involve infinite series, as follows

$$G^{i}_{EM,\phi z} = \frac{ke^{-jk(R-\cos\theta R'\cos\theta')}}{4\pi R}\sum_{n=1}^{\infty}(2-\delta_0)(j)^{n+1}(\cos n\phi+\sin n\phi)$$

$$\times\left\{ j\frac{\cos\theta}{2}(\cos\theta+\sin\theta)\left[\left(J_{n-1}(k\sin\theta R'\sin\theta')\right)-\left(J_{n+1}(k\sin\theta R'\sin\theta')\right)\right.\right.$$

$$\left.+a_{\substack{e\\o}n}\left(H^{(1)}_{n-1}(k\sin\theta R'\sin\theta')-H^{(1)}_{n+1}(k\sin\theta R'\sin\theta')\right)\right]$$

$$\left.+(\cos n\phi'+\sin n\phi')(\cos\theta-\sin\theta)\left[J_n(k\sin\theta R'\sin\theta')+a_{\substack{e\\o}n}H^{(1)}_n(k\sin\theta R'\sin\theta')\right]\right\}$$

(5.20)

and

$$G^{i}_{EM,\phi z} = \frac{e^{-jk(R-\cos\theta R'\cos\theta')}}{4\pi R\sin\theta R'\sin\theta'}\sum_{n=1}^{\infty}n(2-\delta_0)(j)^{n+1}(\cos n\phi+\sin n\phi)$$

$$\times(\cos n\phi'-\sin n\phi')(\cos\theta+\sin\theta)\left[J_n(k\sin\theta R'\sin\theta')+b_{\substack{e\\o}n}H^{(1)}_n(k\sin\theta R'\sin\theta')\right]$$

(5.21)

By using the same procedure as described in the case of a circumferential slot array, the unknown coefficients, a_{sj} and b_f are obtained. Then unknown currents $\bar{M}(\bar{R}_i')$ and $\bar{J}(\bar{R}')$ will be solved. The antenna characteristics can be subsequently determined by using these currents.

5.4.1 Radiation Pattern of an Axial Slot Array

The electric field radiates from the *i*th axial slot on the infinite circular cylinder consist of components of electric field in θ and ϕ directions, are given by (5.16), which is written as

$$\bar{E}^{i}(\bar{R}) = \iint_{s_i}\left[G^{i}_{EM,\theta z'}\hat{\theta}+G^{i}_{EM,\phi z'}\hat{\phi}\right]\cdot[M^{'i}_{z}\hat{z}][\sin\theta'(R')^2]d\theta' d\phi' \quad . \tag{5.22}$$

Finally, the total electric field can be obtained by (5.18) with various element spacing at $d = 0.75\lambda$, 1.0λ, 1.25λ, 1.5λ, 1.75λ, and 2.0λ as shown in Fig.5.5.

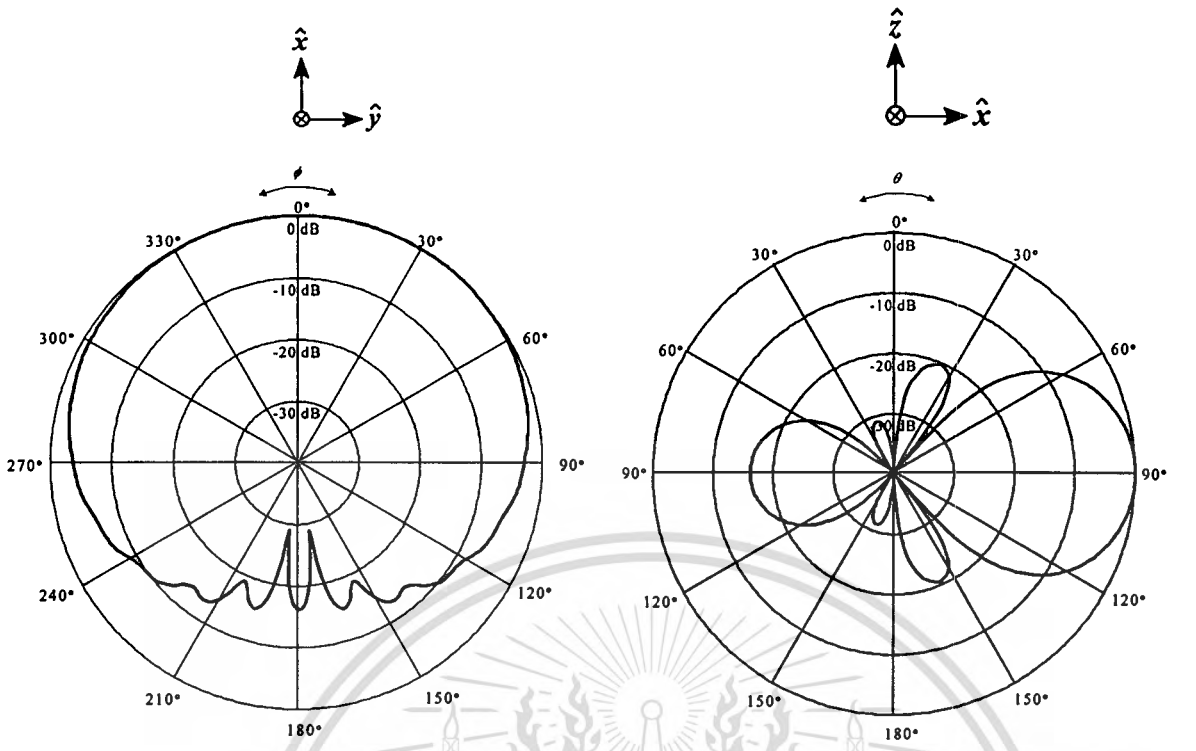

(a) $d = 0.75\lambda$

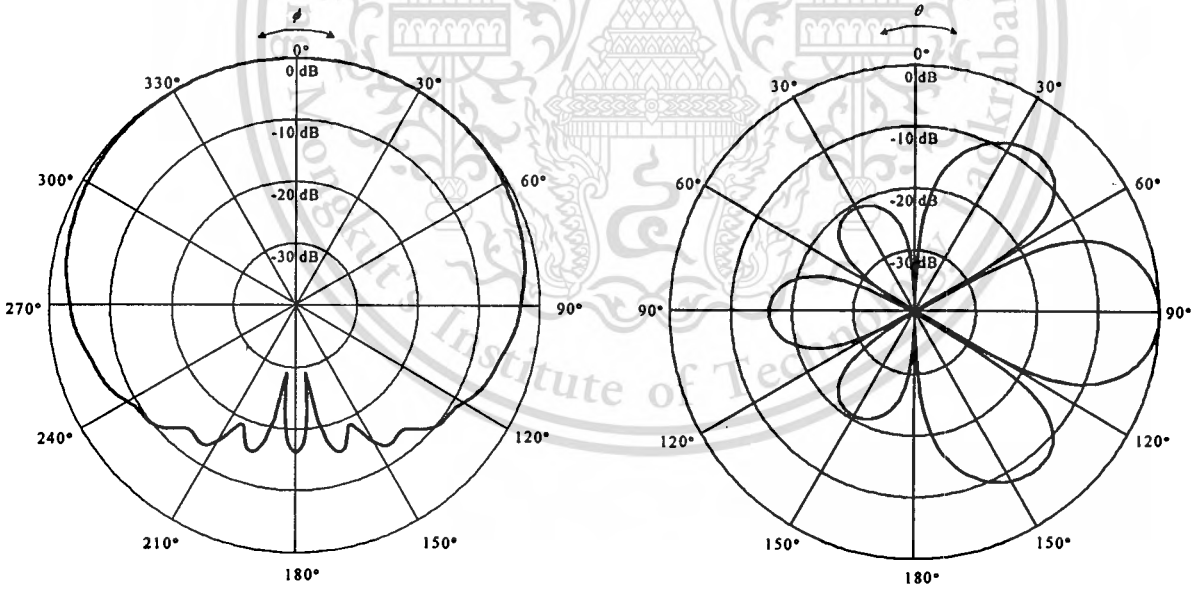

(b) $d = 1.0\ \lambda$

Fig.5.5 Radiation patterns of two axial slots array as a function of the element spacing between two slots

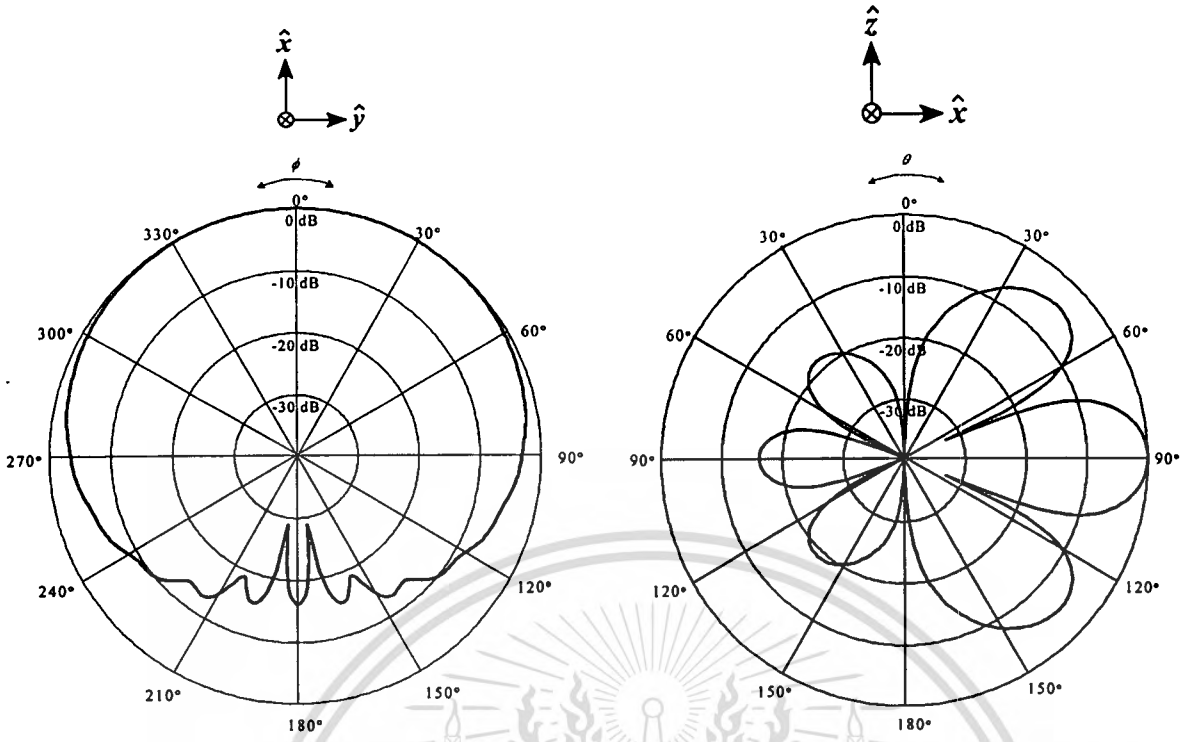

(c) $d = 1.25\ \lambda$

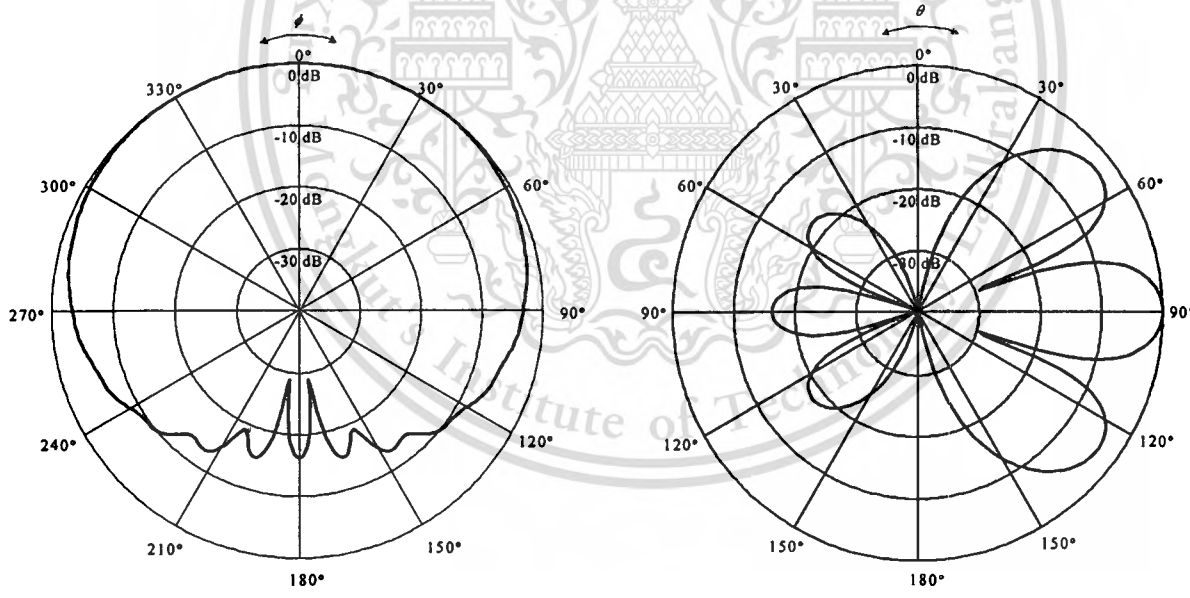

(d) $d = 1.5\ \lambda$

Fig.5.5 Continued. Radiation patterns of two axial slots array as a function of the element spacing between two slots

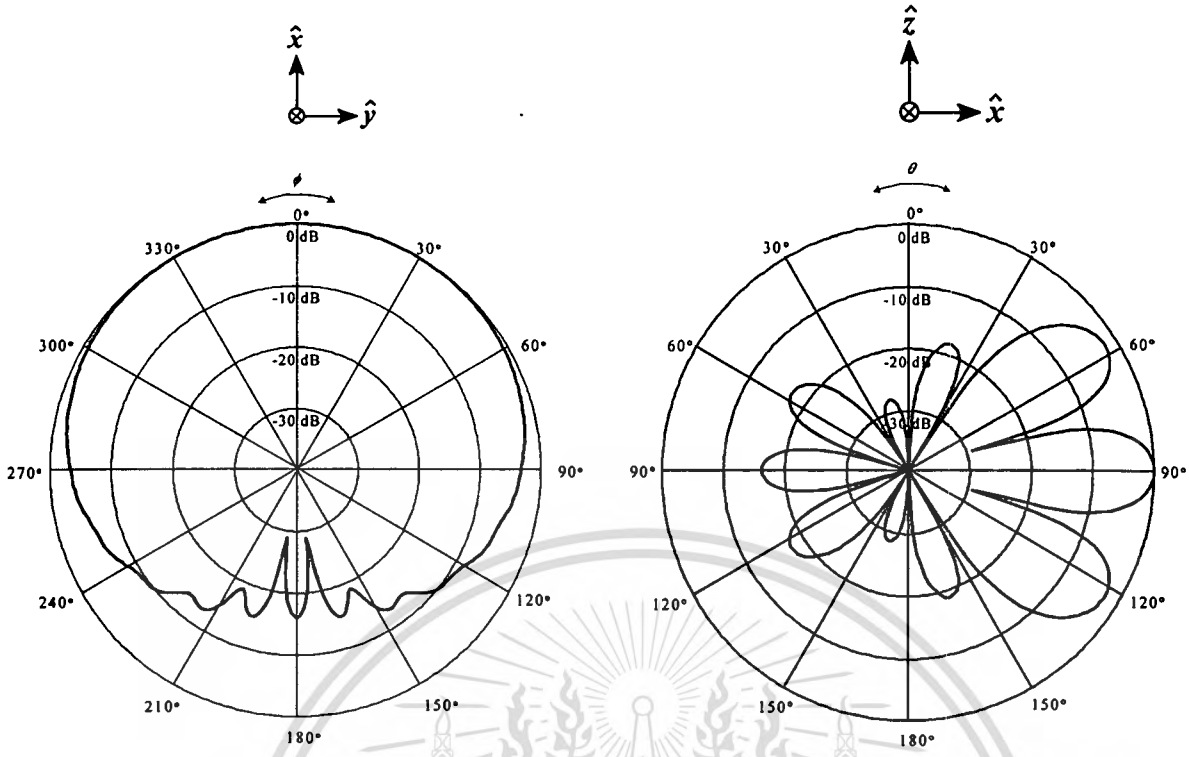

(e) $d = 1.75\ \lambda$

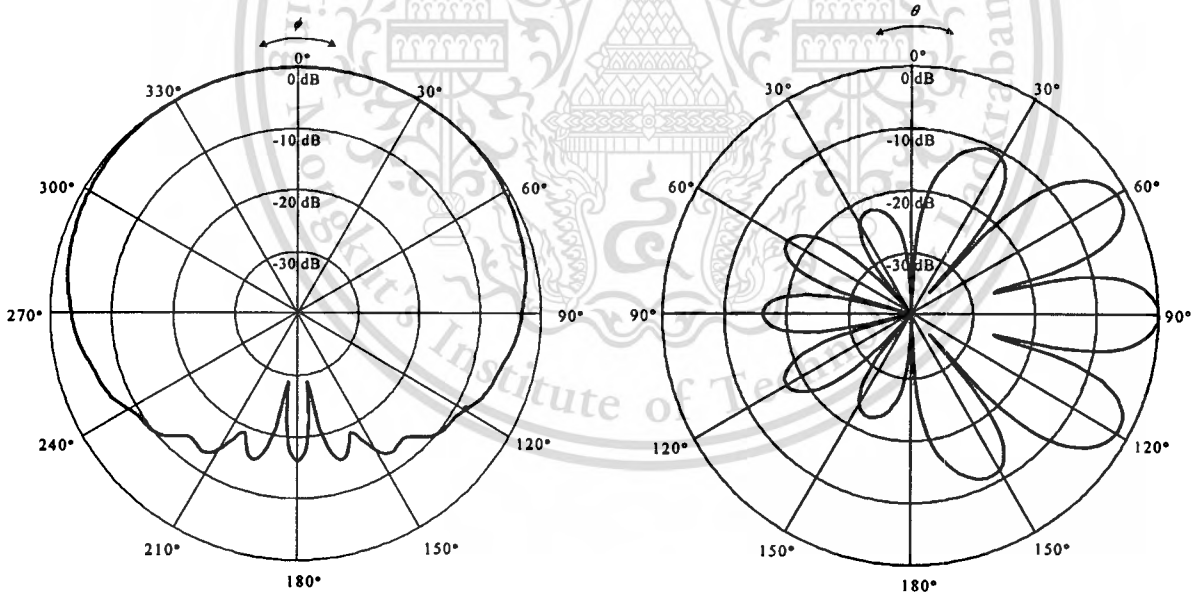

(f) $d = 2.0\ \lambda$

Fig.5.5 Continued. Radiation patterns of two axial slots array as a function of the element spacing between two slots

The radiation patterns of a two-slot array with d = 0.75λ, 1.0λ, 1.25λ, 1.5λ, 1.75λ, and 2.0λ, are plotted in Fig.5.5 (a) through (f). The separation d does not cause the change of radiation pattern in xy–plane. The patterns of each condition of element spacing are identical. However, it yields wider 3-dB beamwidth of 174° when compare to the 3-dB beamwidth in azimuthal plane of a circumferential slot array that is equal to 106°. Furthurmore, spacing of slots will considerably influence for beam forming of this antenna in xz-plane. It is evident that when separation d between slots is further increased along z-direction, the 3-dB beamwidth of radiation pattern is gradually decreased, (HPBW is equal to 40°, 28°, 22°, 19°, 16° and 14° when d = 0.75λ, 1.0λ, 1.25λ, 1.5λ, 1.75λ, and 2.0λ, respectively). It is observed that back lobe of each pattern are almost identical of –16.16 dB. It shows that spacing between slot does not have impact on front-to-back ratio level of radiation pattern of an axial slot array. Furthermore, number of minor lobes is increased and level of such minor lobes is higher when the spacing d is wider. However, in practice, designer can select the other proper parameters to achieve the desired beam shape. Another way is to increase number of radiating slots, which will illustrate a prototype in the next chapter.

5.4.2 Impedance Characteristics of an Axial Slot Array

This section presents the impedance characteristics of an axial two-slot array with a variety of element spacing of 0.75λ, 1.0λ, 1.25λ, 1.5λ, 1.75λ, and 2.0λ, which were utilized for considering the radiation pattern of antenna in above section. The spacing of shorter than 0.75λ is not used because the length of each slot equals λ/2, which causes spacing between slots is too close. The numerical results of the input impedance and return loss of antenna, which are effected with such element spacings, will be shown in Fig.5.6 (a) through (c).

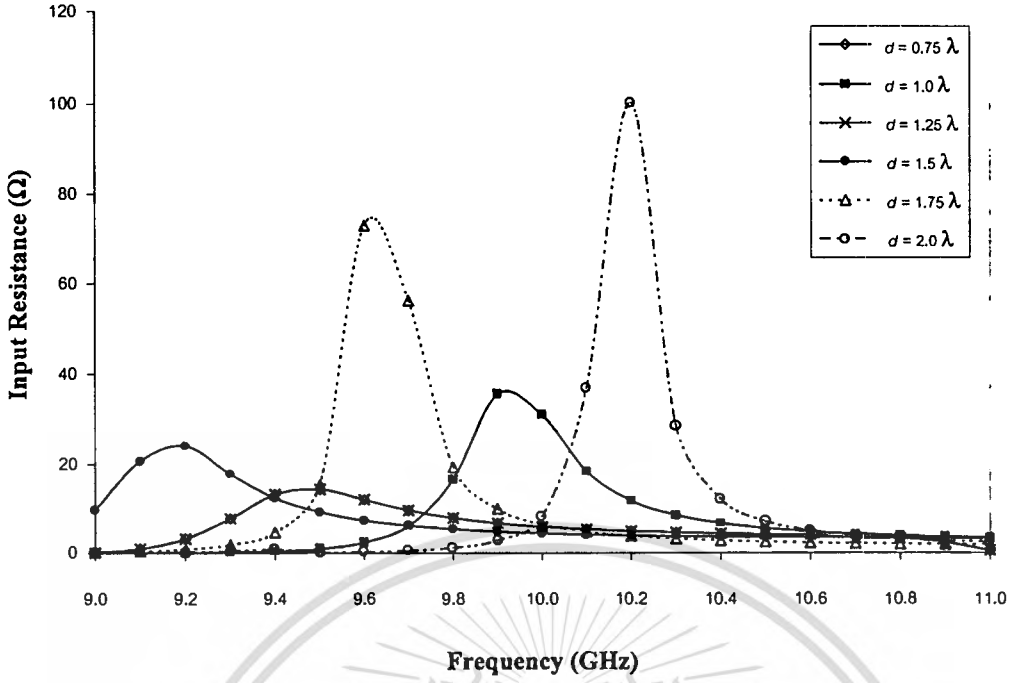

(a) input resistance

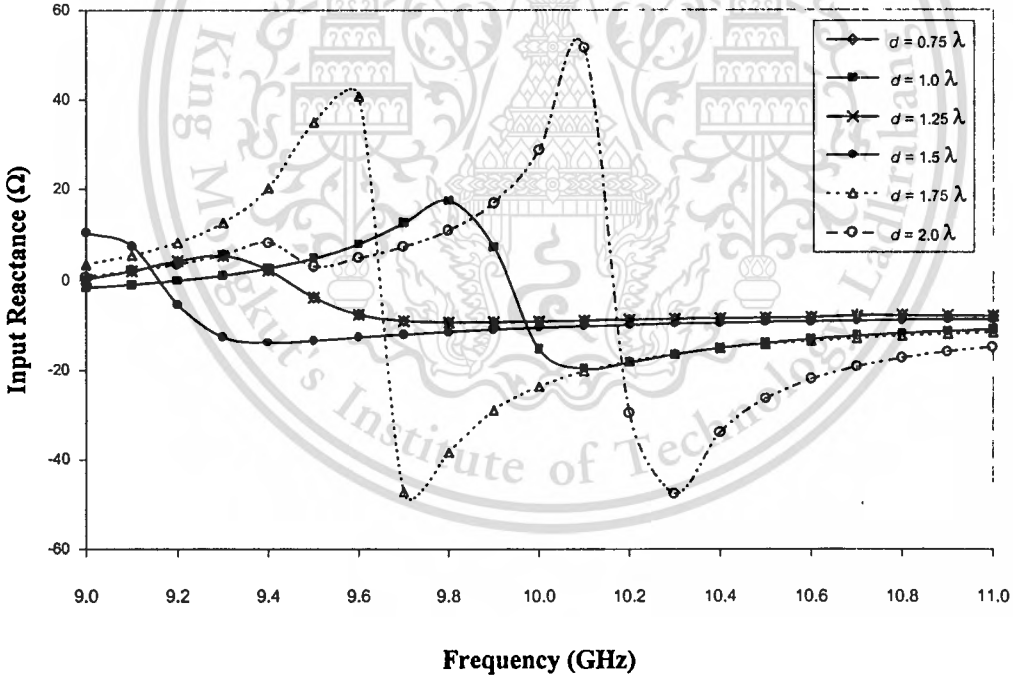

(b) input reactance

Fig. 5.6 Impedance characteristics of an axial two-slot antenna for various element spacings

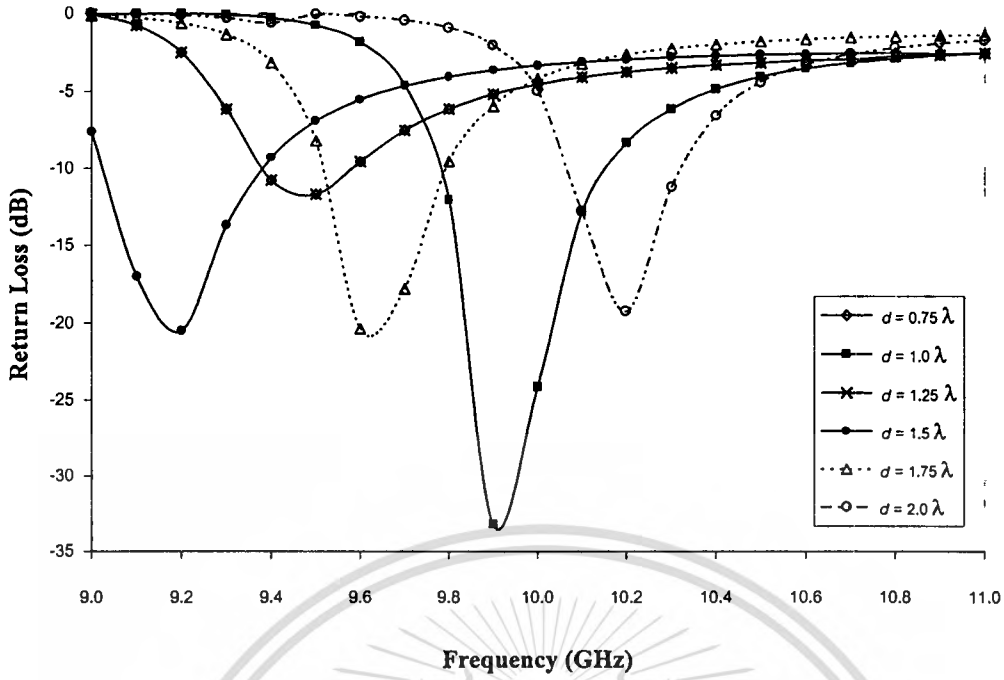

(c) return loss

Fig. 5.6 Continued. Impedance characteristics of an axial two-slot antenna for various element spacings

Input resistance, input reactance and return loss of an axial two-slot array on the surface of a sectoral cylindrical cavity excited by probe are shown in Fig.5.6 (a), (b), and (c), respectively. It is observed that value of input resistance and reactance is largest and the resonant frequency is higher than desired resonant frequency when element spacing equals twice of wavelength as shown in Fig.5.6 (a) and (b). When the spacing between slots is shorten, it can be seen that the value of input resistance, input reactance, and the resonant frequency are lower. The resonant frequency of 10 GHz is realized when d is slightly larger than one wavelength. Finally, Fig. 5.6 (c) shows return loss with different element spacings. The proper distance of slot spacing can also be determined by using the appropriated value of return loss, parallel to considering input resistance and input reactance. The optimum level of the return loss of –33.85 dB is accomplished of the frequency of 9.89 GHz when element spacing of two

slots is 1.0λ. However, we can compromise these related parameters for yielding desired resonant frequency.

5.5 Conclusions

Polarization of electromagnetic wave, which radiated by antenna, is an important characteristic that specify transmitting and receiving signal between two users. A sectoral cylindrical cavity-backed slot array antenna excited by probe can be used in case of either vertical polarization or horizontal polarization. By cutting slots on the outer surface of the cavity in circumferential direction, it will yield the vertical polarization. It will provide the horizontal polarization by cutting slots in axial direction of the cavity. Furthermore, this chapter presents the influence of the outer radius of cavity, the spacing between slots that affects radiation pattern and impedance characteristics of antenna. In order to investigate radiation pattern and impedance characteristics of this antenna, the straightforward procedure is applied. By utilizing the integral equations of the structure based on boundary condition, then the components of dyadic Green functions for circumferential and axial slot are chosen. The entire domain basis function of each direction of the slot and the basis function the probe are used in the Method of Moments to solve for electric current density on the probe and the magnetic current density on the slot. The input impedance and radiation pattern can be found from these currents subsequently. The effects of the parameters of an antenna are studied as a function of element spacing between slot for analyzing the radiation pattern and as a function of frequency for analyzing the input impedance. From numerical results, We can accurately predict them in both of axial slot and circumferential slot at the appropriated element spacing d=1.0λ at the frequency 10.2 GHz and d=0.933λ at the frequency 9.89 GHz, respectively, which yield the good matching condition.

References

[5.1] N.Pasri, "A Circumferential Slot Array Antenna on a Concentric Sectoral Cylindrical Cavity Excited by a Probe," Chap.6, Master Thesis, King Mongkut' s Institute of Technology Ladkrabang, 2003.

[5.2] C.Phongcharoenpanich, P.Wounchoum, S.Kosulvit and M.Krairiksh, "A Horizontally Polarized Omnidirectional Beam Antenna using Array of Axial Slot on Cylindrical Surface," *Proceedings of the 3rd International Conference on Microwave and Millimeter Wave Technology*, Beijing, pp.576-579, Aug. 2002.

Chapter 6

Antenna Measurements

6.1 Introduction

In order to verify the proposed principles that have been explained in the preceding chapters, the prototypes of the antenna that the parameters are optimized as mentioned in the previous chapter were fabricated. The antenna measurements are set up to test the characteristics of a sectoral cylindrical cavity-backed slot array antenna. The radiation patterns in both elevational and azimuthal planes are measured. The impedance characteristics such as the input impedance are tested by using the Network Analyzer.

6.2 Antenna Fabrication

To verify the theoretical calculation, the axial slot cut on the sectoral cylindrical cavity excited by a probe is fabricated. The experiment was set up at the operating frequency of 10 GHz to measure the elevational and azimuthal radiation patterns and impedance characteristics. This frequency is chosen corresponding to the available equipment in the Wireless Communication Laboratory. The antenna design parameters are used from the optimum conditions as specified in the previous section. They are tabulated in Table 6.1 [6.1].

The prototype of the antenna was fabricated and the photograph is depicted in Fig.6.1. It is made of the aluminum that is cutting by the wire cut machine to form the sectoral cylindrical waveguide. The tolerance of this machine is ±5 μm. This structure was shorted by the aluminum wall via the metallic glue. The slot is cut at the outer surface of the cavity using the EDM (Electrode Discharged Machine). The tolerance of the EDM is ±5 μm. This structure is excited by the linear electric probe that is the copper rod of the

diameter 0.5 mm via SMA connector. The impedance characteristics such as input impedance and return loss are measured using HP8722D Network Analyzer.

Table 6.1 Antenna parameters used in the calculations and measurements

Antenna Parameters	*Electrical Size*	*Physical Size at 10GHz*
Inner cylindrical radius (ρ_a)	1.050λ	3.150 cm
Outer cylindrical radius (ρ_b)	1.575λ	4.725 cm
Angle of sectoral cylinder (ϕ_c)	60°	60°
Sectoral cylindrical cavity length (z_d)	1.300λ	3.900 cm
Slot location in ϕ direction (ϕ_s)	15°	15°
Slot location in z direction (z_s)	0.650λ	1.950 cm
Slot length (l_s)	0.500λ	1.500 cm
Slot width (w_s)	0.030λ	0.90 cm
Probe location in ϕ direction (ϕ_f)	30°	30°
Probe location in z direction (z_f)	0.650λ	1.950 cm
Probe length (l_f)	0.280λ	0.840 cm

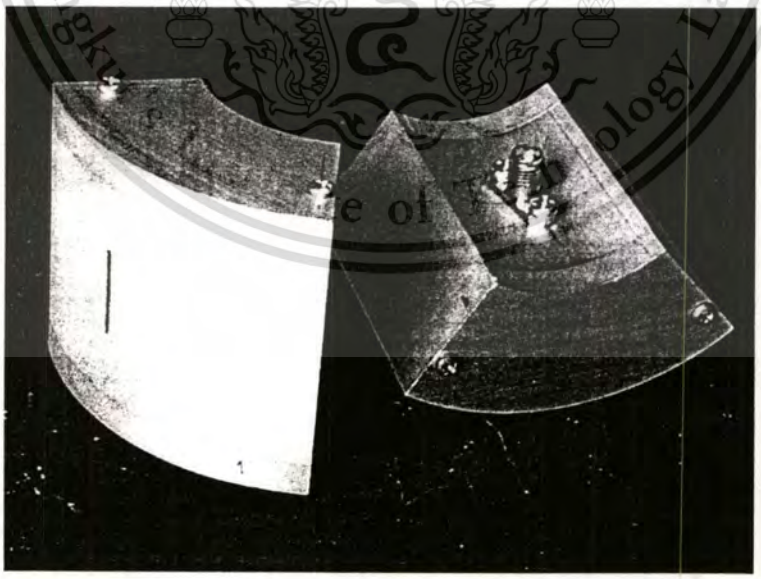

Fig 6.1 Photograph of the fabricated antenna prototype

6.3 Radiation Pattern

The radiation pattern was measured in the in house anichoic chamber and the far-field range of 1 m. is used [6-2]-[6-3]. A pyramidal horn antenna with the gain of 12.5 dB was employed to transmit a linearly polarized wave, and the antenna under test was rotated to receive the transmitted wave at 5° per step until the angle of 360°. These angles of measurement are chosen in order that the elevational beam peak in *xz*-plane can be determined. Therefore, the vertically polarized pattern of the angles between 0° and 360° is measured. The measurements set up to test the radiation patterns in elevational plane are depicted in Fig.6.2. After the elevational pattern is measured, the elevational beam peak is determined.

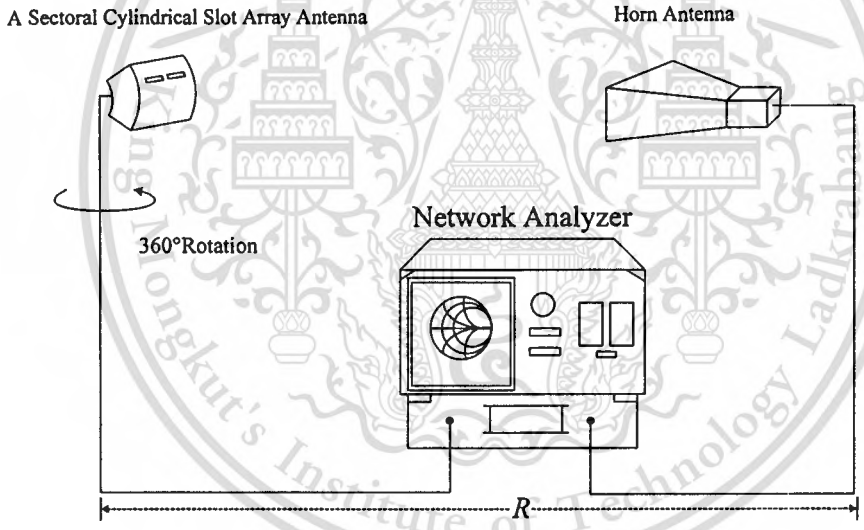

Fig.6.2 Measurement set up of radiation pattern in the elevational plane

The radiation pattern measurement in azimuthal plane is set up where the distance between the transmitting and the receiving antennas is equal to the distance of the radiation pattern measurement in elevational plane. Then, the antenna under test is also rotate 5° per step from 0° to 360°. The measurement set up to test the radiation pattern in azimuthal plane is showsn in Fig.6.3.

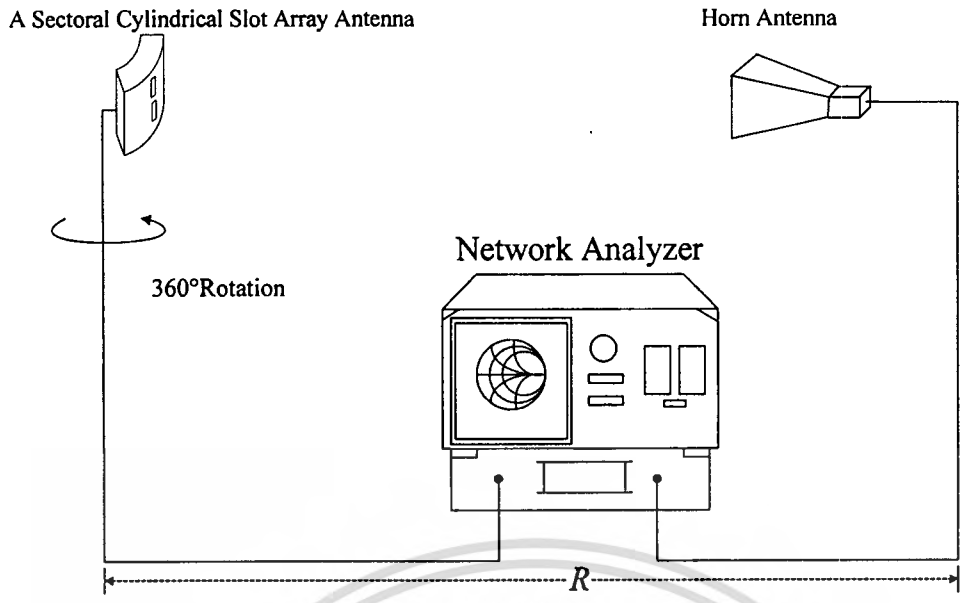

Fig.6.3 Measurement set up of the radiation pattern in the azimuthal plane

Experimental result of radiation pattern in the elevational and azimuthal plane is plotted and compared with the calculation as shown in Fig. 6.4 and Fig.6.5, respectively.

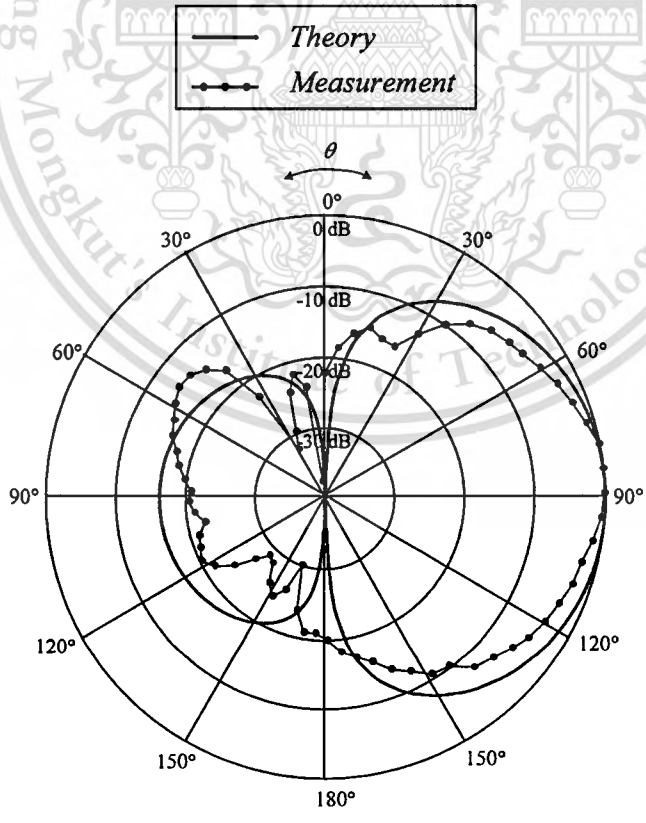

Fig.6.4 Radiation pattern in elevational plane

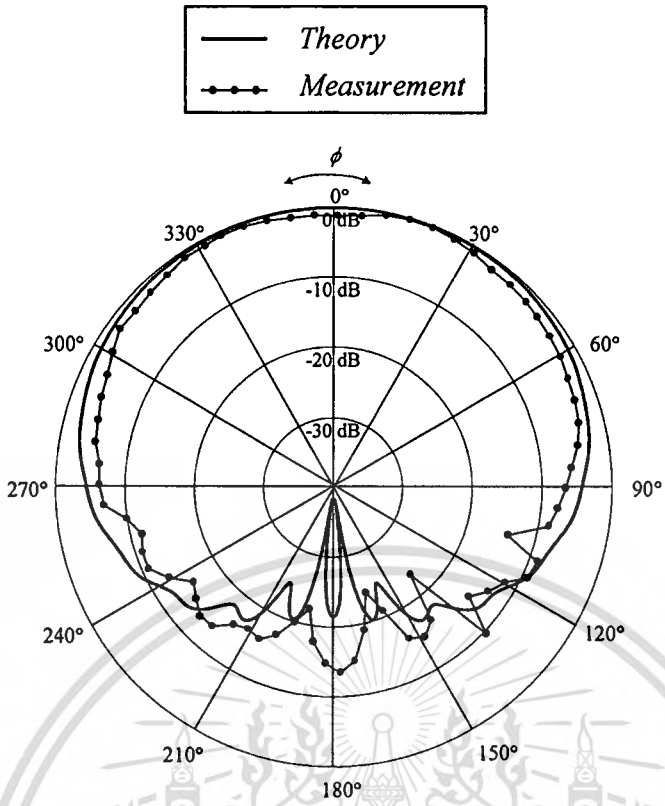

Fig.6.5 Radiation pattern in azimuthal plane

From this comparison, we can see that these results are in good agreement i.e., the beam peak is at 90°. However, there are some errors on account of the diffraction at the edge of the cavity, the imperfect fabrication and the test-site situations [6-4], which causes the radiation pattern in this plane is somewhat distorted in both major lobe and back lobe. In addition, 3-dB beamwidth of the measured pattern is narrower than the calculated one. The calculated result has 3-dB beamwidth about 78° while the result from experiment is 52°. Fig. 6.5 shows the azimuthal pattern of the antenna at the beam peak direction is at 0°. The 3-dB beamwidth for theory is 176° while for experiment is 128°. The theoretical and experimental results are comparatively illustrated. These results agree very well, except the back lobe of measured result is slightly high.

In addition, we fabricated the two-axial-slot array by using the same dimensions of antenna that summarized in Table 6.1, except the cavity length is

specified at 2λ, and the separation between slots is 1λ. The calculated and experimental results are comparatively illustrated in Fig.6.6.

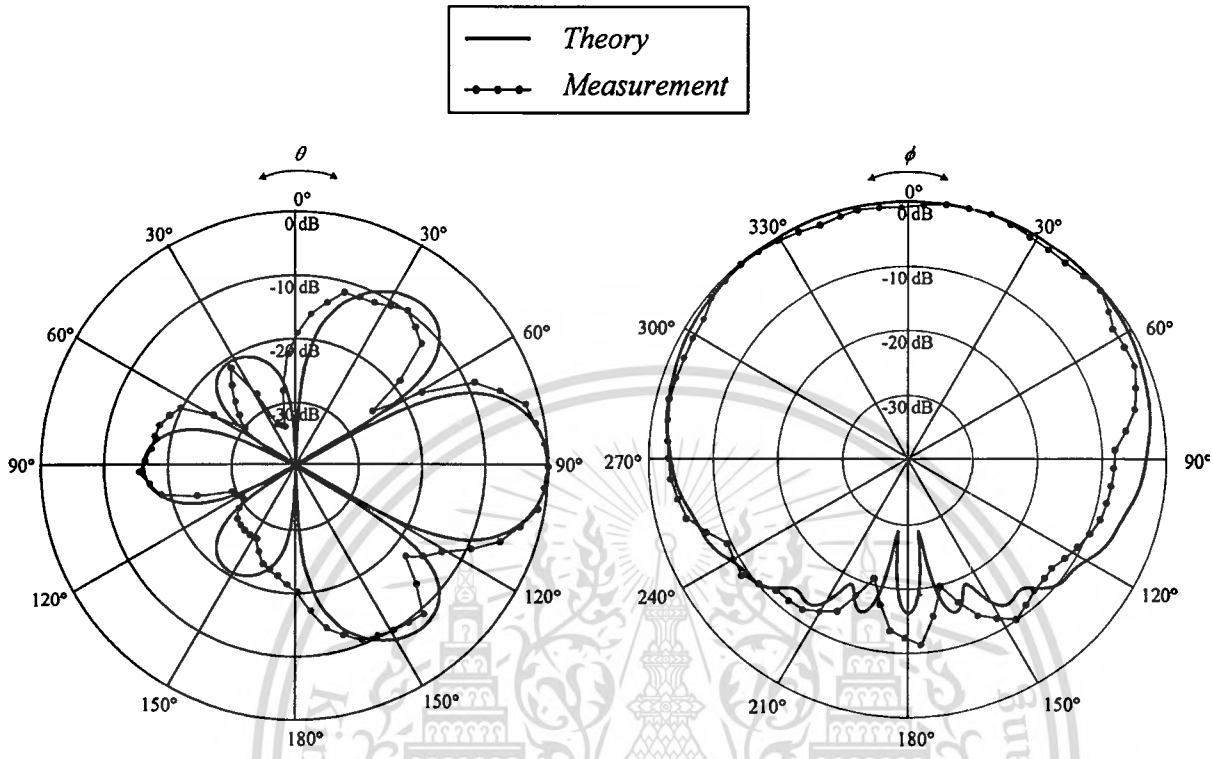

(a) Elevational pattern (b) Azimuthal plane

Fig.6.6 Radiation Pattern of the two-axial-slot array on a sectoral cylindrical cavity

Fig.6.6 (a) and (b) show the radiation patterns of the two slots array on a sectoral cylindrical cavity in elevation and azimuthal plane, respectively. The azimuthal patterns of theory and experiment have the same tendency. The values of half-power beamwidth in elevation plane are almost identical (theory: 28°, experiment: 27°). The difference of azimuthal pattern is beamwidth that the theoretical result is 174° whereas the experiment result is 147°. The other different one is the values of front-to-back ratio, which the theoretical result is –16.16 dB while the experiment result is –17.578 dB. Nevertheless, the trend of comparative results is almost identical.

6.4 The Impedance Characteristics

The impedance characteristics such as input impedance and return loss are measured using HP8722D Network Analyzer. To measure the impedance characteristics of the antenna, the experiment is set up as shown in Fig.6.7 by setting up for S_{11} mode. The measured results of one slot on the sectoral cylindrical cavity are plotted and compared with the theoretical one as figured in Fig.6.8 [6-1].

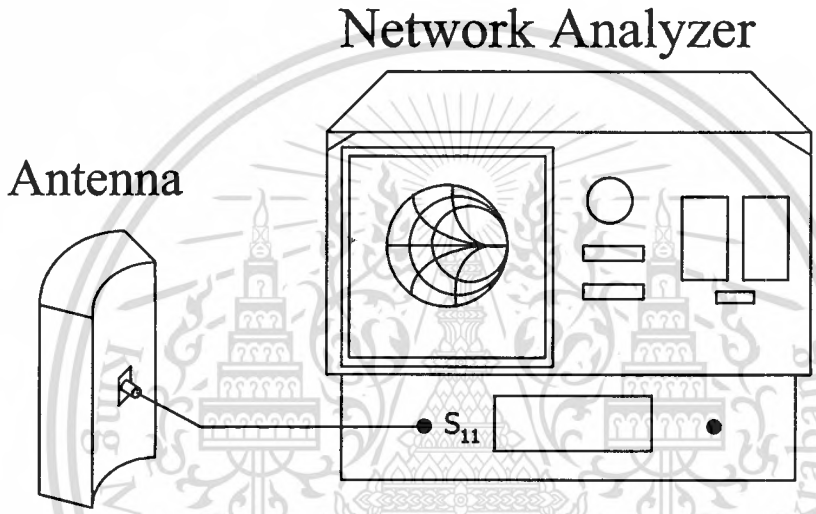

Fig.6.7 Measurement set up of the impedance characteristics

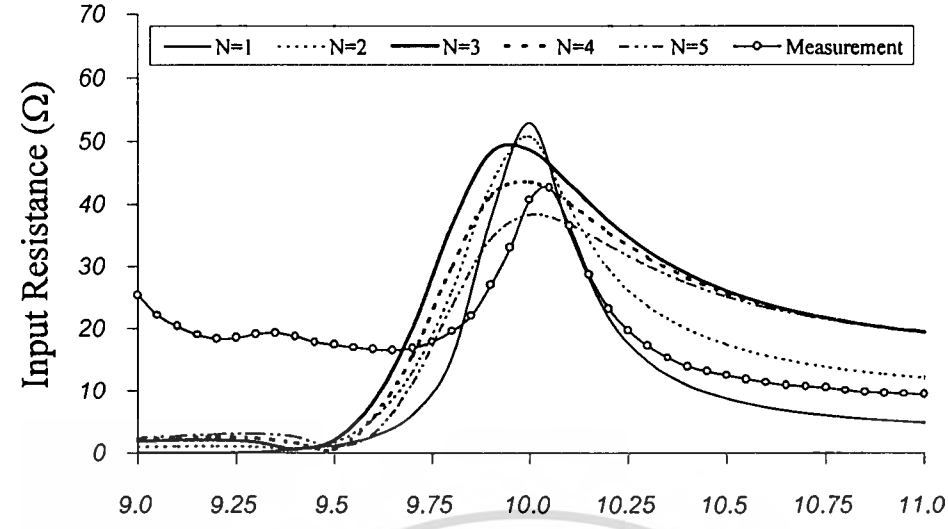

(a) Input resistance

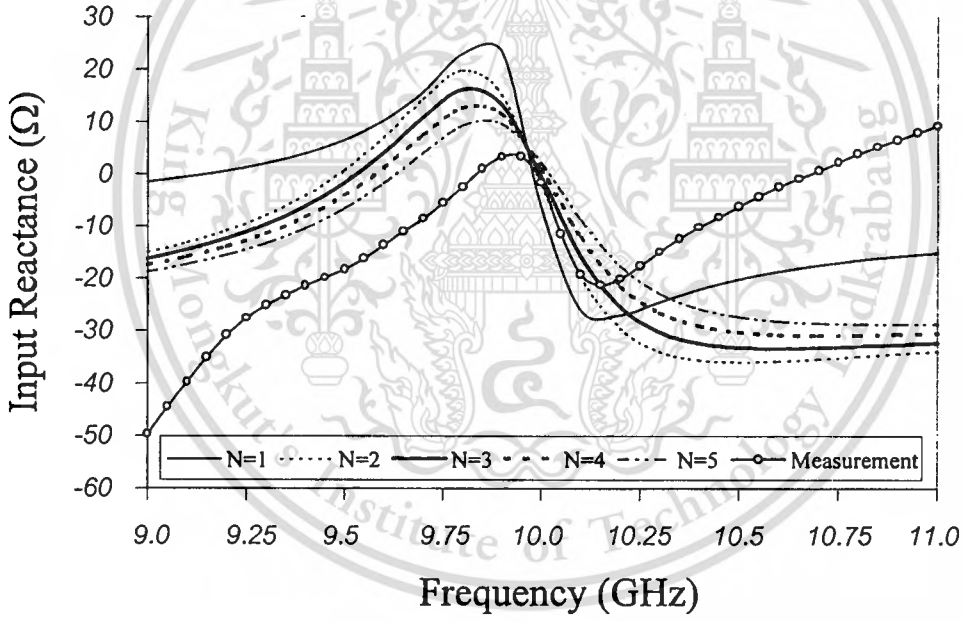

(b) Input reactance

Fig. 6.8 Comparison between calculated and measured results of one slot on the sectoral cylindrical cavity

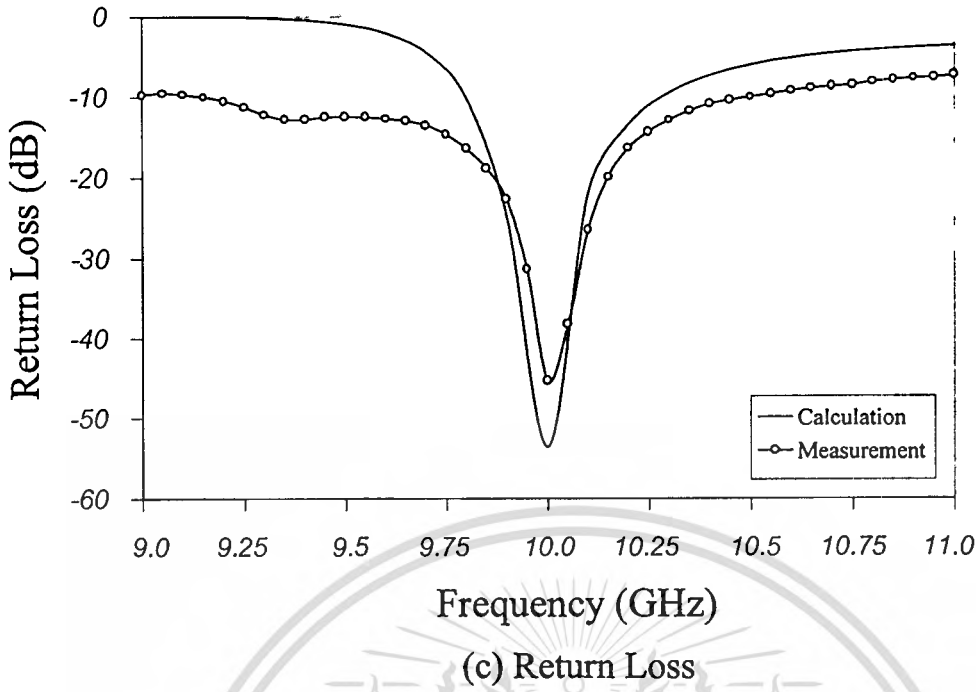

(c) Return Loss

Fig. 6.8 Continued. Comparison between calculated and measured results of one slot on the sectoral cylindrical cavity

Fig. 6.8(a) through Fig.6.8(c) illustrates the compared results between theoretical calculation and measured results. The solid line represents the calculated results whereas the circle line expresses the measured results. Looking at Fig. 6.8(a) and (b) at the designed frequency of 10 GHz, the value of resistance and reactance approach the measured results when N is increased from 1 to 4. The values for N equals 5 are not significantly changed. Hence we choose N to be equal to 4. When frequency is varied from 9 GHz to 11 GHz to illustrate the behavior of the input impedance and return loss over 20% bandwidth, we find that the resistance starts from a very small value at 9 GHz and reaches its peak value of 43 Ω at 10 GHz. Then it reduces to small value as the frequency is increased. For reactance, it starts from very small positive value and reaches its peak value at 9.8 GHz. The resonance takes place at 10 GHz and the value turns out to be negative. The results are in good agreement only at the designed frequency of 10 GHz since the basis functions in (4.1) and (4.2) is frequency independent. Therefore notable discrepancy at the frequencies far

from the designed frequency can be observed. The return loss in Fig. 6.8(c) shows the accurate result at the designed frequency. The calculated and measured results are 54 dB and 46 dB, respectively. Although the calculated results of return loss at the designed frequency are different from the measured results about 8 dB or 14.81%, but both of the results are lower than –10 dB. It is the acceptable minimum value of return loss. The difference in the value of return loss at the frequencies far from 10 GHz come from the frequency independent of the basis functions used in this work. This discrepancy may be improved by selecting the more suitable basis functions. It will be left for further study.

The next step, we measured the impedance characteristic of the two slots array on the sectoral cylindrical cavity. Their values of return loss from theory and experiment are comparatively illustrated in Fig.6.9.

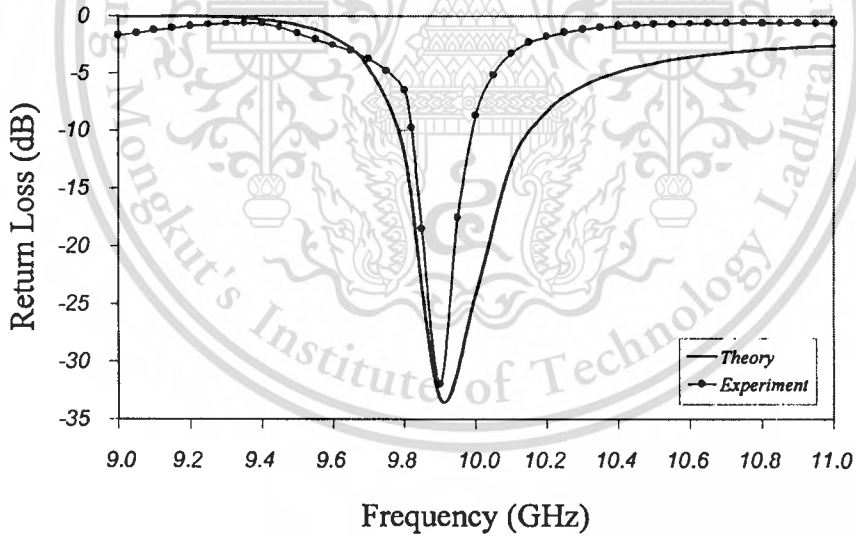

Fig. 6.9 Return loss comparison between calculated and measured results of the two slots on the sectoral cylindrical cavity

It is obvious that the calculated results are coincided with the measured ones. The calculated and measured results of resonant frequency are 9.9 GHz and 9.88 GHz, which are different from the 10 GHz-designed frequency around

0.1 GHz and 0.12 GHz or 1% and 1.2%, respectively. Beside that, both of the results are different in that the bandwidth of return loss ≤ -10 dB and the measured results are narrower than the calculated ones. However, the differences of calculated and measured results are 33.2 dB and 31.16 dB, respectively. The measured value of return loss is different from the calculated results about 1.6 dB or 4.82%.

6.5 Antenna Bandwidth

The bandwidth of the antenna means the frequency range in which the antenna can be well-operated. In the case of a sectoral cylindrical cavity-backed slot array antenna, the characteristics that have to be considered consist of the radiation pattern and the impedance characteristics. The impedance condition must be well-matched viz., the standing wave ratio with no more than 2.0 or the return loss with no more than –10 dB. The frequency band that meets all of these requirements is nominated to be the bandwidth of the antenna. From the information as described above, it is obvious that the antenna bandwidth is constrained by the impedance bandwidth that is around 5% for one slot and 2% for two-slot-array, of the operating frequency, respectively.

6.6 Gain

The technique to make relative-gain measurement are based on Friis transmission formula [6-7]. The antennas are separated by a distance R, and it must satisfy the far-field criterion of each antennas. For polarization matched antennas, aligned for maximum directional radiation, the formula can be written in logarithmic decibel form as

$$(G_{0t})_{dB} + (G_{0r})_{dB} = 20\log_{10}\left(\frac{4\pi R}{\lambda}\right) + 10\log_{10}\left(\frac{P_r}{P_t}\right) \qquad (6.1)$$

where $(G_{0t})_{dB}$ denotes gain of the transmitting antenna. In the measurement, the pyramidal horn antenna with gain 12.4 dB at the operating frequency 10 GHz is employed to be the transmitting antenna. $(G_{0r})_{dB}$ represents gain of the antenna under test. P_r and P_t are the received and transmitted power, respectively, and λ is the operating wavelength. The measured relative-gain of one slot and the slot array on the sectoral cylindrical cavity is shown in Fig. 6.13.

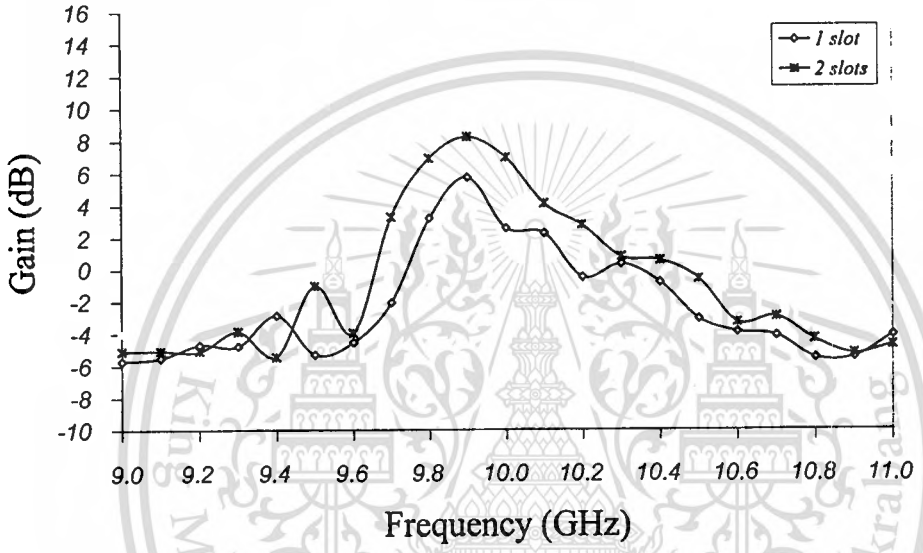

Fig.6.10 Relative-gain of one slot and two-slot array on the sectoral cylindrical cavity

In Fig.6.10, it is noted that the relative gain in the bandwidth of 20%, in case of one slot on the sectoral cylindrical cavity has smallest value, around 5.83 dB at the frequency 9.96 GHz. The relative-gain of two axial slots on the cavity has maximum value, around 8.31 dB at the frequency 9.9 GHz. Likewise, the bandwidth of the two-slot array is wider than one slot on the cavity.

6.7 The Antenna Prototype for UHF TV Broadcasting Station

As mentioned in the Chapter1 is this antenna will be developed and utilized for the broadcasting station antenna. The standard bandwidth of television transmission is based on 6 MHz RF assignments [6-5] in most parts

of the world. For the HDTV (High Definition Television), 30 MHz of video and sound can be digitized and compressed before transmitting in 6 MHz of this specific bandwidth [6-6]. To verify that the proposed antenna has sufficiently wide bandwidth that can respond this standard, we design an antenna at the operating frequency of 806 MHz (UHF TV channel 69) in true scale by using geometrical scale modeling [6-7], as shown in Fig.6.11.

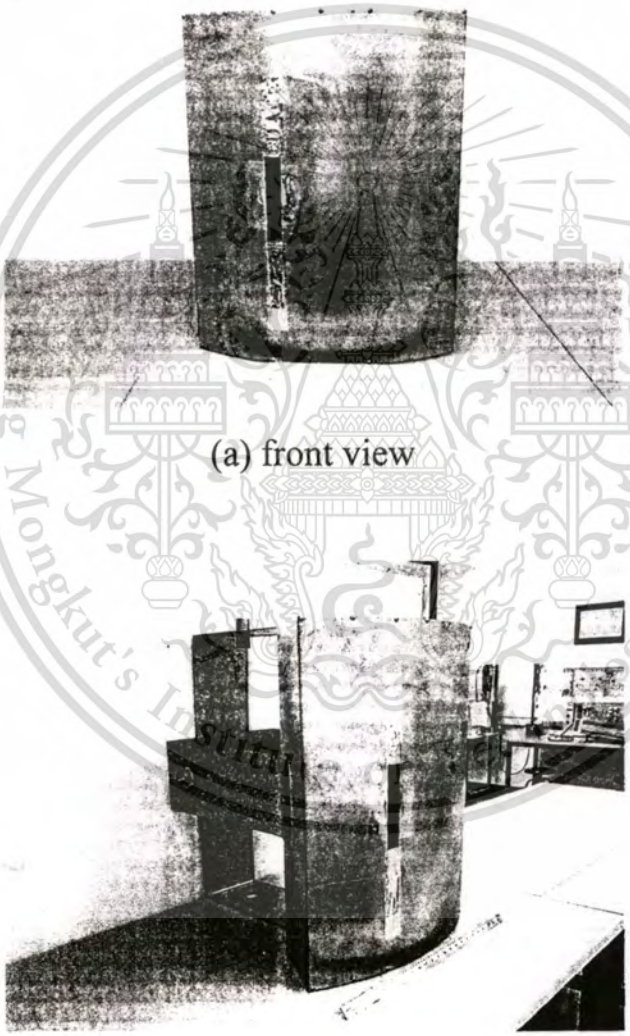

(a) front view

(b) side view

Fig.6.11 Photograph of a slot on the sectoral cylindrical cavity at 806 MHz (UHF TV channel)

Since the fabricated antenna in Fig.6.11 is constructed by using geometrical scale modeling, therefore only the experimental results will be illustrated. The radiation pattern and the impedance characteristics of this antenna are shown in Fig.6.12 and Fig.6.13.

The radiation Pattern in both elevational and azimuthal plane of a slot on the sectoral cylindrical cavity at the operating frequency of 806 MHz, as shown in Fig. 6.12 are similar to those of the antenna which is designed at the operating frequency of 10 GHz. The 3-dB beamwidth of the elevational and azimuthal patterns of 806 MHz-antenna are around 32.5° and 130°, respectively, while of 10 GHz-antenna are 53° and 128°, respectively.

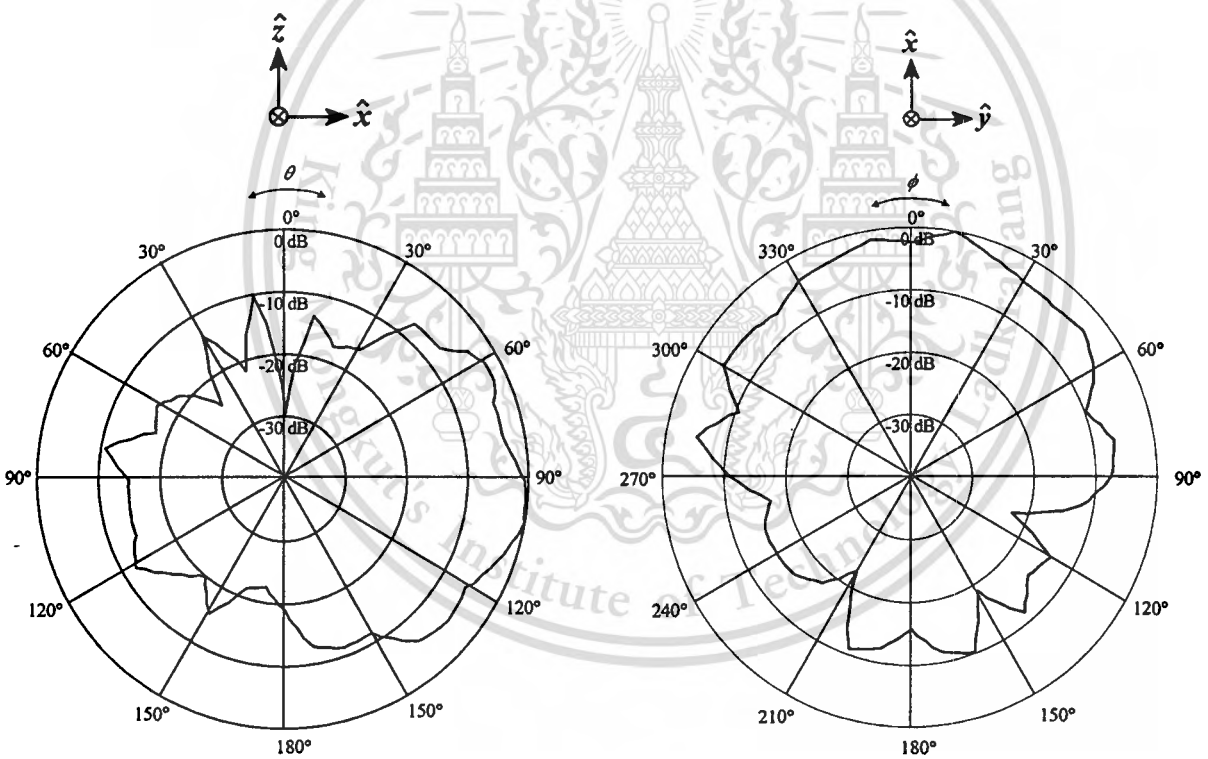

(a) Elevation pattern (b) Azimuthal pattern

Fig.6.12 Radiation pattern of a slot at 806 MHz

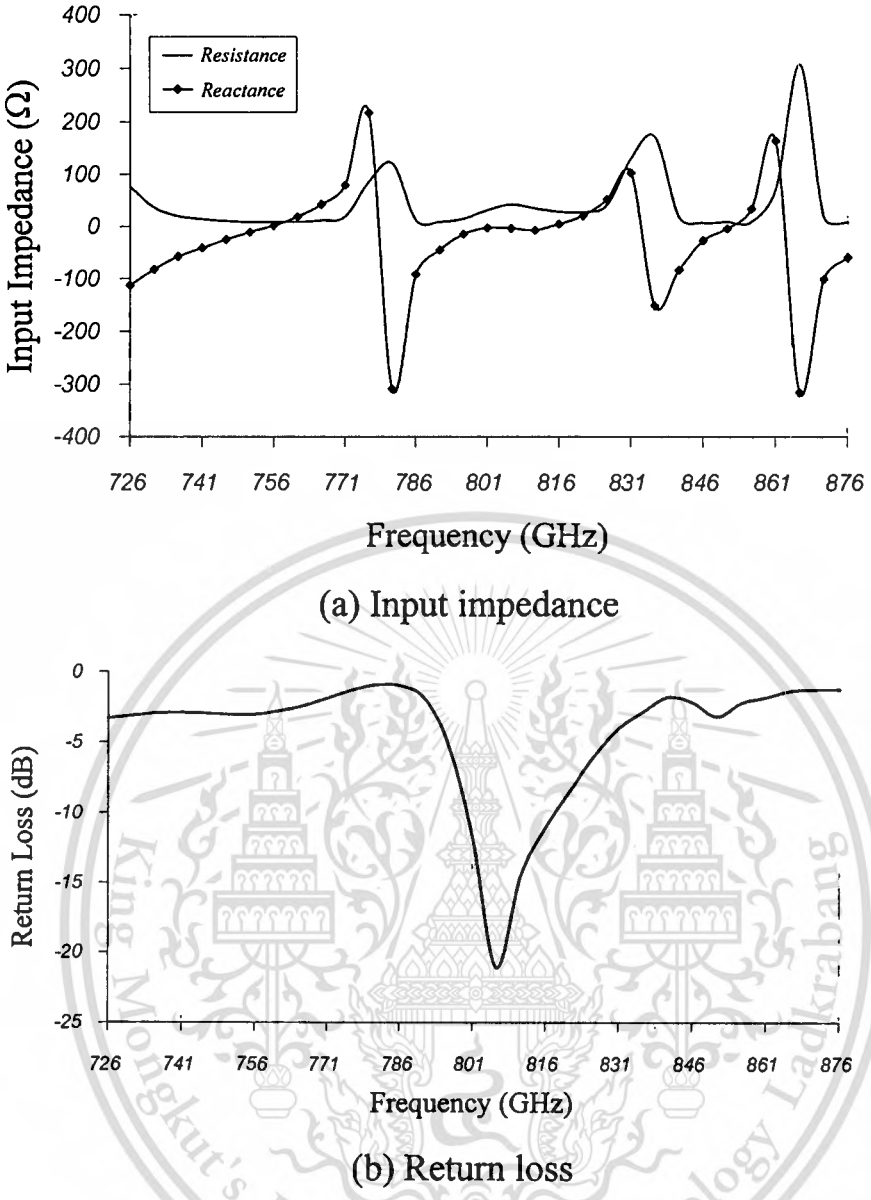

Fig.6.13 Impedance characteristics of a slot at 806 MHz

Fig.6.13 (a) shows the measured input impedance of the antenna by using HP8722D Network Analyzer. It is observed that the input resistance starts from value about 75.73 Ω at 726 MHz, then turns down to very small value and reaches the first peak value of 216.09 Ω at 776 MHz. It reduces to smaller value as the frequency is increased and reaches the second peak value of 42.89 Ω at 806 MHz. After that, it reduces again to smaller value as the frequency is increased and reaches the third peak value of 171.41 Ω at 836 MHz. Finally, it is decreased and reaches the last peak value of 306.2 Ω at 866 MHz. For

reactance, it starts from very small negative value of –112.57 Ω at 726 MHz and reaches its peak value at 776 MHz. The first resonance takes place at 753.5 MHz and the value turns out to be negative and becomes positive, alternately. From such phenomenon, the reactance will cross the zero value of 6 points. They are at 753.5, 778.5, 813.5, 833.5, 853.5, and 863.5 MHz. However, in Fig.6.13 (b), it is found that, the minimum value of return loss is at –21.089 dB at 806 MHz, precisely. Therefore, the bandwidth of this antenna will be determined at this point.

The bandwidth is determined at the value of return loss with no more than –10 dB respect to the minimum return loss at the operating frequency. From the information as described above, it is obvious that the antenna bandwidth is constrained by the impedance bandwidth that is around 2.25% of the operating frequency, or equal to 18 MHz. However, the accurate result within this 2.25% bandwidth is sufficient for many applications including the TV broadcasting [6-8].

Finally, gain of this prototype is also measured by using the same formula as described in the previous section, which is illustrated in Fig. 6.14.

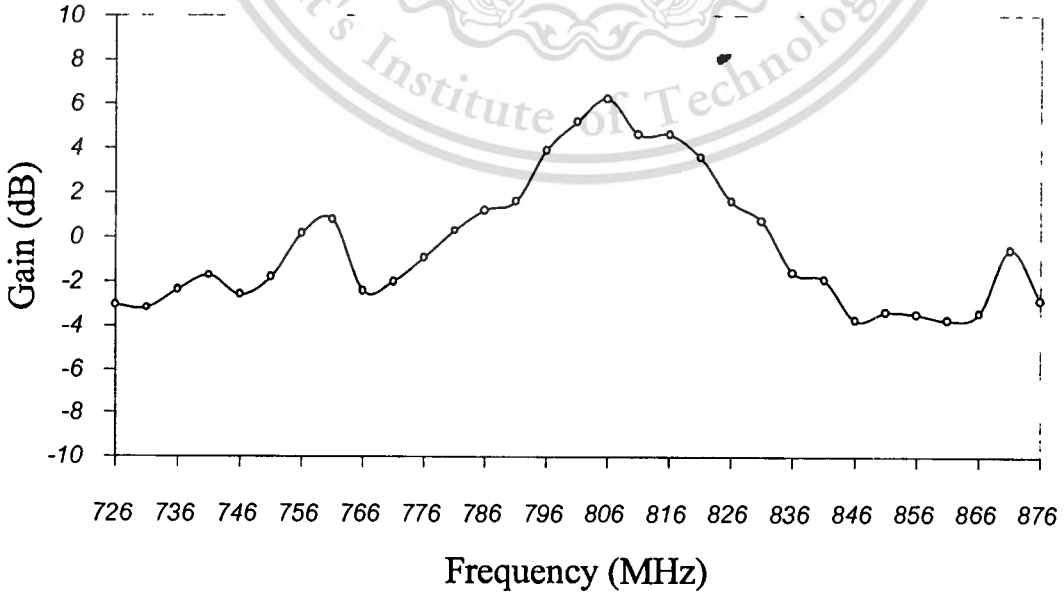

Fig. 6.14 Gain of the one slot at 806 MHz

In Fig.6.14, it is noted that the measured gain of the antenna prototype as shown in Fig. 6.14, is similar to of the one slot on the sectoral cylindrical cavity, which is operated at the frequency 10 GHz. The maximum value of gain at the operating frequency 806 MHz is about 6.04 dB. The values of –3dB are at the approximated frequency 793 MHz and 826 MHz, respectively. If we consider its bandwidth by using this criterion, the bandwidth will be at about 32 MHz.

6.8 Conclusions

The experiments of the radiation pattern and impedance characteristics were set up to verify the antenna characteristics that are theoretically investigated. It is apparent that the theoretical and experimental results are reasonably meet in agreement. These results exhibit that the antenna can work well in the practical situation. In addition, we can predict it accurately within a bandwidth of 2.25% at the operating frequency 806 MHz, which is sufficiently wide for applying to be the antenna for UHF TV broadcasting station in general applications.

References

[6-1] RWongsan, C.Phongcharoenpanich, M.Krairiksh and J.Takada, "Impedance Characteristic Analysis of an Axial Slot Antenna on a Sectoral Cylindrical Cavity Excited by a Probe using Method of Moments," *IEICE Trans. Fundamentals*, vol. E85-A, No.6, June 2003.

[6-2] *IEEE Standard Test Procedures for Antennas*, IEEE Std 149-1979, published by IEEE, Inc., 1979, distributed by Wiley-Interscience.

[6-3] G.E.Evans, *Antenna Measurement Techniques*, Sec.4.2, Artech House, Norwood, MA, 1990.

[6-4] International, Transmitting antenna characteristics at VHF and UHF, Recommendation ITU-R BS.1195, Telecommunication Union,1995.

[6-5] R.L.Freeman, *Telecommunication Transmission Handbook*, Sec.13.6, John Wiley & Sons Inc., Toronto, 1996.

[6-6] C.A.Balanis, *Antenna Theory*, Sec.16.10, John Wiley & Sons Inc., Toronto, 1982.

[6-7] C.Eilers, "Digital Television Transmission Parameters – Analysis and Discussion," *IEEE Trans. On Broadcasting*, vol. 45, No.4, December 1999.

Chapter 7

Discussions and Conclusions

Synopses of this thesis and discussions of the future studies are included in this chapter.

7.1 Summary of Preceding Chapters

As mentioned in the first chapter, this thesis proposes the so-called Sectoral Cylindrical Cavity-Backed Slot Array Antenna. This antenna type is categorized into the group of conformal antenna. The advantage of this antenna type is that its structure is simple since the power divider and the feeding structure are integrated into a single structure. Furthermore, this thesis is concentrated on the design of this antenna type to radiate in both vertically and horizontally polarized beam pattern for applying as the antenna for the base station of the mobile communication and the broadcasting station of the UHF television, which can radiate either unidirectional or omnidirectional pattern in azimuthal angle.

Then, the preliminarily geometry of a sectoral cylindrical cavity-backed slot array antenna is illustrated in Chapter 2. The expressions of the integral equations of two canonical regions of a sectoral cylindrical cavity-backed slot antenna that excited by a probe, in the form of the integration of the product between dyadic Green's functions and two unknown currents, are formulated by applying the Field Equivalent Principle and the boundary condition.

In Chapter 3, the various kinds of internal dyadic Green's functions of a sectoral cylindrical cavity that are essential to find the electromagnetic field inside this cavity is derived, rigorously, in series form, by using the eigenfunction expansions. Finally, the modal solutions of dyadic components of Green's functions for external region of the circular cylinder are shown. These

functions will be substituted into the integral equations and subsequently solved by Method of Moments in Chapter 4.

In Chapter 4, Method of Moments technique has been used to compute the magnetic current and the electric current at the aperture and the probe, respectively. Then the electric field is solved by using these currents. Subsequently, the radiation pattern of an axial half-wavelength slot on infinite cylindrical cavity with various sizes of outer radius is obtained. The radiation patterns both elevational and azimuthal ones are shown to analyze their radiation characteristics. It is obvious that the forming beams with various sizes of outer radius are slightly different and its back lobe can be adjusted by varying the outer radius of the cavity. The directivity and front-to-back ratio of this antenna is calculated to find the optimum parameters that is sufficient for using in practical applications. Finally, the impedance characteristics of the antenna at desired resonant frequency are analyzed to clarify matching condition of the antenna when connected to the 50 Ω-transmission line. The matching condition is improved by adjusting the cavity length, cavity radius ratio, slot location, slot length, and probe length. According to the results of the analysis, the antenna with the acceptable properties is designed for verifying with the experiment in Chapter 6.

Chapter 5 expresses the formulas of a slot array on the sectoral cylindrical cavity excited by probe. This antenna yields either vertical or horizontal polarization by cutting slots on the outer surface of cavity in circumferential and axial direction, respectively. Furthermore, this chapter analyzes the influence of the outer radius of cavity, the spacing between slots that affects radiation pattern and impedance characteristics of the antenna.

Chapter 6 verifies the principle and theory presented in the previous chapters. With the appropriate parameters, the antenna prototype is fabricated to test its characteristics. The experiments were set up to measure the radiation

pattern, input impedance and return loss of the antenna. The reasonably agreement between the theoretical and experimental results are acquired. From the comparison, it confirms that this antenna is very useful and serviceable for the mobile base station and UHF-television broadcasting station. Finally, the summaries of the material in this thesis and the discussion for the future studies are included in chapter 7, the last chapter. Appendices consist of, the first, includes the Bessel and Neumann function of the sectoral cylindrical cavity and the second presents the components of dyadic Green's functions for the sectoral cylindrical cavity.

7.2 Remark for Future Studies

Since the aim of this thesis is to study the sectoral cylindrical cavity-backed slot array antenna, the antenna characteristics are investigated and analyzed. The ultimate goal of this thesis is to design the antenna to radiate either the horizontally or vertically polarized radiation for the specific application as previously described. However, there are many strategies to design this antenna for various aspects of the applications. Therefore, the antenna feature will be different from one presented in this thesis, for example it is possible to employ this antenna to radiate the omnidirectional beam instead of only the unidirectional beam that is out of scope of this thesis. Moreover, omnidirectional beam antenna design to use the single excited probe, for power divider saving, is also left for further study.

In addition, this thesis is mainly concerned with the investigation of the sectoral cylindrical cavity-backed slot array antenna, which yields the horizontal polarization. The feasibility for applications of the UHF TV broadcasting base station antenna is offered. Nevertheless, to really apply this antenna to this application, the propagation model taken into account that the environment should be significantly conducted. This is left for further works as well.

Moreover, the radome that is very useful to prevent this antenna from any environmental damage is another topic that is open for other researchers.

In the theoretical viewpoint, since the assumption of the calculation is based on the infinite length of circular cylinder of the external dyadic Green's functions, the effect of the shadow region of the actual structure is neglected. Therefore, the diffraction effect of the finite sectoral cylindrical surface should be taken into consideration to get more precise results. This work is left for future investigations.

Last but not least, the wall thickness of the sectoral cylindrical cavity enclosed by the conducting surface in this thesis is ideally assumed to be very thin and disregarded. Beside that, the excited probe is also ideally assumed to be very thin so as to disregard the diameter. For more accurate results, this phenomenon should be taken into account in the calculations.

Appendices

Appendix A

Bessel and Neumann Functions of the Sectoral Cylindrical Cavity

The structure of the sectoral cylindrical cavity is modified from the basic configuration of coaxial cylinder. Therefore, the dyadic Green's functions are also based on formulating with Bessel-Neumann combination function in radial coordinate together with the trigonometric function in ϕ - coordinates and the exponential function in z- coordinates as of coaxial cylinder [A-1]. Nevertheless, the dyadic Green's function can be solved when we know the roots of zero of the ordinary sectoral cylindrical Bessel-Neumann function ratio. Therefore, this appendix explains only Bessel-Neumann combination function of the sectoral cylindrical cavity and the means for solving required roots in both TM and TE modes.

A-1 TM Modes: Sectoral Cylindrical Cavity

By expanding the transverse component wave equation for E_z in cylindrical coordinates:

$$\frac{1}{\rho}\frac{\partial}{\partial\rho}\left(\rho\frac{\partial E_z}{\partial\rho}\right)+\frac{1}{\rho^2}\frac{\partial^2 E_z}{\partial\phi^2}+k_e^2E_z=0 \tag{A.1}$$

By using the separation of variable method. The results is

$$E_z(\rho,\phi)=\left(A'\cos\upsilon\phi+B'\sin\upsilon\phi\right)\left[C'J_\upsilon(k_e\rho)+D'Y_\upsilon(k_e\rho)\right] \tag{A.2}$$

We select the reference for $\phi=0$ so we have only the cosine variation. Setting $B'=0$ and multiplying the constant A' into the C' and D' to get new constants C and D yields

$$E_z(\rho,\phi)=\left[CJ_\upsilon(k_e\rho)+DY_\upsilon(k_h\rho)\right]\cos\upsilon\phi \tag{A.3}$$

Since E_z will be a tangential component of electric field at the metal boundaries at $\rho=\rho_a$ and $\rho=\rho_b$ it must be zero there. This yields the two boundary conditions

$$E_z(\rho_a,\phi)=\left[CJ_\upsilon(k_e\rho_a)+DY_\upsilon(k_h\rho_a)\right]\cos\upsilon\phi=0$$

$$E_z(\rho_b,\phi)=\left[CJ_\upsilon(k_e\rho_b)+DY_\upsilon(k_h\rho_b)\right]\cos\upsilon\phi=0$$

Since these must be true for any ϕ, the cos $n\phi$ coefficients must be zero:

$$\left.\begin{aligned}CJ_\upsilon(k_e\rho_a)+DY_\upsilon(k_e\rho_a)=0\\ CJ_\upsilon(k_e\rho_b)+DY_\upsilon(k_e\rho_b)=0\end{aligned}\right\} \tag{A.4}$$

We have used all the independent boundary conditions. There are, however, three unknowns, C, D, and k_e. One obvious solution is to have $C = D = 0$. This will not do since E_z from (A.3) would be zero everywhere. Thus C and D are not zero. From linear algebra we know that a set of equations in unknowns C and D that are all equal to zero can have nonzero solutions for C and D if the determinant of the coefficients is zero. Therefore

$$\begin{vmatrix}J_\upsilon(k_e\rho_a) & Y_\upsilon(k_e\rho_a)\\ J_\upsilon(k_e\rho_b) & Y_\upsilon(k_e\rho_b)\end{vmatrix}=0$$

$$J_\upsilon(k_e\rho_a)Y_\upsilon(k_e\rho_b)-J_\upsilon(k_e\rho_b)Y_\upsilon(k_e\rho_a)=0 \tag{A.5}$$

This is called the Bessel-Neumann combination boundary condition. For a given integer υ (circumferential mode number) and given guide dimensions ρ_a and ρ_b, only k_e remains to be determined. Since the equation is transcendental it must be solved either numerically or graphically. The graphical solution is obtained by first

moving the negative term to the right side of the equation and then naming each side as a function of k_e. We then set

$$y_1(k_e) = J_\upsilon(k_e\rho_a)Y_\upsilon(k_e\rho_b) = J_\upsilon(k_e\rho_b\rho_a)Y_\upsilon(k_e\rho_a) = y_2(k_e) \tag{A.6}$$

We next plot y_1 and y_2 versus k_e (for given υ, ρ_a and ρ_b) on the same set of axes. The intersections of y_1 and y_2 identify the allowed values of k_e. Since there will be several intersections for each value of υ we identify them with a second subscript l.

The modes would be denoted by the mode conversion

$$\mathrm{TM}_{\upsilon l}, \quad \text{when} \quad \upsilon = \frac{m\pi}{\phi_c}, \qquad m = 1,2,3,\ldots \quad l = 1,2,3,\ldots$$

The lower-order values of k_e are given in Table A.1. Note that the table does not give k_e directly but depends upon a modification of Bessel-Neumann combination, Eq.(A.5). Letting this

$$x = k_e\rho_a$$

from which

$$k_e = \frac{x}{\rho_a} \tag{A.7}$$

Substituting this into Eq. (A.5)

$$J_\upsilon(x)Y_\upsilon\left(\frac{\rho_b}{\rho_a}x\right) - J_\upsilon\left(\frac{\rho_b}{\rho_a}x\right)Y_\upsilon(x) = 0 \tag{A.8}$$

Table A.1 Roots of Bessel-Neumann boundary condition (Eq.A.8):

Table values are $(\rho_b/\rho_a - 1)x_{vl}$

ρ_b / ρ_a	vl 01	11	21	31	02	12	22	32
1.0	*3.142*	*3.142*	*3.142*	*3.142*	*6.283*	*6.283*	*6.283*	*6.283*
1.1	*3.141*	*3.143*	*3.147*	*3.154*	*6.283*	*6.284*	*6.286*	*6.289*
1.2	*3.140*	*3.146*	*3.161*	*3.187*	*6.282*	*6.285*	*6.293*	*6.306*
1.3	*3.139*	*3.150*	*3.182*	*3.236*	*6.282*	*6.287*	*6.304*	*6.331*
1.4	*3.137*	*3.155*	*3.208*	*3.294*	*2.281*	*2.290*	*2.317*	*6.362*
1.5	*3.135*	*3.161*	*3.237*	*3.36*	*6.280*	*6.293*	*6.332*	*6.387*
1.6	*3.133*	*3.168*	*3.27*	*3.43*	*6.279*	*6.296*	*6.349*	*6.437*
1.8	*3.128*	*3.182*	*3.36*	*3.6*	*6.276*	*6.304*	*6.387*	*6.523*
2.0	*3.123*	*3.197*	*3.4*	*3.7*	*6.273*	*6.312*	*6.43*	*6.62*

ρ_b / ρ_a	vl 03	13	23	33	04	14	24	34
1.0	*9.425*	*9.425*	*9.425*	*9.425*	*12.566*	*12.566*	*12.566*	*12.566*
1.1	*9.425*	*9.425*	*9.427*	*9.429*	*12.566*	*12.567*	*12.568*	*12.569*
1.2	*9.424*	*9.426*	*9.431*	*9.440*	*12.566*	*12.567*	*12.571*	*12.578*
1.3	*9.424*	*9.427*	*9.438*	*9.457*	*12.566*	*12.568*	*12.577*	*12.590*
1.4	*9.423*	*9.429*	*9.447*	*9.478*	*12.565*	*12.570*	*12.583*	*12.606*
1.5	*9.423*	*9.431*	*9.458*	*9.502*	*12.565*	*12.571*	*12.591*	*12.624*
1.6	*9.422*	*9.434*	*9.469*	*9.528*	*12.564*	*12.573*	*12.600*	*12.644*
1.8	*9.420*	*9.439*	*9.495*	*9.587*	*12.563*	*12.577*	*12.619*	*12.689*
2.0	*9.418*	*9.444*	*9.523*	*9.652*	*12.561*	*12.581*	*12.640*	*12.738*

The values in the table are $(\rho_b/\rho_a - 1)x_{vl}$, so for given values of ρ_a , ρ_b, v, and l we read the value from the table and then obtain $k_{e,vl}$, using

$$k_{e,\upsilon l} = \frac{x_{\upsilon l}}{\rho_a} = \frac{\left[\dfrac{\text{table mode value}}{\left(\dfrac{\rho_b}{\rho_a} - 1\right)}\right]}{\rho_a} = \frac{\text{table mode value}}{\rho_b - \rho_a} \tag{A.9}$$

Once the value of k_e has been determined the value of D (or C, the choice is immaterial) can be obtained using either equation in the boundary condition set of (A.4). Solving the second of those equations for D, we obtain

$$D = -\frac{J_\upsilon(k_e\rho_b)}{Y_\upsilon(k_e\rho_b)}C \tag{A.10}$$

Finally, we obtain the solution for $E_z(\rho,\phi)$ using this result in (A.2)

$$E_z(\rho,\phi) = C\left[J_\upsilon(k_e\rho) - \frac{J_\upsilon(k_e\rho_b)}{Y_\upsilon(k_e\rho_b)}Y_\upsilon(k_e\rho)\right]\cos\upsilon\phi \tag{A.11}$$

The propagation constant is

$$k_{ge} = \sqrt{k_e^2 - k^2} = j\sqrt{k^2 - k_e^2} = j\sqrt{\omega^2\mu\varepsilon - k_e^2} \tag{A.12}$$

where we use (A.9) for k_e.

A-2 TE Modes: Sectoral Cylindrical Cavity

Values of k_h for this system are found from roots of the Bessel-Neumann derivative combination boundary condition

$$J'_\upsilon(k_h\rho_a)Y'_\upsilon(k_h\rho_b) - J'_\upsilon(k_h\rho_b)Y'_\upsilon(k_h\rho_a) = 0 \tag{A.13}$$

A more convenient form for tabulating values is obtained by letting

$$x' = k_h\rho_a \tag{A.14}$$

from which $k_h = x'/\rho_a$. The boundary condition becomes

$$J'_\upsilon(x')Y'_\upsilon\left(\frac{\rho_b}{\rho_a}x'\right) - J'_\upsilon\left(\frac{\rho_b}{\rho_a}x'\right)Y'_\upsilon(x') = 0 \qquad \text{(A.15)}$$

The boundary equation must be solved graphically, in general, as explained in the preceding section. Table A.2 supplies the first few values from which the k_h can be determined. The resulting modes are denoted by the usual mode convention :

$$\text{TE}_{vl}, \quad \text{when} \quad \upsilon = \frac{m\pi}{\phi_c}, \qquad m = 1,2,3,\ldots. \quad l = 1,2,3,\ldots.$$

Table A.2 Roots of Bessel-Neumann derivative boundary condition (Eq.A.15):

Table values are $(\rho_b/\rho_a - 1)x_{vl}$

ρ_b / ρ_a	vl							
	01	11	21	31	02	12	22	32
1.001	*3.141*	*3.141*	*3.141*	*3.141*	*6.283*	*6.283*	*6.283*	*6.283*
1.1	*3.142*	*0.095*	*0.190*	*0.285*	*6.283*	*3.144*	*3.148*	*3.155*
1.2	*4.145*	*0.182*	*0.364*	*0.546*	*6.285*	*3.150*	*3.166*	*3.193*
1.3	*3.149*	*0.261*	*0.523*	*0.784*	*6.287*	*3.160*	*3.194*	*3.248*
1.4	*3.154*	*0.334*	*0.669*	*1.002*	*6.289*	*3.173*	*3.228*	*3.318*
1.5	*3.160*	*0.402*	*0.804*	*1.203*	*6.293*	*3.188*	*3.269*	*3.400*
1.6	*3.167*	*0.465*	*0.928*	*1.387*	*6.296*	*3.204*	*3.314*	*3.490*
1.8	*3.181*	*0.578*	*1.150*	*1.710*	*6.304*	*3.241*	*3.416*	*3.694*
2.0	*3.196*	*0.677*	*1.340*	*1.978*	*6.312*	*3.282*	*3.531*	*3.920*

ρ_b / ρ_a	vl							
	03	13	23	33	04	14	24	34
1.001	*9.424*	*9.424*	*9.424*	*9.424*	*12.566*	*12.566*	*12.566*	*12.566*
1.1	*9.425*	*6.284*	*6.286*	*6.290*	*12.566*	*9.425*	*9.427*	*9.429*
1.2	*9.426*	*6.287*	*6.295*	*6.309*	*12.567*	*9.427*	*9.433*	*9.442*
1.3	*9.427*	*6.292*	*6.309*	*6.336*	*12.568*	*9.431*	*9.442*	*9.460*
1.4	*9.429*	*6.299*	*6.326*	*6.371*	*12.569*	*9.435*	*9.453*	*9.483*
1.5	*9.431*	*6.306*	*6.346*	*6.412*	*12.571*	*9.440*	*9.466*	*9.510*
1.6	*9.433*	*6.314*	*6.368*	*6.457*	*12.573*	*9.445*	*9.481*	*9.541*
1.8	*9.438*	*6.332*	*6.418*	*6.559*	*12.576*	*9.457*	*9.514*	*9.608*
2.0	*9.444*	*6.353*	*6.474*	*6.673*	*12.581*	*9.471*	*9.551*	*9.684*

For given values of υ and l (mode numbers) we take the value from Table (A.2) and compute k_h using

$$k_{h,\upsilon l} = \frac{\text{table mode value}}{\left(\frac{\rho_b}{\rho_a} - 1\right)} \frac{x_{\upsilon l}}{\rho_a} = \frac{\text{table mode value}}{\rho_b - \rho_a} \tag{A.16}$$

The propagation constant is then found using

$$k_{gh} = \sqrt{k_h^2 - k^2} = j\sqrt{k^2 - k_h^2} = j\sqrt{\omega^2 \mu\varepsilon - k_h^2} \tag{A.17}$$

where we use (A.16) for k_h.

Finally, when k_e and k_h are known. The dyadic Green's function will be fulfilled and solved, subsequently.

References

[A-1] G.F.Miner, Lines and Electromagnetic Fields for Engineers, Sec.9.3, New York: Oxford University Press, 1996.

Appendix B

The Components of Dyadic Green's Functions for a Sectoral Cylindrical Cavity

The dyadic Green's functions inside a sectoral cylindrical cavity can be obtained by the method of scattering superposition [B-1] as described in chapter 3. All components of four sets of dyadic Green's function for electric and magnetic fields due to the electric and magnetic current sources are expanded from their products of vector wave functions. We can use their components to involve any problems of electromagnetic fields in the structure of the sectoral cylindrical cavity that the component selection will be suggested in the end of this appendix.

B-1 Magnetic Field due to the Magnetic Current Source

$$\begin{aligned}\overline{\overline{G}}_{HM}\left(\bar{R},\bar{R}'\right) = &-\frac{1}{k^2}\hat{z}\hat{z}\delta\left(\bar{R}-\bar{R}'\right) \\ &+2j\sum_{m,n}\begin{cases}\dfrac{A_h}{\sin\left(k_{gh}z_d\right)}\begin{bmatrix}\bar{N}_{h,odd}\left(z_d-z\right)\bar{N}'_{h,odd}\left(z'\right)\\ \bar{N}_{h,odd}\left(z\right)\bar{N}'_{h,odd}\left(z_d-z'\right)\end{bmatrix} \\ -\dfrac{A_e}{\sin\left(k_{ge}z_d\right)}\begin{bmatrix}\bar{M}_{e,even}\left(z_d-z\right)\bar{M}'_{e,even}\left(z'\right)\\ \bar{M}_{e,even}\left(z\right)\bar{M}'_{e,even}\left(z_d-z'\right)\end{bmatrix}\end{cases}, \begin{matrix} z>z' \\ z<z'\end{matrix}\end{aligned} \tag{B.1}$$

when $z > z'$, the vector wave functions in bracket can be expanded as follow

$$\begin{aligned}\bar{N}_{h,odd}\left(z_d-z\right)\bar{N}'_{h,odd}\left(z'\right) = \frac{1}{k^2}\Bigg\{ &-k_{gh}^2\frac{\partial B_\upsilon\left(k_h\rho\right)}{\partial\rho}\frac{\partial B_\upsilon\left(k_h\rho'\right)}{\partial\rho'}\cos\left(\upsilon\phi\right)\cos\left(\upsilon\phi'\right)\sin k_{gh}\left(z_d-z\right)\sin\left(k_{gh}z'\right)\hat{\rho}\hat{\rho} \\ &-\frac{\upsilon k_{gh}^2}{\rho'}\frac{\partial B_\upsilon\left(k_h\rho\right)}{\partial\rho}B_\upsilon\left(k_h\rho'\right)\cos\left(\upsilon\phi\right)\sin\left(\upsilon\phi'\right)\sin k_{gh}\left(z_d-z\right)\sin\left(k_{gh}z'\right)\hat{\rho}\hat{\phi} \\ &+k_{gh}k_h^2\frac{\partial B_\upsilon\left(k_h\rho\right)}{\partial\rho}B_\upsilon\left(k_h\rho'\right)\cos\left(\upsilon\phi\right)\cos\left(\upsilon\phi'\right)\sin k_{gh}\left(z_d-z\right)\cos\left(k_{gh}z'\right)\hat{\rho}\hat{z}\end{aligned}$$

$$+\frac{\upsilon k_{gh}^2}{\rho}B_\upsilon(k_h\rho)\frac{\partial B_\upsilon(k_h\rho')}{\partial\rho'}\sin(\upsilon\phi)\cos(\upsilon\phi')\sin k_{gh}(z_d-z)\sin(k_{gh}z')\hat{\phi}\hat{\rho}$$

$$+\frac{\upsilon^2 k_{gh}^2}{\rho\rho'}B_\upsilon(k_h\rho)B_\upsilon(k_h\rho')\sin(\upsilon\phi)\sin(\upsilon\phi')\sin k_{gh}(z_d-z)\sin(k_{gh}z')\hat{\phi}\hat{\phi}$$

$$-\frac{\upsilon k_{gh}k_h^2}{\rho}B_\upsilon(k_h\rho)B_\upsilon(k_h\rho')\sin(\upsilon\phi)\cos(\upsilon\phi')\sin k_{gh}(z_d-z)\cos(k_{gh}z')\hat{\phi}\hat{z}$$

$$-k_{gh}k_h^2B_\upsilon(k_h\rho)\frac{\partial B_\upsilon(k_h\rho')}{\partial\rho'}\cos(\upsilon\phi)\cos(\upsilon\phi')\cos k_{gh}(z_d-z)\sin(k_{gh}z')\hat{z}\hat{\rho}$$

$$-\frac{nk_{gh}k_h^2}{\rho'}B_\upsilon(k_h\rho)B_\upsilon(k_h\rho')\cos(\upsilon\phi)\sin(\upsilon\phi')\cos k_{gh}(z_d-z)\sin(k_{gh}z')\hat{z}\hat{\phi}$$

$$+k_h^4B_\upsilon(k_h\rho)B_\upsilon(k_h\rho')\cos(\upsilon\phi)\cos(\upsilon\phi')\cos k_{gh}(z_d-z)\sin(k_{gh}z')\hat{z}\hat{z}\Big\}$$

(B.2)

$$\bar{M}_{e,even}(z_d-z)\bar{M}'_{e,even}(z')=\frac{\upsilon^2}{\rho\rho'}B_\upsilon(k_e\rho)B_\upsilon(k_e\rho')\cos(\upsilon\phi)\cos(\upsilon\phi')\sin k_{ge}(z_d-z)\sin(k_{ge}z')\hat{\rho}\hat{\rho}$$

$$-\frac{\upsilon}{\rho}B_\upsilon(k_e\rho)\frac{\partial B_\upsilon(k_e\rho')}{\partial\rho'}\cos(\upsilon\phi)\sin(\upsilon\phi')\sin k_{ge}(z_d-z)\sin(k_{ge}z')\hat{\rho}\hat{\phi}$$

$$-\frac{\upsilon}{\rho'}\frac{\partial B_\upsilon(k_e\rho)}{\partial\rho}B_\upsilon(k_e\rho')\sin(\upsilon\phi)\cos(\upsilon\phi')\sin k_{ge}(z_d-z)\sin(k_{ge}z')\hat{\phi}\hat{\rho}$$

$$+\frac{\partial B_\upsilon(k_e\rho)}{\partial\rho}\frac{\partial B_\upsilon(k_e\rho')}{\partial\rho'}\sin(\upsilon\phi)\sin(\upsilon\phi')\sin k_{ge}(z_d-z)\sin(k_{ge}z')\hat{\phi}\hat{\phi}$$

(B.3)

when $z<z'$, the vector wave functions in bracket can be expanded as follow

$$\bar{N}_{h,odd}(z)\bar{N}'_{h,odd}(z_d-z')=\frac{1}{k^2}\Big\{-k_{gh}^2\frac{\partial B_\upsilon(k_h\rho)}{\partial\rho}\frac{\partial B_\upsilon(k_h\rho')}{\partial\rho'}\cos(\upsilon\phi)\cos(\upsilon\phi')\sin(k_{gh}z)\sin k_{gh}(z_d-z')\hat{\rho}\hat{\rho}$$

$$+\frac{\upsilon k_{gh}^2}{\rho'}\frac{\partial B_\upsilon(k_h\rho)}{\partial\rho}B_\upsilon(k_h\rho')\cos(\upsilon\phi)\sin(\upsilon\phi')\sin(k_\mu z)\sin k_\mu(z_d-z')\hat{\rho}\hat{\phi}$$

$$-k_{gh}^2k_h^{\,2}\frac{\partial B_\upsilon(k_h\rho)}{\partial\rho}B_\upsilon(k_h\rho')\cos(\upsilon\phi)\cos(\upsilon\phi')\sin(k_{gh}z)\cos k_{gh}(z_d-z')\hat{\rho}\hat{z}$$

$$-\frac{\upsilon k_{gh}^2}{\rho}B_\upsilon(k_h\rho)\frac{\partial B_\upsilon(k_h\rho')}{\partial\rho'}\sin(\upsilon\phi)\cos(\upsilon\phi')\sin(k_{gh}z)\sin k_{gh}(z_d-z')\hat{\phi}\rho$$

$$+\frac{\upsilon^2 k_{gh}^2}{\rho\rho'} B_\upsilon(k_h\rho) B_\upsilon(k_h\rho') \sin(\upsilon\phi) \sin(\upsilon\phi') \sin(k_{gh} z) \sin k_{gh}(z_d - z') \hat{\phi}\hat{\phi}$$

$$-\frac{\upsilon k_{gh} k_h^{\,2}}{\rho} B_\upsilon(k_h\rho) B_\upsilon(k_h\rho') \sin(\upsilon\phi) \cos(\upsilon\phi') \sin(k_{gh} z) \cos k_{gh}(z_d - z') \hat{\phi}\hat{z}$$

$$+k_{gh} k_h^2 B_\upsilon(k_h\rho) \frac{\partial B_\upsilon(k_h\rho')}{\partial\rho'} \cos(\upsilon\phi) \cos(\upsilon\phi') \cos(k_{gh} z) \sin k_{gh}(z_d - z') \hat{z}\hat{\rho}$$

$$-\frac{\upsilon k_{gh} k_h^2}{\rho'} B_\upsilon(k_h\rho) B_\upsilon(k_h\rho') \cos(\upsilon\phi) \sin(\upsilon\phi') \cos(k_{gh} z) \sin k_{gh}(z_d - z') \hat{z}\hat{\phi}$$

$$+k_h^4 B_\upsilon(k_h\rho) B_\upsilon(k_h\rho') \cos(\upsilon\phi) \cos(\upsilon\phi') \cos(k_{gh} z) \sin k_{gh}(z_d - z') \hat{z}\hat{z}\Big\} \tag{B.4}$$

$$\bar{M}_{e,even}(z) \bar{M}'_{e,even}(z_d - z') = \frac{\upsilon^2}{\rho\rho'} B_\upsilon(k_e\rho) B_\upsilon(k_e\rho') \cos(\upsilon\phi) \cos(\upsilon\phi') \sin(k_{ge} z) \sin k_{ge}(z_d - z') \hat{\rho}\hat{\rho}$$

$$-\frac{\upsilon}{\rho} B_\upsilon(k_e\rho) \frac{\partial B_\upsilon(k_e\rho')}{\partial\rho'} \cos(\upsilon\phi) \sin(\upsilon\phi') \sin(k_{ge} z) \sin k_{ge}(z_d - z') \hat{\rho}\hat{\phi}$$

$$-\frac{\upsilon}{\rho'} \frac{\partial B_\upsilon(k_e\rho)}{\partial\rho} B_\upsilon(k_e\rho') \sin(\upsilon\phi) \cos(\upsilon\phi') \sin(k_{ge} z) \sin k_{ge}(z_d - z') \hat{\phi}\hat{\rho}$$

$$+\frac{\partial B_\upsilon(k_e\rho)}{\partial\rho} \frac{\partial B_\upsilon(k_e\rho')}{\partial\rho'} \sin(\upsilon\phi) \sin(\upsilon\phi') \sin(k_{ge} z) \sin k_{ge}(z_d - z') \hat{\phi}\hat{\phi} \tag{B.5}$$

B-2 Electric Field due to the Electric Current Source

$$\bar{\bar{G}}_{EJ}(\bar{R}, \bar{R}') = -\frac{1}{k^2} \hat{z}\hat{z} \delta(\bar{R} - \bar{R}')$$

$$+2j \sum_{m,n} \left\{ \frac{A_h}{\sin(k_{gh} z_d)} \begin{bmatrix} \bar{M}_{h,odd}(z_d - z) \bar{M}'_{h,odd}(z') \\ \bar{M}_{h,odd}(z) \bar{M}'_{h,odd}(z_d - z') \end{bmatrix} \right.$$

$$\left. -\frac{A_e}{\sin(k_{ge} z_d)} \begin{bmatrix} \bar{N}_{e,even}(z_d - z) \bar{N}'_{e,even}(z') \\ \bar{N}_{e,even}(z) \bar{N}'_{e,even}(z_d - z') \end{bmatrix} \right\} \begin{matrix} z > z' \\ , z < z' \end{matrix} \tag{B.6}$$

when $z > z'$, the expansion of vector wave functions in bracket are

$$\begin{aligned}\bar{M}_{o,odd}(z_d - z)\bar{M}'_{o,odd}(z') = {} & \frac{\upsilon^2}{\rho\rho'} B_\upsilon(k_h\rho) B_\upsilon(k_h\rho') \sin(\upsilon\phi)\sin(\upsilon\phi')\sin k_{gh}(z_d - z)\sin(k_{gh}z')\hat{\rho}\hat{\rho} \\ & + \frac{\upsilon}{\rho} B_\upsilon(k_h\rho)\frac{\partial B_\upsilon(k_h\rho')}{\partial\rho'}\sin(\upsilon\phi)\cos(\upsilon\phi')\sin k_{gh}(z_d - z)\sin(k_{gh}z')\hat{\rho}\hat{\phi} \\ & - \frac{\upsilon}{\rho'}\frac{\partial B_\upsilon(k_h\rho)}{\partial\rho} B_\upsilon(k_h\rho')\cos(\upsilon\phi)\sin(\upsilon\phi')\sin k_{gh}(z_d - z)\sin(k_{gh}z')\hat{\phi}\hat{\rho} \\ & + \frac{\partial B_\upsilon(k_h\rho)}{\partial\rho}\frac{\partial B_\upsilon(k_h\rho')}{\partial\rho'}\cos(\upsilon\phi)\cos(\upsilon\phi')\sin k_{gh}(z_d - z)\sin(k_{gh}z')\hat{\phi}\hat{\phi}\end{aligned} \tag{B.7}$$

$$\begin{aligned}\bar{N}_{e,even}(z_d - z)\bar{N}'_{e,even}(z') = \frac{1}{k^2}\Big\{ & -k_{ge}^2\frac{\partial B_\upsilon(k_e\rho)}{\partial\rho}\frac{\partial B_\upsilon(k_e\rho')}{\partial\rho'}\cos(\upsilon\phi)\cos(\upsilon\phi')\sin k_\lambda(z_d - z)\sin(k_\lambda z')\hat{\rho}\hat{\rho} \\ & + \frac{\upsilon k_{ge}^2}{\rho'}\frac{\partial B_\upsilon(k_e\rho)}{\partial\rho} B_\upsilon(k_e\rho')\cos(\upsilon\phi)\sin(\upsilon\phi')\sin k_{ge}(z_d - z)\sin(k_{ge}z')\hat{\rho}\hat{\phi} \\ & - k_{ge}k_e^2\frac{\partial B_\upsilon(k_e\rho)}{\partial\rho} B_\upsilon(k_e\rho')\cos(\upsilon\phi)\cos(\upsilon\phi')\sin k_{ge}(z_d - z)\cos(k_{ge}z')\hat{\rho}\hat{z} \\ & + \frac{\upsilon k_{ge}^2}{\rho} B_\upsilon(k_e\rho)\frac{\partial B_\upsilon(k_e\rho')}{\partial\rho'}\sin(\upsilon\phi)\cos(\upsilon\phi')\sin k_{ge}(z_d - z)\sin(k_{ge}z')\hat{\phi}\hat{\rho} \\ & - \frac{\upsilon^2 k_{ge}^2}{\rho\rho'} B_\upsilon(k_e\rho) B_\upsilon(k_e\rho')\sin(\upsilon\phi)\sin(\upsilon\phi')\sin k_{ge}(z_d - z)\sin(k_{ge}z')\hat{\phi}\hat{\phi} \\ & + \frac{\upsilon k_{ge}k_e^2}{\rho} B_\upsilon(k_e\rho) B_\upsilon(k_e\rho')\sin(\upsilon\phi)\cos(\upsilon\phi')\sin k_{ge}(z_d - z)\cos(k_{ge}z')\hat{\phi}\hat{z} \\ & + k_{ge}k_e^2 B_\upsilon(k_e\rho)\frac{\partial B_\upsilon(k_e\rho')}{\partial\rho'}\cos(\upsilon\phi)\cos(\upsilon\phi')\cos k_{ge}(z_d - z)\sin(k_{ge}z')\hat{z}\hat{\rho} \\ & - \frac{\upsilon k_{ge}k_e^2}{\rho'} B_\upsilon(k_e\rho) B_\upsilon(k_e\rho')\cos(\upsilon\phi)\sin(\upsilon\phi')\cos k_{ge}(z_d - z)\sin(k_{ge}z')\hat{z}\hat{\phi} \\ & + k_e^4 B_\upsilon(k_e\rho) B_\upsilon(k_e\rho')\cos(\upsilon\phi)\cos(\upsilon\phi')\cos k_{ge}(z_d - z)\sin(k_{ge}z')\hat{z}\hat{z}\Big\}\end{aligned} \tag{B.8}$$

when $z < z'$, the expansion of vector wave functions in bracket are

$$\begin{aligned}\bar{M}_{h,odd}(z)\bar{M}'_{h,odd}(z_d-z') = {} & \frac{\upsilon^2}{\rho\rho'}B_\upsilon(k_h\rho)B_\upsilon(k_h\rho')\sin(\upsilon\phi)\sin(\upsilon\phi')\sin(k_{gh}z)\sin k_{gh}(z_d-z')\hat{\rho}\hat{\rho} \\ & + \frac{\upsilon}{\rho}B_\upsilon(k_h\rho)\frac{\partial B_\upsilon(k_h\rho')}{\partial\rho'}\sin(\upsilon\phi)\cos(\upsilon\phi')\sin(k_{gh}z)\sin k_{gh}(z_d-z')\hat{\rho}\hat{\phi} \\ & + \frac{\upsilon}{\rho'}\frac{\partial B_\upsilon(k_h\rho)}{\partial\rho}B_\upsilon(k_h\rho')\cos(\upsilon\phi)\sin(\upsilon\phi')\sin(k_{gh}z)\sin k_{gh}(z_d-z')\hat{\phi}\hat{\rho} \\ & + \frac{\partial B_\upsilon(k_h\rho)}{\partial\rho}\frac{\partial B_\upsilon(k_h\rho')}{\partial\rho'}\cos(\upsilon\phi)\cos(\upsilon\phi')\sin(k_{gh}z)\sin k_{gh}(z_d-z')\hat{\phi}\hat{\phi}\end{aligned} \tag{B.9}$$

$$\begin{aligned}\bar{N}_{e,even}(z)\bar{N}'_{e,even}(z_d-z') = \frac{1}{k^2}\Big\{ & -k_{ge}^2\frac{\partial B_\upsilon(k_e\rho)}{\partial\rho}\frac{\partial B_\upsilon(k_e\rho')}{\partial\rho'}\sin(\upsilon\phi)\sin(\upsilon\phi')\sin(k_{ge}z)\sin k_{ge}(z_d-z')\hat{\rho}\hat{\rho} \\ & + \frac{\upsilon k_{ge}^2}{\rho'}\frac{\partial B_\upsilon(k_e\rho)}{\partial\rho}B_\upsilon(k_e\rho')\sin(\upsilon\phi)\cos(\upsilon\phi')\sin(k_{ge}z)\sin k_{ge}(z_d-z')\hat{\rho}\hat{\phi} \\ & + k_{ge}k_e^2\frac{\partial B_\upsilon(k_e\rho)}{\partial\rho}B_\upsilon(k_e\rho')\sin(\upsilon\phi)\sin(\upsilon\phi')\sin(k_{ge}z)\sin k_{ge}(z_d-z')\hat{\rho}\hat{z} \\ & + \frac{\upsilon k_{ge}^2}{\rho}B_\upsilon(k_e\rho)\frac{\partial B_\upsilon(k_e\rho')}{\partial\rho'}\cos(\upsilon\phi)\sin(\upsilon\phi')\sin(k_{ge}z)\sin k_{ge}(z_d-z')\hat{\phi}\hat{\rho} \\ & - \frac{\upsilon^2k_{ge}^2}{\rho\rho'}B_\upsilon(k_e\rho)B_\upsilon(k_e\rho')\cos(\upsilon\phi)\cos(\upsilon\phi')\sin(k_{ge}z)\sin k_{ge}(z_d-z')\hat{\phi}\hat{\phi} \\ & - \frac{\upsilon k_{ge}k_e^2}{\rho}B_\upsilon(k_e\rho)B_\upsilon(k_e\rho')\cos(\upsilon\phi)\sin(\upsilon\phi')\sin(k_{ge}z)\cos k_{ge}(z_d-z')\hat{\phi}\hat{z} \\ & - k_{ge}k_e^2B_\upsilon(k_e\rho)\frac{\partial B_\upsilon(k_e\rho')}{\partial\rho'}\sin(\upsilon\phi)\sin(\upsilon\phi')\cos(k_{ge}z)\sin k_{ge}(z_d-z')\hat{z}\hat{\rho} \\ & + \frac{\upsilon k_{ge}k_e^2}{\rho'}B_\upsilon(k_e\rho)B_\upsilon(k_e\rho')\sin(\upsilon\phi)\cos(\upsilon\phi')\cos(k_{ge}z)\sin k_{ge}(z_d-z')\hat{z}\hat{\phi} \\ & + k_e^4B_\upsilon(k_e\rho)B_\upsilon(k_e\rho')\sin(\upsilon\phi)\sin(\upsilon\phi')\cos(k_{ge}z)\cos k_{ge}(z_d-z')\hat{z}\hat{z}\Big\}\end{aligned} \tag{B.10}$$

B-3 Electric Field due to the Magnetic Current Source

$$\overline{\overline{G}}_{EM}\left(\bar{R},\bar{R}'\right)=2jk\sum_{n,m}\left\{\frac{A_h}{\sin\left(k_{gh}z_d\right)}\begin{bmatrix}\bar{M}_{h,odd}\left(z_d-z\right)\bar{N}'_{h,odd}\left(z'\right)\\ \bar{M}_{h,odd}\left(z\right)\bar{N}'_{h,odd}\left(z_d-z'\right)\end{bmatrix}\right.$$
$$\left.-\frac{A_e}{\sin\left(k_{ge}z_d\right)}\begin{bmatrix}\bar{N}_{e,even}\left(z_d-z\right)\bar{M}'_{e,even}\left(z'\right)\\ \bar{N}_{e,even}\left(z\right)\bar{M}'_{e,even}\left(z_d-z'\right)\end{bmatrix}\right\}\begin{matrix}z>z'\\ ,z<z'\end{matrix} \tag{B.11}$$

when $z > z'$, the products of vector wave functions in bracket are

$$\begin{aligned}\bar{M}_{h,odd}\left(z_d-z\right)\bar{N}'_{h,odd}\left(z'\right)=\frac{1}{k^2}\Bigg\{&-\frac{\upsilon k_{gh}}{\rho}B_\upsilon\left(k_h\rho\right)\frac{\partial B_\upsilon\left(k_h\rho'\right)}{\partial\rho'}\sin\left(\upsilon\phi\right)\cos\left(\upsilon\phi'\right)\cos k_{gh}\left(z_d-z\right)\cos\left(k_{gh}z'\right)\hat{\rho}\hat{\rho}\\ &-\frac{\upsilon^2k_{gh}}{\rho\rho'}B_\upsilon\left(k_h\rho\right)B_\upsilon\left(k_h\rho'\right)\sin\left(\upsilon\phi\right)\sin\left(\upsilon\phi'\right)\cos k_{gh}\left(z_d-z\right)\cos\left(k_{gh}z'\right)\hat{\rho}\hat{\phi}\\ &-\frac{\upsilon k_h^2}{\rho}B_\upsilon\left(k_h\rho\right)B_\upsilon\left(k_h\rho'\right)\sin\left(\upsilon\phi\right)\cos\left(\upsilon\phi'\right)\cos k_{gh}\left(z_d-z\right)\sin\left(k_{gh}z'\right)\hat{\rho}\hat{z}\\ &-k_{gh}\frac{\partial B_\upsilon\left(k_h\rho\right)}{\partial\rho}\frac{\partial B_\upsilon\left(k_h\rho'\right)}{\partial\rho'}\cos\left(\upsilon\phi\right)\cos\left(\upsilon\phi'\right)\cos k_{gh}\left(z_d-z\right)\cos\left(k_{gh}z'\right)\hat{\phi}\hat{\rho}\\ &-\frac{\upsilon k_{gh}}{\rho'}\frac{\partial B_\upsilon\left(k_h\rho\right)}{\partial\rho}B_\upsilon\left(k_h\rho'\right)\cos\left(\upsilon\phi\right)\sin\left(\upsilon\phi'\right)\cos k_{gh}\left(z_d-z\right)\cos\left(k_{gh}z'\right)\hat{\phi}\hat{\phi}\\ &-k_h^2\frac{\partial B_\upsilon\left(k_h\rho\right)}{\partial\rho}B_\upsilon\left(k_h\rho'\right)\cos\left(\upsilon\phi\right)\cos\left(\upsilon\phi'\right)\cos k_{gh}\left(z_d-z\right)\sin\left(k_{gh}z'\right)\hat{\phi}\hat{z}\Bigg\}\end{aligned} \tag{B.12}$$

$$\begin{aligned}\bar{N}_{e,even}\left(z_d-z\right)\bar{M}'_{e,even}\left(z'\right)=\frac{1}{k}\Bigg\{&-\frac{\upsilon k_{ge}}{\rho'}\frac{\partial B_\upsilon\left(k_e\rho\right)}{\partial\rho}B_\upsilon\left(k_e\rho'\right)\sin\left(\upsilon\phi\right)\cos\left(\upsilon\phi'\right)\cos k_{ge}\left(z_d-z\right)\cos\left(k_{ge}z'\right)\hat{\rho}\hat{\rho}\\ &-k_{ge}\frac{\partial B_\upsilon\left(k_e\rho\right)}{\partial\rho}\frac{\partial B_\upsilon\left(k_e\rho'\right)}{\partial\rho'}\sin\left(\upsilon\phi\right)\sin\left(\upsilon\phi'\right)\cos k_{ge}\left(z_d-z\right)\cos\left(k_{ge}z'\right)\hat{\rho}\hat{\phi}\\ &-\frac{\upsilon^2k_{ge}}{\rho\rho'}B_\upsilon\left(k_e\rho\right)B_\upsilon\left(k_e\rho'\right)\cos\left(\upsilon\phi\right)\cos\left(\upsilon\phi'\right)\cos k_{ge}\left(z_d-z\right)\cos\left(k_{ge}z'\right)\hat{\phi}\hat{\rho}\\ &+\frac{\upsilon k_{ge}}{\rho}B_\upsilon\left(k_e\rho\right)\frac{\partial B_\upsilon\left(k_e\rho'\right)}{\partial\rho'}\cos\left(\upsilon\phi\right)\sin\left(\upsilon\phi'\right)\cos k_{ge}\left(z_d-z\right)\cos\left(k_{ge}z'\right)\hat{\phi}\hat{\phi}\end{aligned}$$

$$-\frac{\upsilon k_e^2}{\rho'}B_\upsilon(k_e\rho)B_\upsilon(k_e\rho')\sin(\upsilon\phi)\cos(\upsilon\phi')\sin k_{ge}(z_d-z)\cos(k_{ge}z')\hat{z}\hat{\rho}$$
$$-\lambda^2 B_n(\lambda\rho)\frac{\partial B_n(\lambda\rho')}{\partial\rho'}\sin(n\phi)\sin(n\phi')\sin k_\lambda(z_d-z)\cos(k_\lambda z')\hat{z}\hat{\phi}\Big\} \quad \text{(B.13)}$$

when $z < z'$, the products of vector wave functions in bracket are

$$\bar{M}_{h,odd}(z)\bar{N}'_{h,odd}(z_d-z') = \frac{1}{k^2}\Big\{\frac{\upsilon k_{gh}}{\rho}B_\upsilon(k_h\rho)\frac{\partial B_\upsilon(k_h\rho')}{\partial\rho'}\sin(\upsilon\phi)\cos(\upsilon\phi')\cos(k_{gh}z)\cos k_{gh}(z_d-z')\hat{\rho}\hat{\rho}$$
$$-\frac{\upsilon^2 k_{gh}}{\rho\rho'}B_\upsilon(k_h\rho)B_\upsilon(k_h\rho')\sin(\upsilon\phi)\sin(\upsilon\phi')\cos(k_{gh}z)\cos k_{gh}(z_d-z')\hat{\rho}\hat{\phi}$$
$$-\frac{\upsilon\mu^2}{\rho}B_\upsilon(k_h\rho)B_\upsilon(k_h\rho')\sin(\upsilon\phi)\cos(\upsilon\phi')\cos(k_{gh}z)\sin k_{gh}(z_d-z')\hat{\rho}\hat{z}$$
$$+k_{gh}\frac{\partial B_\upsilon(k_h\rho)}{\partial\rho}\frac{\partial B_\upsilon(k_h\rho')}{\partial\rho'}\cos(\upsilon\phi)\cos(\upsilon\phi')\cos(k_{gh}z)\sin(z_d-z')\hat{\phi}\hat{\rho}$$
$$-\frac{\upsilon k_{gh}}{\rho'}\frac{\partial B_\upsilon(k_h\rho)}{\partial\rho}B_\upsilon(k_h\rho')\cos(\upsilon\phi)\sin(\upsilon\phi')\cos(k_{gh}z)\sin k_{gh}(z_d-z')\hat{\phi}\hat{\phi}$$
$$-k_h^2\frac{\partial B_\upsilon(k_h\rho)}{\partial\rho}B_\upsilon(k_h\rho')\cos(\upsilon\phi)\cos(\upsilon\phi')\cos(k_{gh}z)\cos k_{gh}(z_d-z')\hat{\phi}\hat{z}\Big\} \quad \text{(B.14)}$$

$$\bar{N}_{e,even}(z)\bar{M}'_{e,even}(z_d-z') = \frac{1}{k}\Big\{\frac{\upsilon k_{ge}}{\rho'}\frac{\partial B_\upsilon(k_e\rho)}{\partial\rho}B_\upsilon(k_e\rho')\sin(\upsilon\phi)\cos(\upsilon\phi')\cos(k_{ge}z)\cos k_{ge}(z_d-z')\hat{\rho}\hat{\rho}$$
$$-k_{ge}\frac{\partial B_\upsilon(k_e\rho)}{\partial\rho}\frac{\partial B_\upsilon(k_e\rho')}{\partial\rho'}\sin(\upsilon\phi)\sin(\upsilon\phi')\cos(k_{ge}z)\cos k_{ge}(z_d-z')\hat{\rho}\hat{\phi}$$
$$+\frac{\upsilon^2 k_{ge}}{\rho\rho'}B_\upsilon(k_e\rho)B_\upsilon(k_e\rho')\cos(\upsilon\phi)\cos(\upsilon\phi')\cos(k_{ge}z)\cos k_{ge}(z_d-z')\hat{\phi}\hat{\rho}$$
$$-\frac{\upsilon k_{ge}}{\rho}B_\upsilon(k_e\rho)\frac{\partial B_\upsilon(k_e\rho')}{\partial\rho'}\cos(\upsilon\phi)\sin(\upsilon\phi')\cos(k_{ge}z)\cos k_{ge}(z_d-z')\hat{\phi}\hat{\phi}$$
$$+\frac{\upsilon k_e^2}{\rho'}B_\upsilon(k_e\rho)B_\upsilon(k_e\rho')\sin(\upsilon\phi)\cos(\upsilon\phi')\sin(k_{ge}z)\cos k_{ge}(z_d-z')\hat{z}\hat{\rho}$$
$$-k_e^2 B_\upsilon(\lambda\rho)\frac{\partial B_\upsilon(\lambda\rho')}{\partial\rho'}\sin(\upsilon\phi)\sin(\upsilon\phi')\sin(k_\lambda z)\cos k_{ge}(z_d-z')\hat{z}\hat{\phi}\Big\} \quad \text{(B.15)}$$

B-4 Magnetic Field due to the Electric Current Source

$$\overline{\overline{G}}_{HJ}\left(\bar{R},\bar{R}'\right)=2jk\sum_{n,m}\left\{\frac{A_h}{\sin\left(k_{gh}z_d\right)}\begin{bmatrix}\bar{N}_{h,odd}\left(z_d-z\right)\bar{M}'_{h,odd}\left(z'\right)\\ \bar{N}_{h,odd}\left(z\right)\bar{M}'_{h,odd}\left(z_d-z'\right)\end{bmatrix}\right.$$
$$\left.-\frac{A_e}{\sin\left(k_{ge}z_d\right)}\begin{bmatrix}\bar{M}_{e,even}\left(z_d-z\right)\bar{N}'_{e,even}\left(z'\right)\\ \bar{M}_{e,even}\left(z\right)\bar{N}'_{e,even}\left(z_d-z'\right)\end{bmatrix}\right\}\begin{matrix}z>z'\\ ,z<z'\end{matrix}$$

(B.16)

when $z > z'$, the products of vector wave functions in bracket are

$$\bar{N}_{h,odd}\left(z_d-z\right)\bar{M}'_{h,odd}\left(z'\right)=\frac{1}{k}\left\{\frac{\upsilon k_{gh}}{\rho'}\frac{\partial B_\upsilon\left(k_e\rho\right)}{\partial\rho}B_\upsilon\left(k_e\rho'\right)\cos\left(\upsilon\phi\right)\sin\left(\upsilon\phi'\right)\cos k_{gh}\left(z_d-z\right)\cos\left(k_{gh}z'\right)\hat{\rho}\hat{\rho}\right.$$
$$+k_{gh}\frac{\partial B_\upsilon\left(k_e\rho\right)}{\partial\rho}\frac{\partial B_\upsilon\left(k_e\rho'\right)}{\partial\rho'}\cos\left(\upsilon\phi\right)\cos\left(\upsilon\phi'\right)\cos k_{gh}\left(z_d-z\right)\cos\left(k_{gh}z'\right)\hat{\rho}\hat{\phi}$$
$$-\frac{\upsilon^2k_{gh}}{\rho\rho'}B_\upsilon\left(k_h\rho\right)B_\upsilon\left(k_h\rho'\right)\sin\left(\upsilon\phi\right)\sin\left(\upsilon\nu\phi'\right)\cos k_{gh}\left(z_d-z\right)\cos\left(k_{gh}z'\right)\hat{\phi}\hat{\rho}$$
$$-\frac{\upsilon k_{gh}}{\rho}B_\upsilon\left(k_h\rho\right)\frac{\partial B_\upsilon\left(k_h\rho'\right)}{\partial\rho'}\sin\left(\upsilon\phi\right)\cos\left(\upsilon\phi'\right)\cos k_{gh}\left(z_d-z\right)\cos\left(k_{gh}z'\right)\hat{\phi}\hat{\phi}$$
$$-\frac{\upsilon k_h^2}{\rho'}B_\upsilon\left(k_h\rho\right)B_\upsilon\left(k_h\rho'\right)\cos\left(\upsilon\phi\right)\sin\left(\upsilon\phi'\right)\sin k_{gh}\left(z_d-z\right)\cos\left(k_{gh}z'\right)\hat{z}\hat{\rho}$$
$$\left.-k_h^2B_\upsilon\left(k_h\rho\right)\frac{\partial B_\upsilon\left(k_h\rho'\right)}{\partial\rho'}\cos\left(\upsilon\phi\right)\cos\left(\upsilon\phi'\right)\sin k_{gh}\left(z_d-z\right)\cos\left(k_{gh}z'\right)\hat{\phi}\hat{z}\right\}$$

(B.17)

$$\bar{M}_{e,even}\left(z_d-z\right)\bar{N}'_{e,even}\left(z'\right)=\frac{1}{k}\left\{\frac{\upsilon k_{ge}}{\rho}B_\upsilon\left(k_e\rho\right)\frac{\partial B_\upsilon\left(k_e\rho'\right)}{\partial\rho}\cos\left(\upsilon\phi\right)\sin\left(\upsilon\phi'\right)\cos k_{ge}\left(z_d-z\right)\cos\left(k_{ge}z'\right)\hat{\rho}\hat{\rho}\right.$$
$$+\frac{\upsilon^2k_{ge}}{\rho\rho'}B_\upsilon\left(k_e\rho\right)B_\upsilon\left(k_e\rho'\right)\cos\left(\upsilon\phi\right)\cos\left(\upsilon\phi'\right)\cos k_{ge}\left(z_d-z\right)\cos\left(k_{ge}z'\right)\hat{\rho}\hat{\phi}$$
$$+\frac{\upsilon k_e^2}{\rho}B_\upsilon\left(k_e\rho\right)B_\upsilon\left(k_e\rho'\right)\cos\left(\upsilon\phi\right)\sin\left(\upsilon\phi'\right)\cos k_{ge}\left(z_d-z\right)\sin\left(k_{ge}z'\right)\hat{\rho}\hat{z}$$
$$\left.-k_{ge}\frac{\partial B_\upsilon\left(k_e\rho\right)}{\partial\rho}\frac{\partial B_\upsilon\left(k_e\rho'\right)}{\partial\rho'}\sin\left(\upsilon\phi\right)\sin\left(\upsilon\phi'\right)\cos k_{ge}\left(z_d-z\right)\cos\left(k_{ge}z'\right)\hat{\phi}\hat{\rho}\right.$$

$$-\frac{\upsilon k_{ge}}{\rho'}\frac{\partial B_\upsilon(k_e\rho)}{\partial\rho}B_\upsilon(k_e\rho')\sin(\upsilon\phi)\cos(\upsilon\phi')\cos k_{ge}(z_d-z)\cos(k_{ge}z')\hat{\phi}\hat{\phi}$$

$$-k_e^2\frac{\partial B_\upsilon(k_e\rho)}{\partial\rho}B_\upsilon(k_e\rho')\sin(\upsilon\phi)\sin(\upsilon\phi')\cos k_{ge}(z_d-z)\sin(k_{ge}z')\hat{\phi}\hat{z}\Big\} \tag{B.18}$$

when $z < z'$, the products of vector wave functions in bracket are

$$\bar{N}_{h,odd}(z)\bar{M}'_{h,odd}(z_d-z') = \frac{1}{k}\Big\{-\frac{\upsilon k_{gh}}{\rho'}\frac{\partial B_\upsilon(k_h\rho)}{\partial\rho}B_\upsilon(k_h\rho')\cos(\upsilon\phi)\sin(\upsilon\phi')\cos(k_{gh}z)\cos k_{gh}(z_d-z')\hat{\rho}\hat{\rho}$$

$$-k_{gh}\frac{\partial B_\upsilon(k_h\rho)}{\partial\rho}\frac{\partial B_\upsilon(k_h\rho')}{\partial\rho'}\cos(\upsilon\phi)\cos(\upsilon\phi')\cos(k_{gh}z)\cos k_{gh}(z_d-z')\hat{\rho}\hat{\phi}$$

$$-\frac{\upsilon^2 k_\mu}{\rho\rho'}B_\upsilon(k_h\rho)B_\upsilon(k_h\rho')\sin(\upsilon\phi)\sin(\upsilon\phi')\cos(k_{gh}z)\cos k_{gh}(z_d-z')\hat{\phi}\hat{\rho}$$

$$-\frac{\upsilon k_\mu}{\rho}B_\upsilon(k_h\rho)\frac{\partial B_\upsilon(k_h\rho')}{\partial\rho'}\sin(\upsilon\phi)\cos(\upsilon\phi')\cos(k_{gh}z)\cos k_{gh}(z_d-z')\hat{\phi}\hat{\phi}$$

$$-\frac{\upsilon k_h^2}{\rho'}B_\upsilon(k_h\rho)B_\upsilon(k_h\rho')\cos(\upsilon\phi)\sin(\upsilon\phi')\sin(k_{gh}z)\cos k_{gh}(z_d-z')\hat{z}\hat{\rho}$$

$$-k_h^2 B_n(k_h\rho)\frac{\partial B_\upsilon(k_h\rho')}{\partial\rho'}\cos(\upsilon\phi)\cos(\upsilon\phi')\sin(k_{gh}z)\cos k_{gh}(z_d-z')\hat{z}\hat{\phi}\Big\} \tag{A.19}$$

$$\bar{M}_{e,even}(z)\bar{N}'_{e,even}(z_d-z') = \frac{1}{k}\Big\{\frac{\upsilon k_{ge}}{\rho}B_\upsilon(k_e\rho)\frac{\partial B_\upsilon(k_e\rho')}{\partial\rho}\cos(\upsilon\phi)\sin(\upsilon\phi')\cos(k_{ge}z)\cos k_{ge}(z_d-z')\hat{\rho}\hat{\rho}$$

$$-\frac{\upsilon^2 k_{ge}}{\rho\rho'}B_\upsilon(k_e\rho)B_\upsilon(k_e\rho')\cos(\upsilon\phi)\cos(\upsilon\phi')\cos(k_{ge}z)\cos k_{ge}(z_d-z')\hat{\rho}\hat{\phi}$$

$$+\frac{\upsilon k_e^2}{\rho}B_\upsilon(k_e\rho)B_\upsilon(k_e\rho')\cos(\upsilon\phi)\sin(\upsilon\phi')\cos(k_{ge}z)\sin k_{ge}(z_d-z')\hat{\rho}\hat{z}$$

$$-k_{ge}\frac{\partial B_\upsilon(k_e\rho)}{\partial\rho}\frac{\partial B_\upsilon(k_e\rho')}{\partial\rho'}\sin(\upsilon\phi)\sin(\upsilon\phi')\cos(k_{ge}z)\cos k_{ge}(z_d-z')\hat{\phi}\hat{\rho}$$

$$+\frac{\upsilon k_{ge}}{\rho'}\frac{\partial B_\upsilon(k_e\rho)}{\partial\rho}B_\upsilon(k_e\rho')\sin(\upsilon\phi)\cos(\upsilon\phi')\cos(k_{ge}z)\cos k_{ge}(z_d-z')\hat{\phi}\hat{\phi}$$

$$-k_e^2\frac{\partial B_\upsilon(k_e\rho)}{\partial\rho}B_\upsilon(k_e\rho')\sin(\upsilon\phi)\sin(\upsilon\phi')\cos(k_{ge}z)\sin k_{ge}(z_d-z')\hat{\phi}\hat{z}\Big\} \tag{A.20}$$

We repeat here the coefficients involved in chapter 3; they are

$$A_h = -j\frac{(2-\delta)}{2\phi_c k_h^2 I_h k_{gh}} \quad , \quad A_e = -j\frac{(2-\delta)}{2\phi_c k_e^2 I_e k_{ge}}$$

$$k_{gh} = \left(k^2 - k_h^2\right)^{1/2} \quad , \quad k_{ge} = \left(k^2 - k_e^2\right)^{1/2}$$

$$I_h = \frac{\rho^2}{2k_h^2} B_\upsilon^2\left(k_h\rho\right)\left[k_h^2 - \frac{\upsilon^2}{\rho^2}\right]_{\rho=\rho_a}^{\rho=\rho_b} \quad , \quad I_e = \frac{\rho^2}{2k_e^2}\left[\frac{\partial B_\upsilon\left(k_e\rho\right)}{\partial\rho}\right]_{\rho=\rho_a}^{\rho=\rho_b}$$

$$\delta_o = \begin{cases} 1, & n = 0 \\ 0, & n \neq 0 \end{cases}$$

where $B_\upsilon(k_\xi\rho)$ denotes the linear combination of the ordinary Bessel function of the first kind $J_\upsilon(k_\xi\rho)$ and the second kind $Y_\upsilon(k_\xi\rho)$ of order υ, as described in chapter 3 and appendix A.

The components of dyadic Green's function in Eq. (B.2)-(B.5), (B.7)-(B.10), (B.12)-(B.15) and (B.17)-(B-20) can be used to substitute in the integral equations for any problems of the sectoral cylindrical cavity[B-2]. By selecting the components of the products of vector wave functions according to field and source positions of problem. Our example is a slot cut in z-direction on the outer surface of the cavity and excited probe is located in ρ-direction at the center of inner surface of cavity. Therefore, we have to choose $\hat{z}\hat{z}$-component for $\overline{\overline{G}}_{HM}\left(\overline{R},\overline{R}'\right)$, $\hat{z}\hat{\rho}$-component for $\overline{\overline{G}}_{HJ}\left(\overline{R},\overline{R}'\right)$, $\hat{\rho}\hat{z}$-component for $\overline{\overline{G}}_{EM}\left(\overline{R},\overline{R}'\right)$ and $\hat{\rho}\hat{\rho}$-component for $\overline{\overline{G}}_{EJ}\left(\overline{R},\overline{R}'\right)$.

References

[B-1] C.T.Tai, *Dyadic Green Function in Electromagnetic Theory*, 2nd Ed. Sec.6.4, New York: IEEE Press, 1993.

[B-2] R.Wongsan, C.Phongcharoenpanich, and M.Krairiksh, "Electromagnetic dyadic Green's functions of a sectoral cylindrical cavity," *Proceedings of the International Forum cum Conference on Information Technology and Communication at the Dawn of the New Millennium*, Bangkok, vol.2, pp.477-486, Aug. 2000.

List of Publications

1. R.Wongsan, C.Phongcharoenpanich, and M. Krairiksh, "Analysis of Input Impedance of a Sectoral Cylindrical Cavity-Backed Slot Antenna Fed by Probe," *Proceedings of the 2000 International Symposium on Antennas and Propagation*, Fukuoka, vol.2, pp.613-616, Aug. 2000.
2. R.Wongsan, C.Phongcharoenpanich, and M. Krairiksh, "Estimations of Impedance Characteristics of a Sectoral Cylindrical Cavity-Backed Slot Antenna Fed by Probe," *Proceedings of the International Forum cum Conference on Information Technology and Communication at the Dawn of the New Millennium*, Bangkok, vol.2, pp.467-475, Aug. 2000.
3. R.Wongsan, C.Phongcharoenpanich, and M. Krairiksh, "Electromagnetic Dyadic Green's Functions of a Sectoral Cylindrical Cavity," *Proceedings of the International Forum cum Conference on Information Technology and Communication at the Dawn of the New Millennium*, Bangkok, vol.2, pp.477-486, Aug. 2000.
4. R.Wongsan, C.Phongcharoenpanich and M.Krairiksh, "Assessment of Input Impedance of an Axial Slot Antenna on a Sectoral Cylindrical Cavity Excited by Probe using Method of Moments," *Proceedings of the 2002 International Conference on Circuits/Systems Computers and Communications* , pp.731-734, July 2001.
5. P.Wounchoum, C.Phongcharoenpanich, R.Wongsan, S.Kosulvit and M.Krairiksh, "Radiation Characteristics of a Slot Antenna on the Cylindrical Surface," *Proceedings of the Second National Symposium on Graduate Research*, p.10, April 2001 (in Thai).

6. N.Pasri, R.Wongsan, C.Phongcharoenpanich and M.Krairiksh, "Input Impedance of the Circumferential Slot Antenna on a Sectoral Cylindrical Cavity Excited by a Probe," *Proceedings of the 24th Electrical Engineering Conference*, pp.711-716, Nov.2001.
7. C.Phongcharoenpanich, P.Wounchoum, S.Kosulvit, R.Wongsan and M.Krairiksh, "Characteristics of an Omnidirectional Antenna using Circular Array of Slot on Cylinder for TV Broadcasting System," *Proceedings of the 2001 International Symposium on Communications and Information Technology*, pp.207-210, Nov.2001.
8. R.Wongsan, C.Phongcharoenpanich, M.Krairiksh and J.Takada, "Impedance Characteristic Analysis of an Axial Slot Antenna on a Sectoral Cylindrical Cavity Excited by a Probe using Method of Moments," *IEICE Trans. Fundamentals*, vol. E85-A, No.6, June 2003.

Cirriculum Vitae

Author: Rangsan Wongsan

Date of Birth: July 27, 1964

Bachelor Degree: B.Eng. in Electronics Engineering

Institution: Faculty of Engineering
Rajamongala Institute of Technology

Year of Graduation: 1989

Master Degree: M.Eng. in Electrical Engineering

Institution: Faculty of Engineering
King Mongkut's Institute of Technology North Bangkok

Year of Graduation: 1994

Master Thesis: Design and Testing of Rectangular Microstrip Antennas Flush-mounted Cylindrical Structures

Scholarship: Local Graduate Scholarship from Ministry of University Affairs (1998-2000)

Experiences:
- Lecturer of Electronics Division, Rajamongala Institute of Technology, North Bangkok Campus (1989-1993)
- Lecturer of School of Telecommunication Engineering, Institute of Engineering, Suranaree University of Technology (since 1994)